材料与能源前沿科学：
“能源转换和储存中的基础科学问题”培训班

铜铟镓硒与铜锌锡硫薄膜太阳能电池

辛　颢

iamhxin@njupt.edu.cn

南京邮电大学化学与生命科学学院

Nanjing University of Posts and Telecommunications

2022-11-03

纲　要

I. 铜铟镓硒薄膜太阳能电池

1. CIGS薄膜太阳能电池简介
2. 真空法CIGS电池性能提高历程
3. 溶液法CIGS电池：材料合成与晶粒生长机制
4. 总结与展望

II. 铜锌锡硫薄膜太阳能电池

1. CZTS薄膜太阳能电池：优势与挑战
2. 吸收层缺陷调控：开路电压损失与晶粒生长机制
3. 异质结界面缺陷：形成机制与消除
4. 总结与展望

III. 致谢

太阳能电池类型

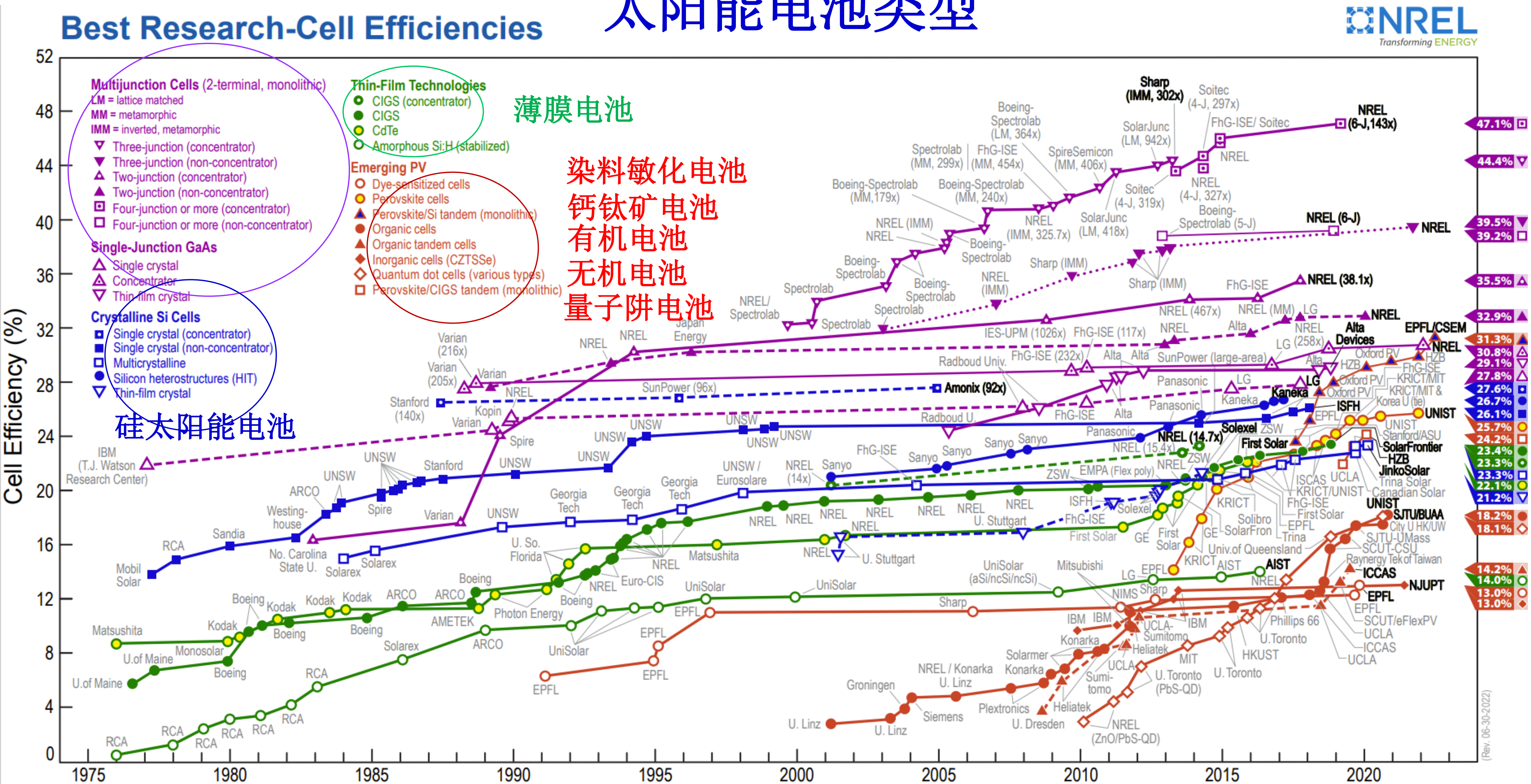

This plot is courtesy of the National Renewable Energy Laboratory, Golden, CO.

1. CIGS薄膜太阳能电池简介

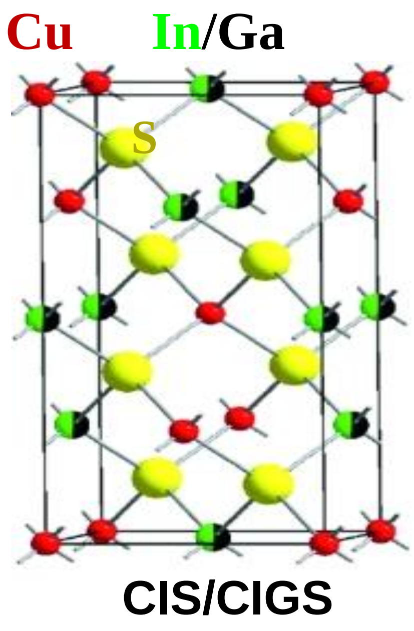

CIGS晶体结构

本征p-型半导体（V_{Cu}）

- 直接带隙
- 吸光系数高（10^5 cm^{-1}）
- 带隙可调（1.04 eV-1.67 eV）
- 理论效率高（32%-33%）
- 多晶薄膜：较高的缺陷耐受度

CIGS电池

- 成本相对低
- 稳定性好
- 效率高
- 轻薄
- 可柔性

真空法：蒸镀法、溅射后硒化法 ⟹

- ◆ 效率高，工艺相对成熟
- ◆ 设备成本高、大面积均匀性难以控制

非真空法：电沉积、喷雾热解、溶液法、纳米晶法 ⟹

- ◆ 制备成本低、组分精确调控、适用于卷对卷工艺生产
- ◆ 效率需进一步提升

Device Structure and Energy Diagram

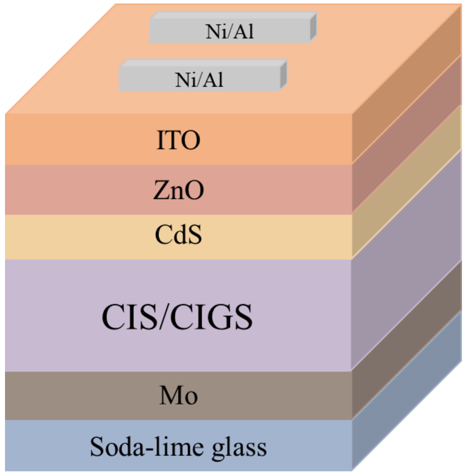

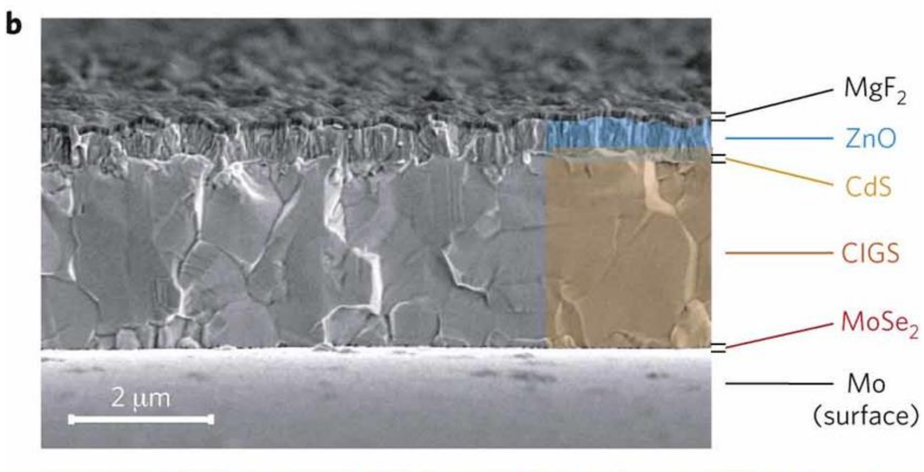

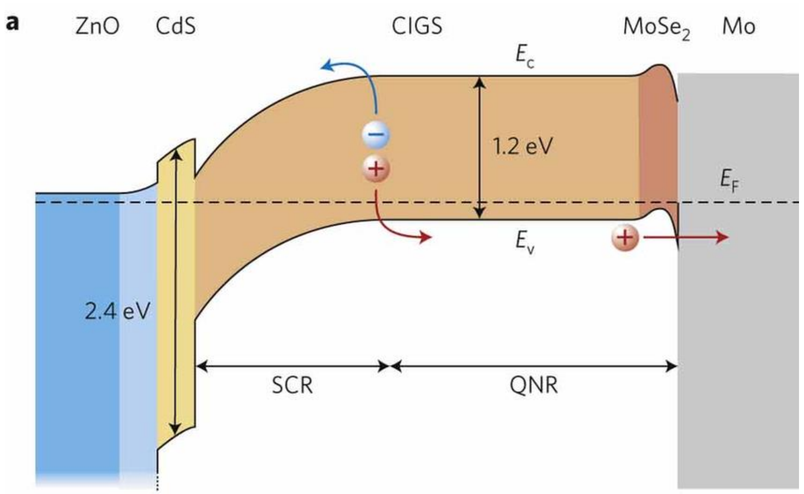

多晶薄膜：晶粒内和晶界处缺陷

晶格匹配

	Zinc-blende	(112)/(111) in-plane cons.	layer distance
CdS	5.848	4.136	3.376
$CuInSe_2$	a=5.781	4.103	3.349

外延型异质结界面

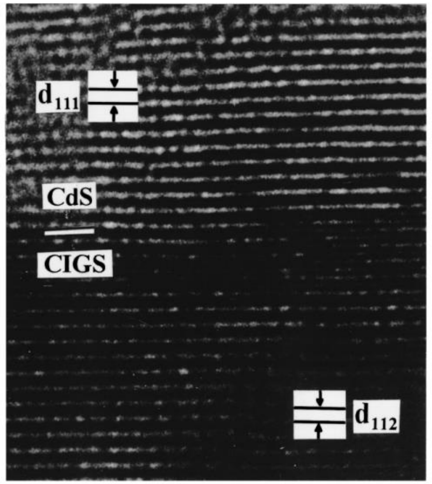

Cu-poor 表面，内埋异质结

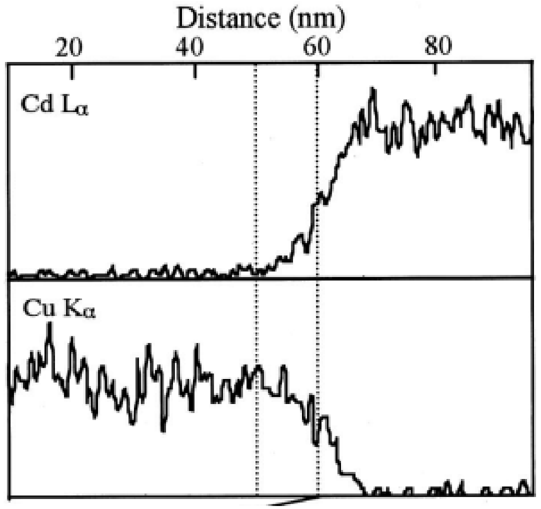

2.真空法CIGS电池提高历程

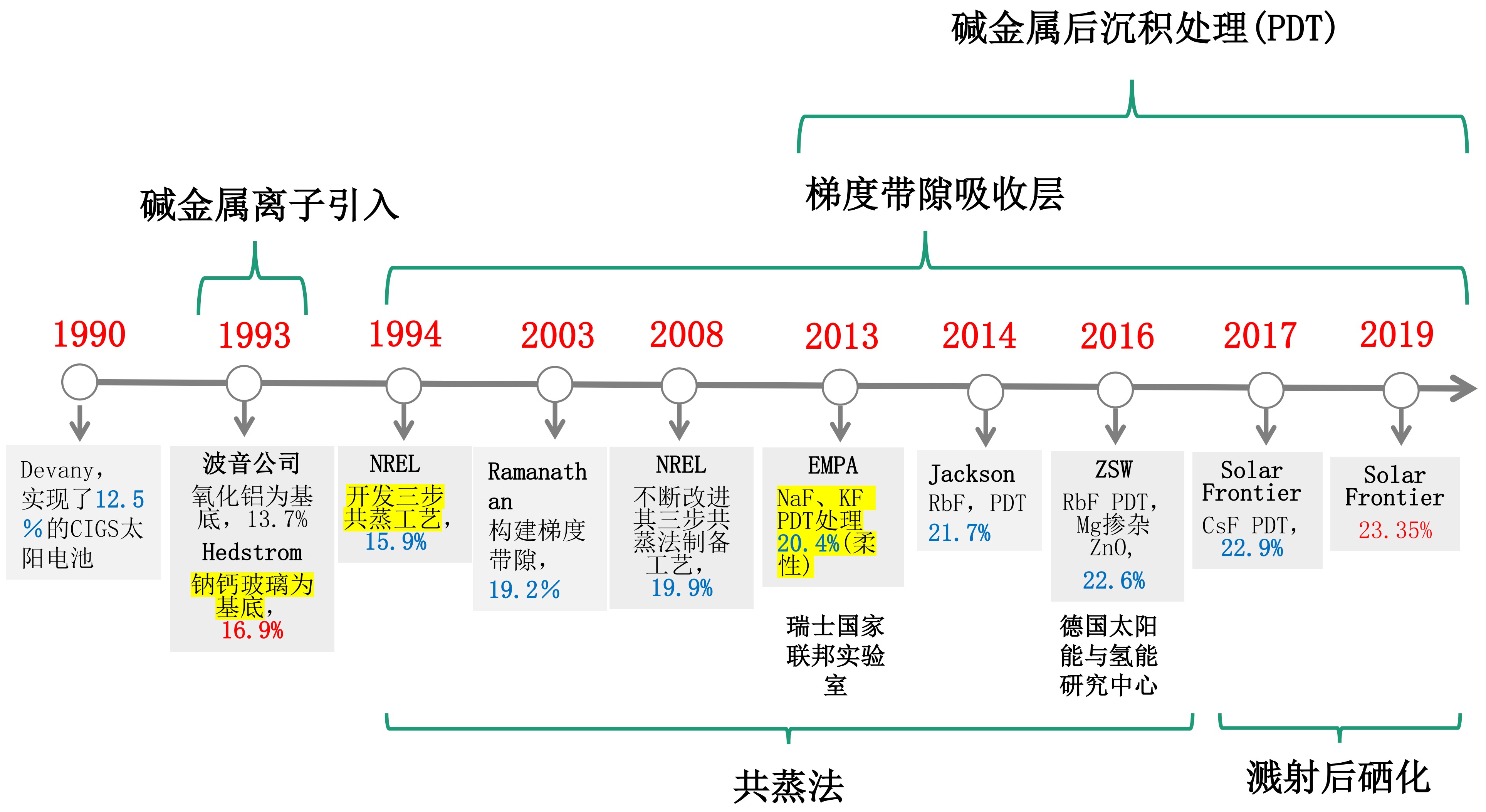

2.1 碱金属离子引入（Na掺杂）

1993年，Hedstrom以钠钙玻璃为基底制备CIGS电池效率16.9%

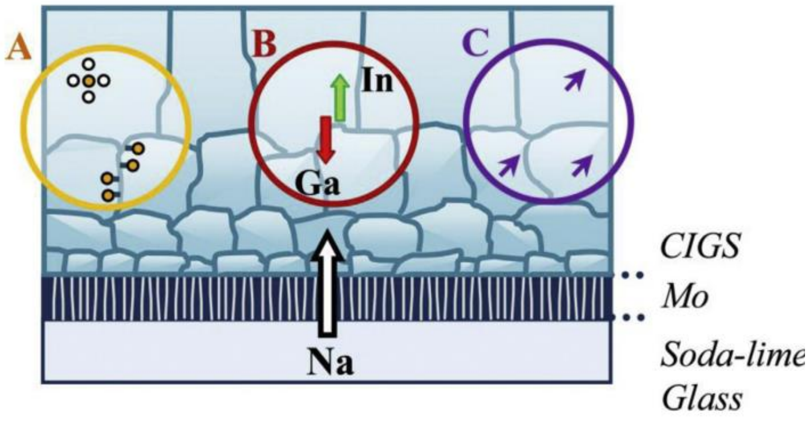

CIGS吸收膜掺入Na可改善器件性能
经Na掺入CIGS薄膜后发生：
（A）载流子密度增加和钝化晶界
（B）镓的偏析
（C）晶面生长取向变化

钠钙玻璃中的Na能扩撒至吸收膜中，对于不含碱金属的衬底可采用如下方法：

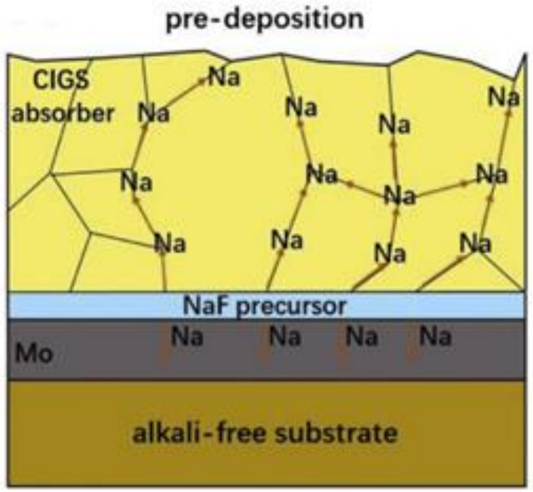

预沉积

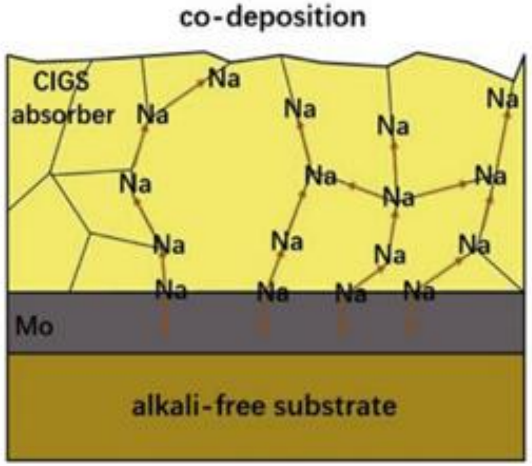

共沉积

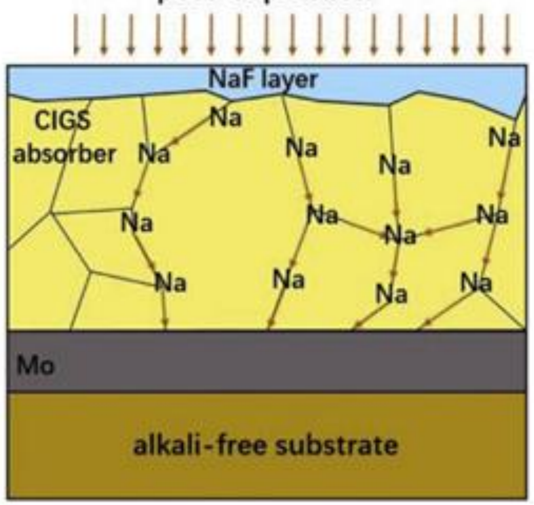

后沉积

2.2 梯度带隙吸收层 （三步共蒸法）

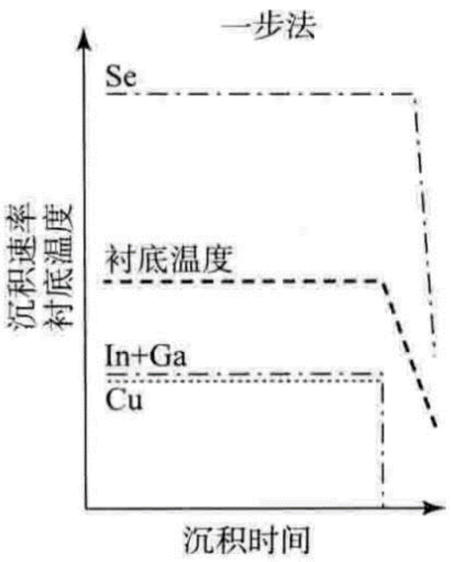

组分贫铜
工艺简单
结晶质量低

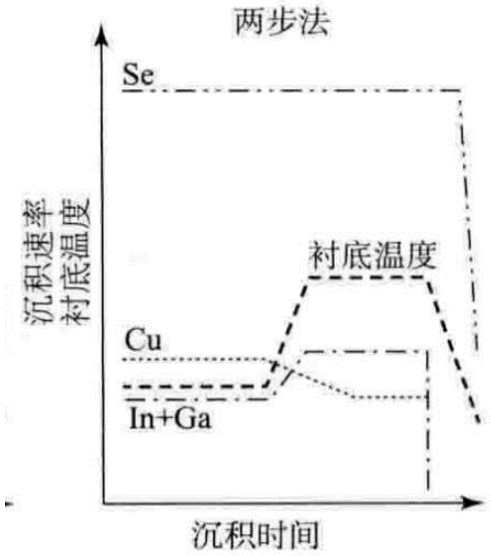

第一步富铜
第二步贫铜
薄膜晶粒大，组分贫铜

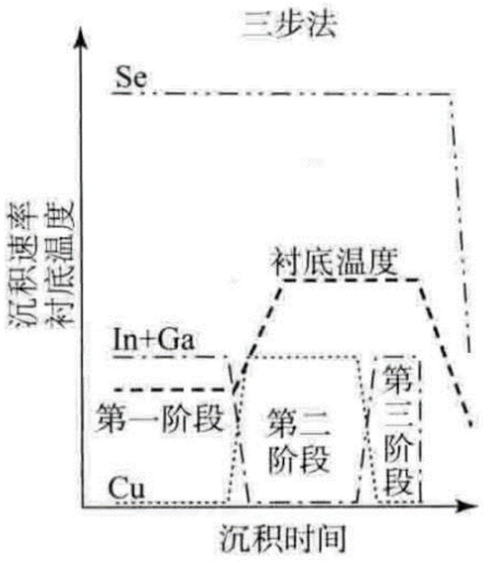

第一、三步沉积In、Ga、Se
第二步沉积Cu、Se
可构建梯度带隙，结晶质量高

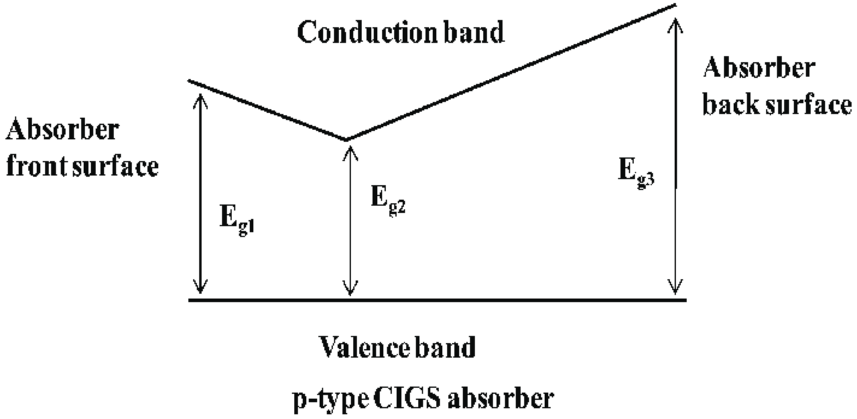

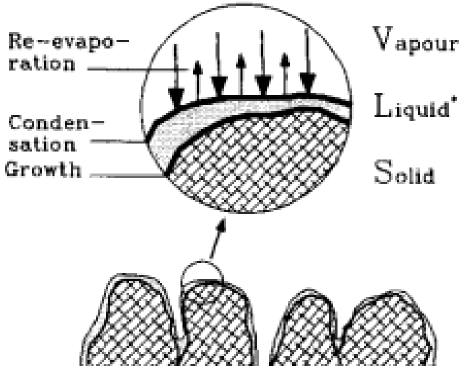

NREL, 首次开发三步共蒸工艺, 15.9%

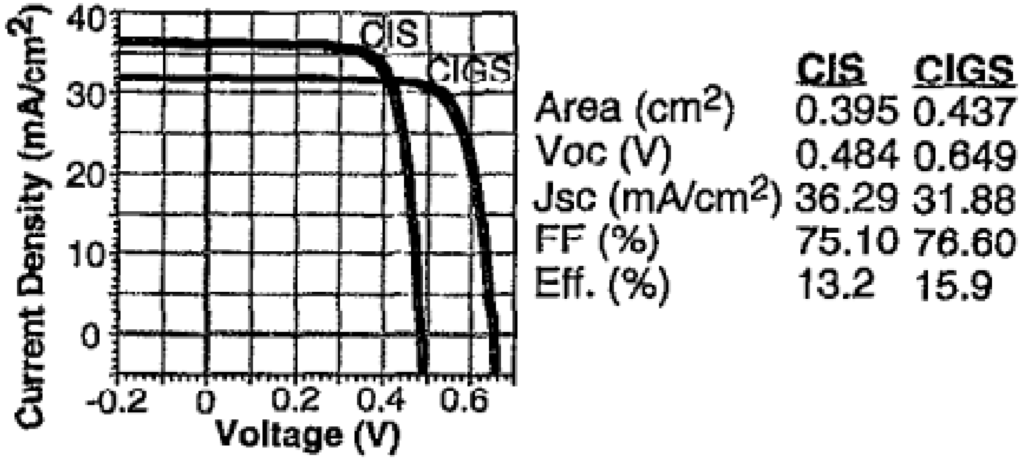

Applied Physics Letters 1994, 65(2):198-200.

不断改进的三步共蒸法制备工艺, 效率19.9%

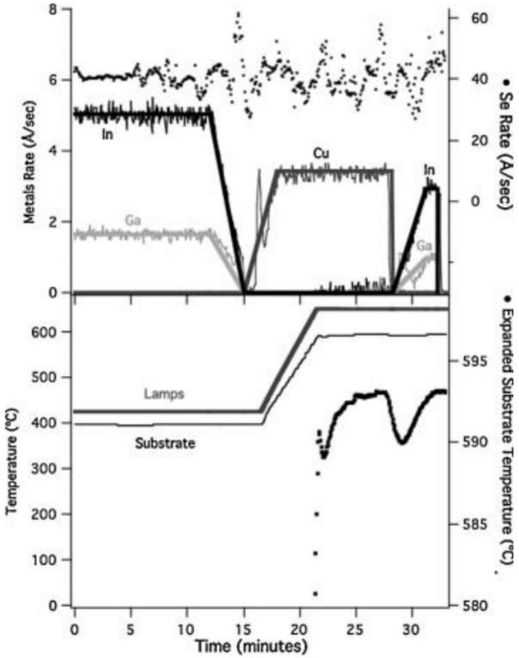

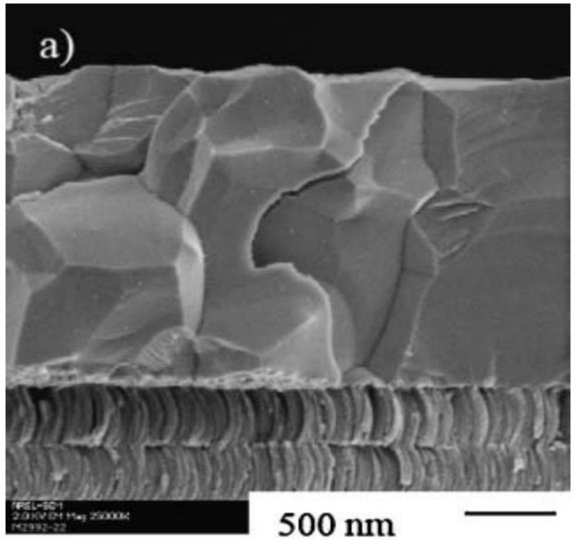

Progress in Photovoltaics: Research and Applications, 2008, 16(3): 23523-9.

2.3. 碱金属后沉积处理(PDT)

Solar Frontier，溅射后硒化法制备吸收层，经CsF PDT处理： 22.9%

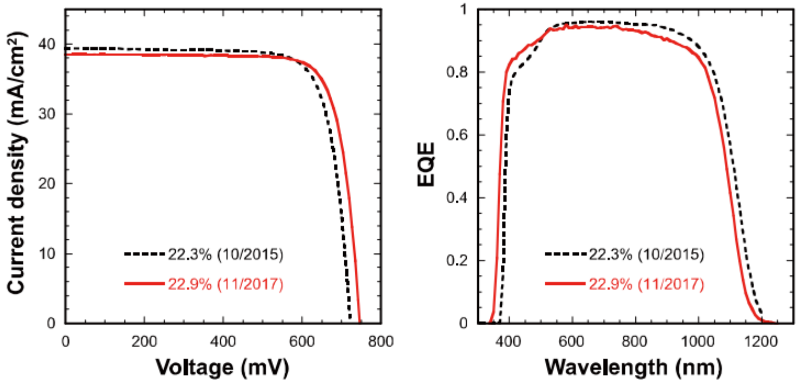

(a) (b)

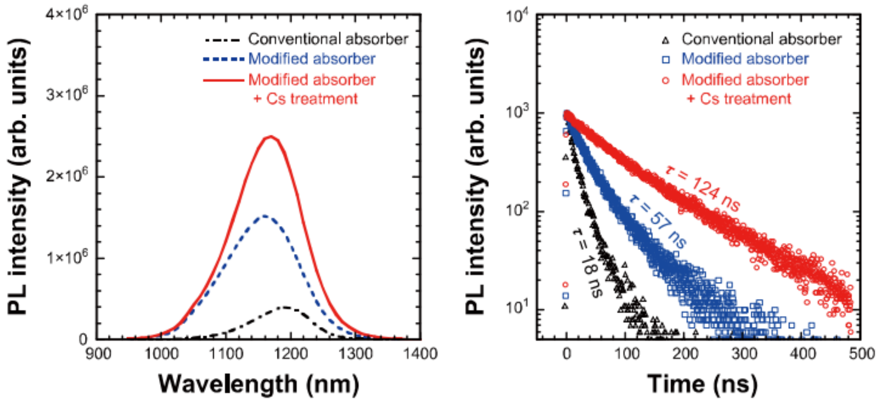

(a) (b)

IEEE Journal of Photovoltaics, 2017, 9(1):325-330

Solar Frontier，溅射后硒化法制备吸收层，经CsF PDT处理，沉积无镉缓冲层：23.35%

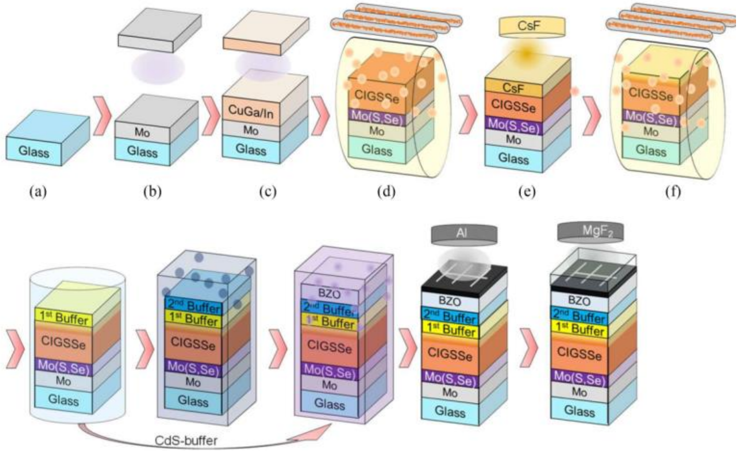

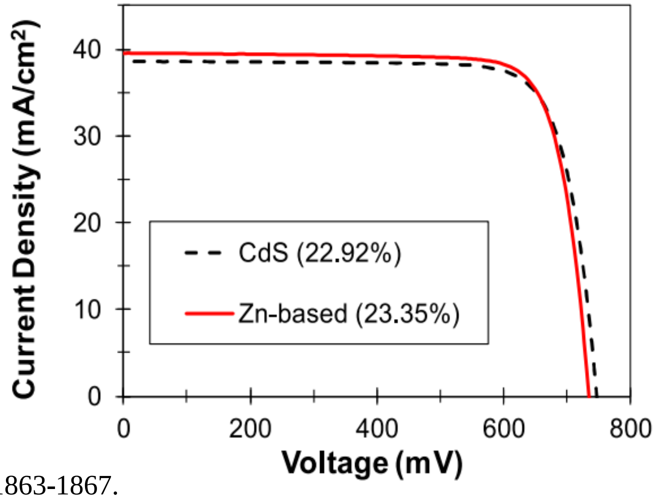

IEEE Journal of Photovoltaics, 2019, 9(6): 1863-1867.

3. 溶液法CIS/CIGS电池：材料合成与晶粒生长机制

New applications

- Adoptable to roll-to-roll processing
- High materials utilization rate
- High throughput
- Property chemical control

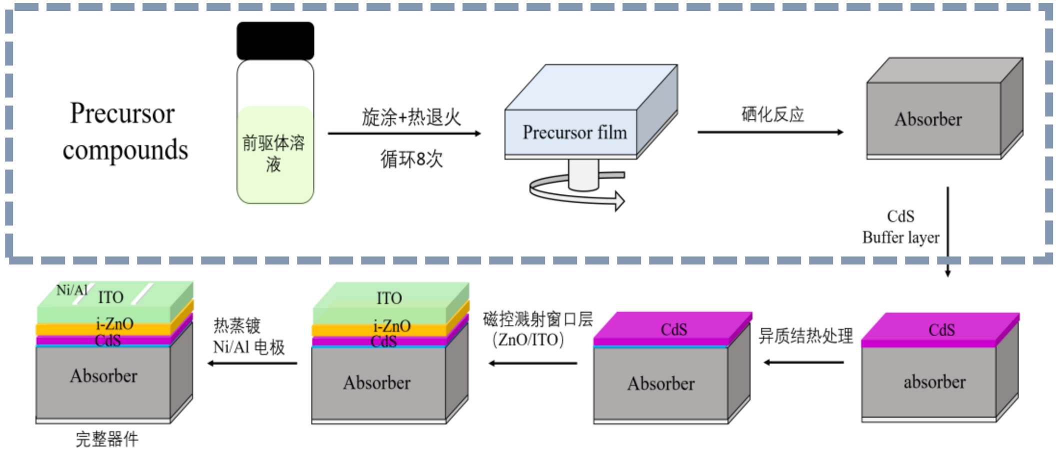

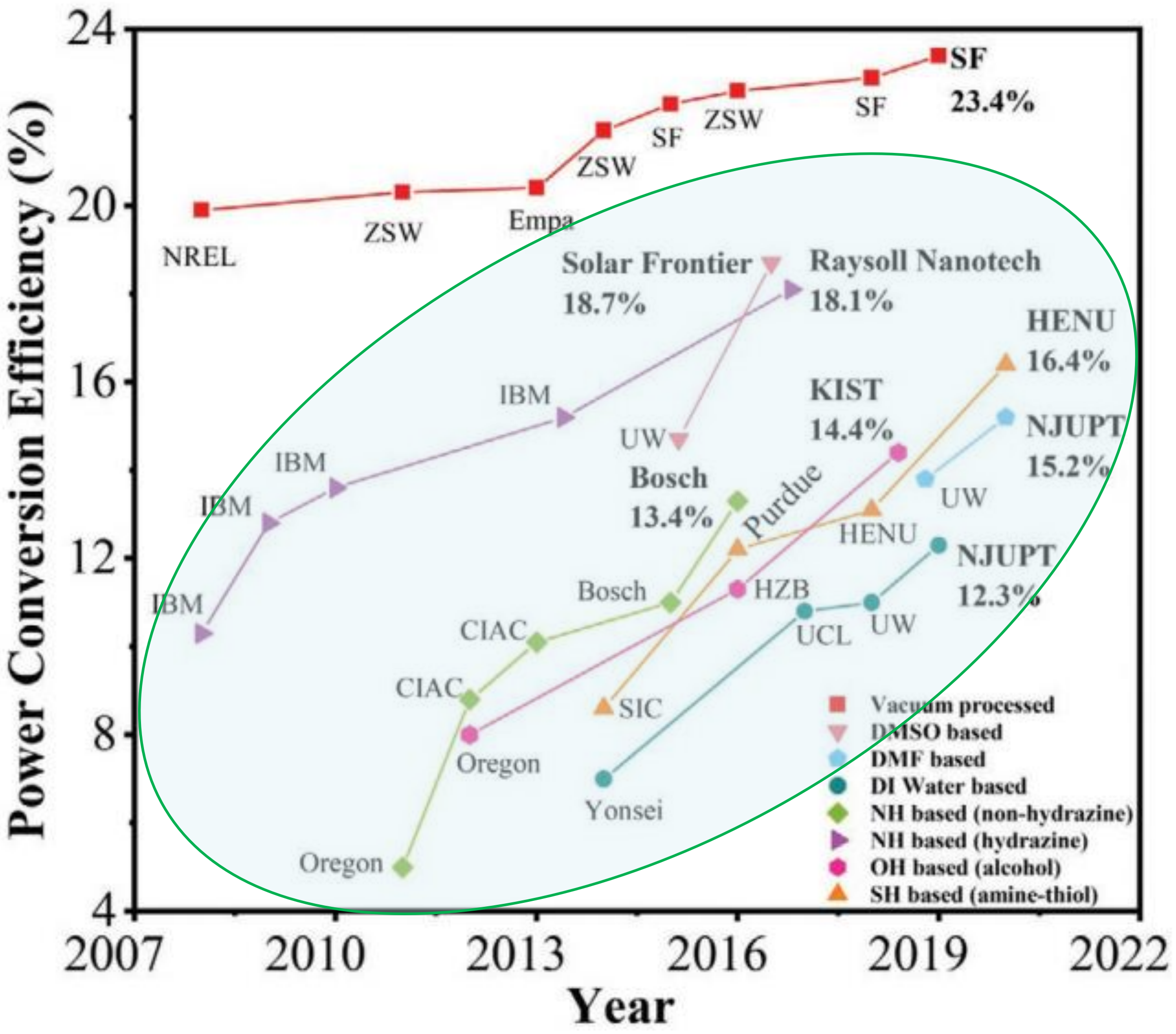

S. Suresh and A. R. Uhl, Adv. Energy Mater. 2021, 2003743

Solution Processed CIS/CIGS

Hydrazine

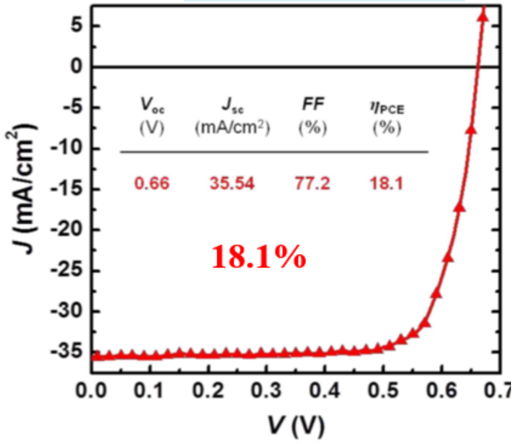

Qian, et al. *Energy Environ. Sci.*, 2016, 9, 3674.

Alcohol

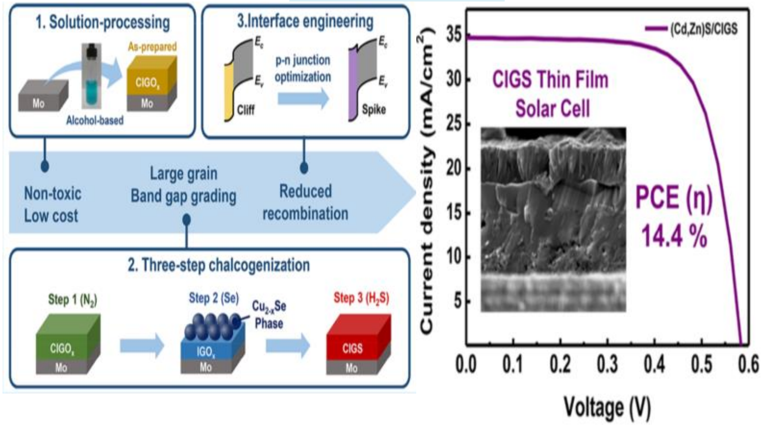

Min, et al. *ACS, AMI*, 2018, 10, 9894.

Amine-thiol

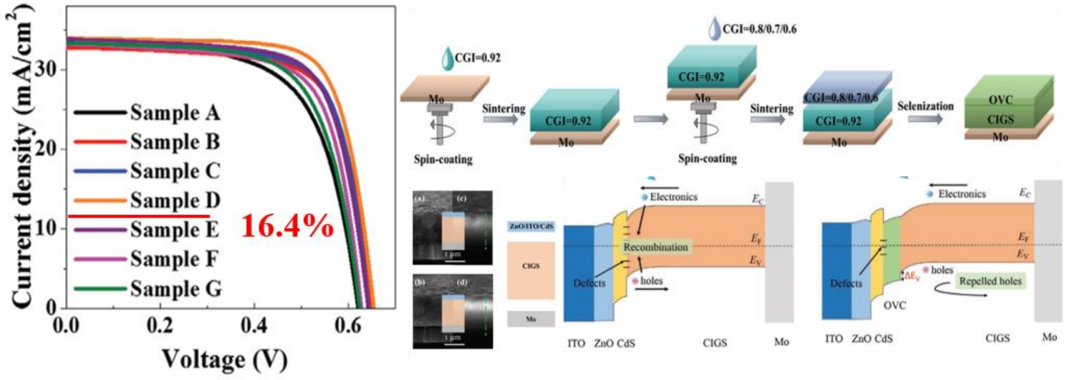

Zhao and Wu, et al. *Adv. Funct. Mater.*, 2020, 31, 2007928.

DMSO

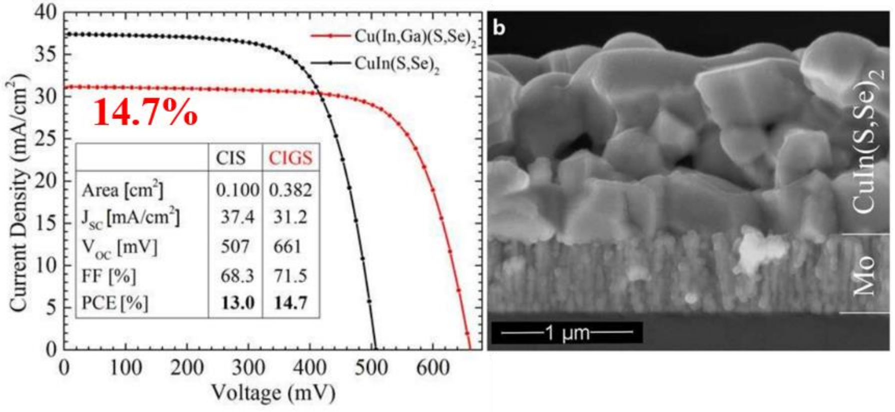

Hillhouse, et al. *Adv. Energy Mater.* 2018, 8, 1801254

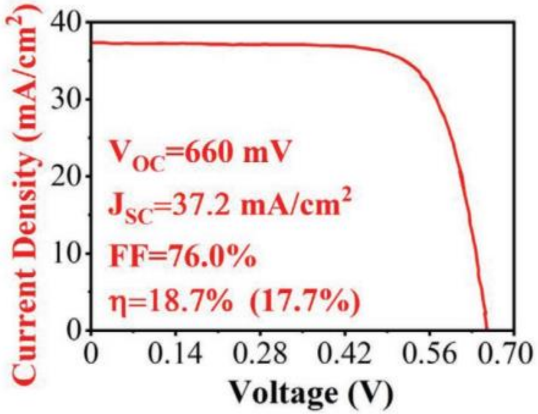

Tetsuya Aramoto, et al. *32nd Eur. Photovoltaic Sol. Energy Conf. and Exhibition*, 2016.

DMF

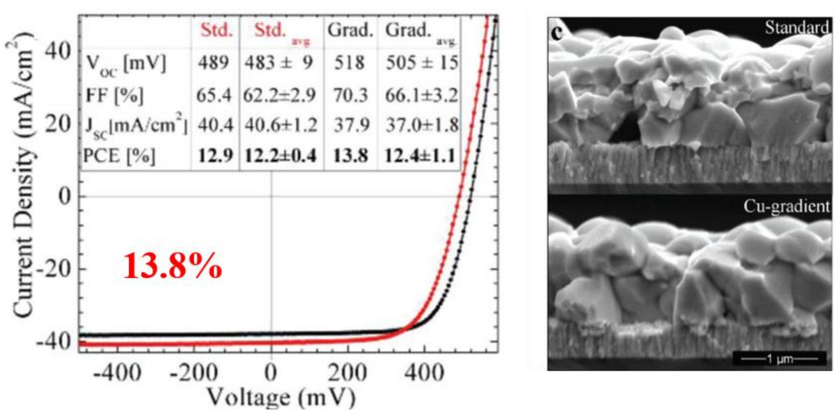

Hillhouse, et al. *Adv. Energy Mater.* 2018, 8, 1801254

Three Examples of Solution Processed CIGS Solar Cells

DMF Solution

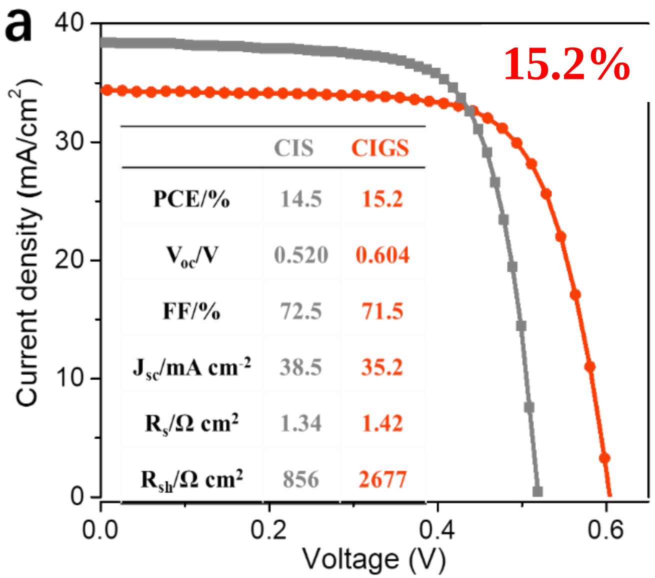

Solar RRL 2018.
Nano Energy 2020.

H_2O Solution

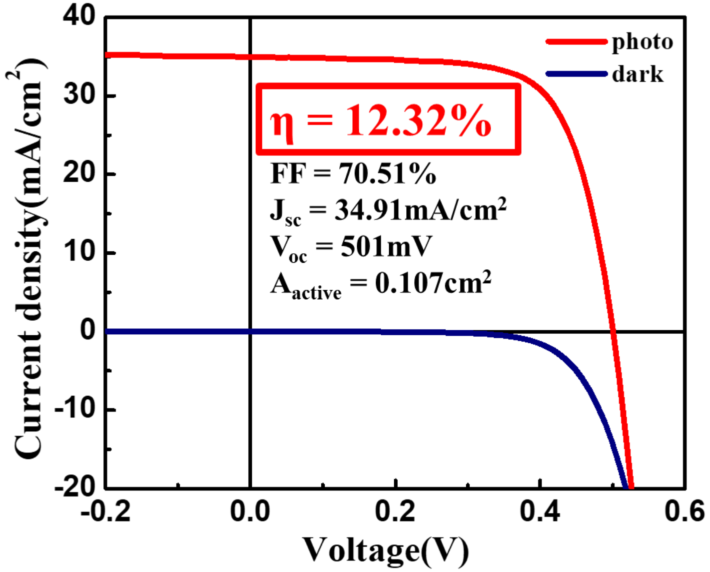

Nano Energy 2019.
Adv. Energy Sustainability Res. 2022.

NMP Solution

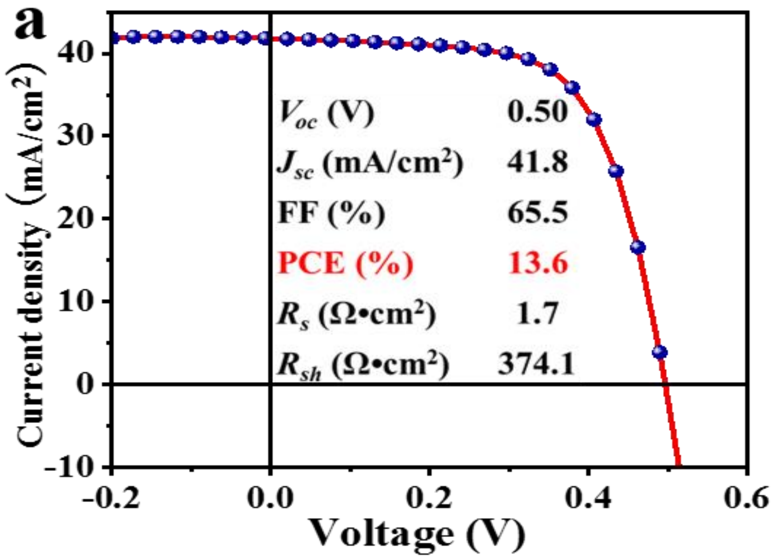

Solar RRL 2019.
Solar Energy 2021.
Adv. Energy Mater. 2022.

2.1 DMF溶液：硒化氛围压力影响

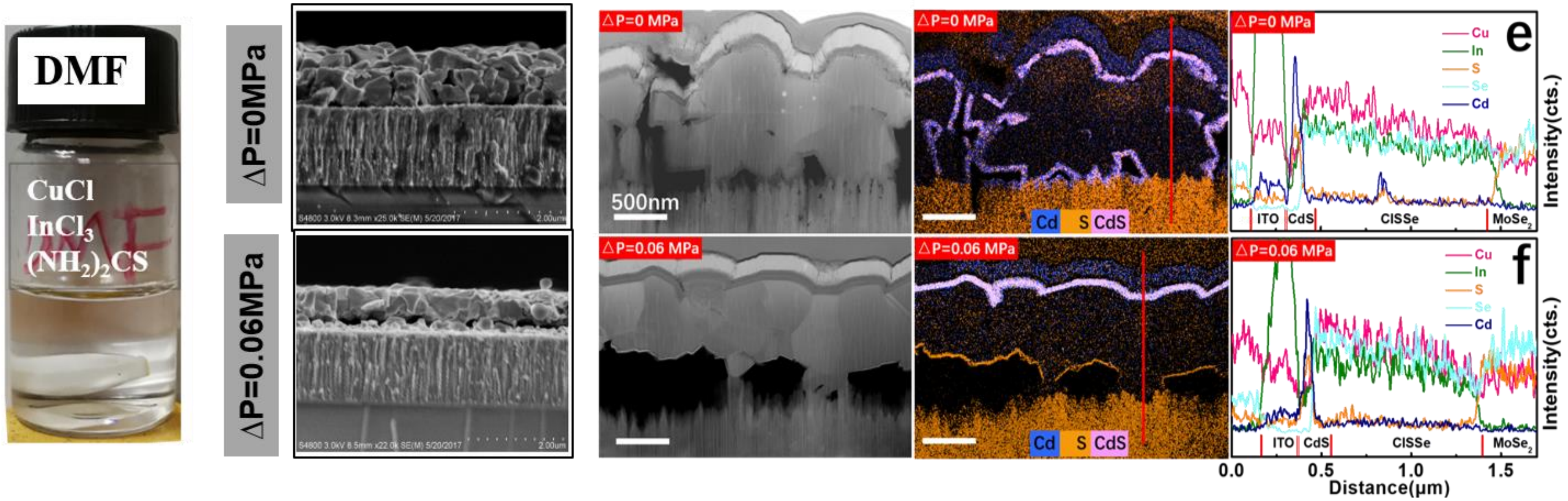

ΔP=0 MPa: loose grains, CdS into the film, Cu-rich near surface

ΔP=0.06 MPa: dense top grains, CdS only on surface, uniform composition

Cu/In=0.85, no etching treatment

- Dissolve all precursors at room temperature.
- Long-time stability
- PCE=10.3%

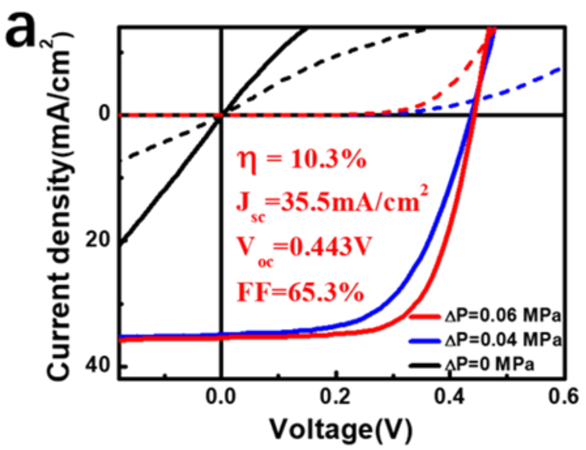

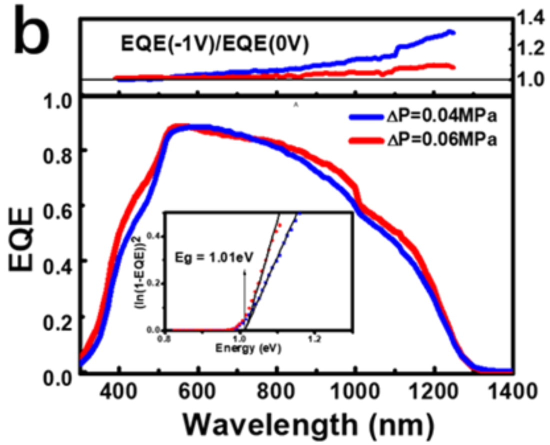

Solar RRL, 2018,1800044.

2.2 DMF溶液：Cu-rich 吸收层

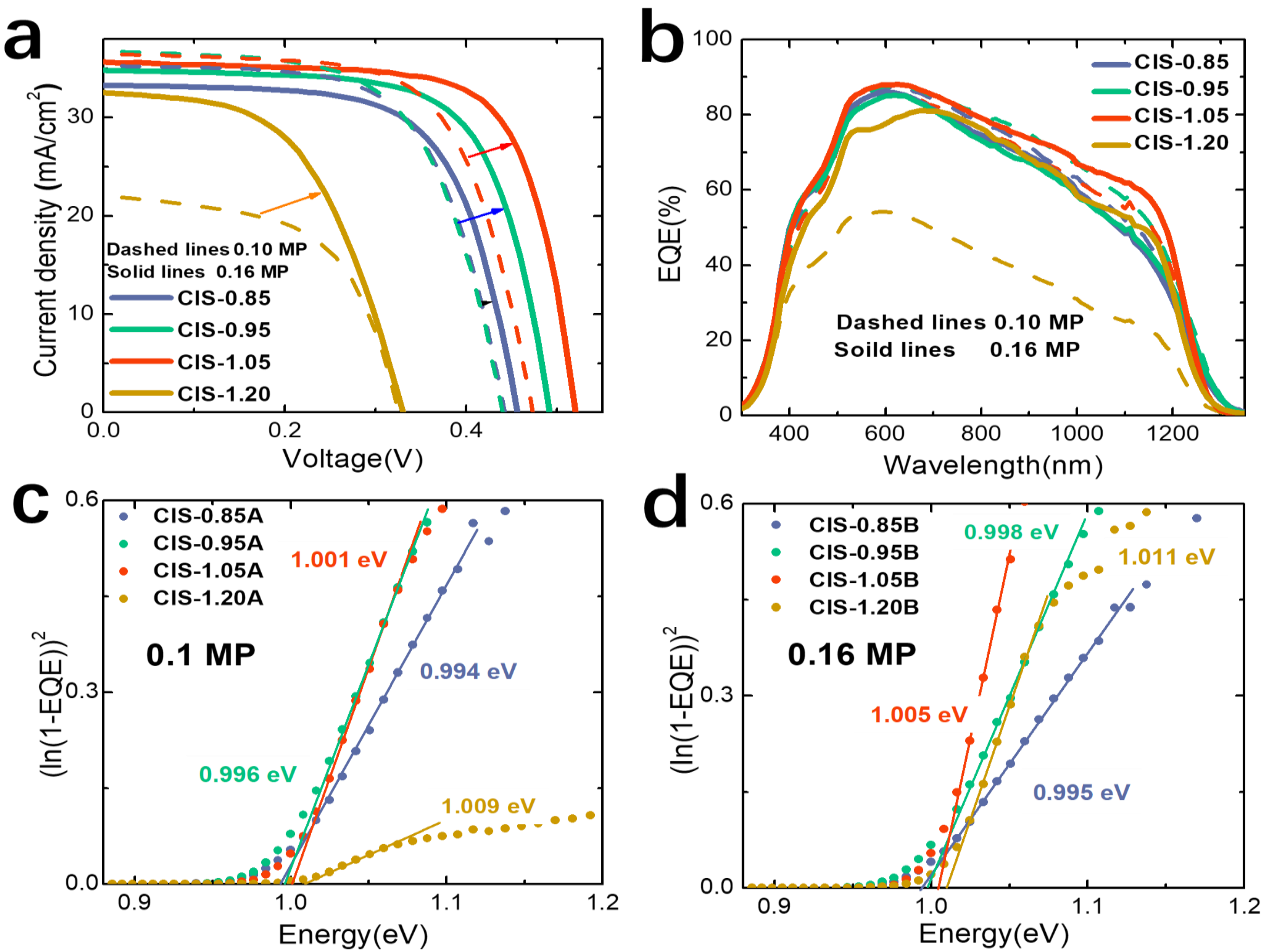

- 常压：Cu/In=1.05 效率最高 PCE=11.3%
- 加压：Cu/In=1.05 效率最高 PCE=13.3%

Cu-poor (Cu/(In+Ga)<0.9)

- State-of-the-art composition
- Avoid $Cu_{2-x}Se$ impurity
  (KCN etching is still needed)
- Order-defect-compound (ODC) layer

Cu-rich

- Lower defect
- Potentially High V_{oc}
- $Cu_{2-x}Se$ impurity
- High performance not achieved yet

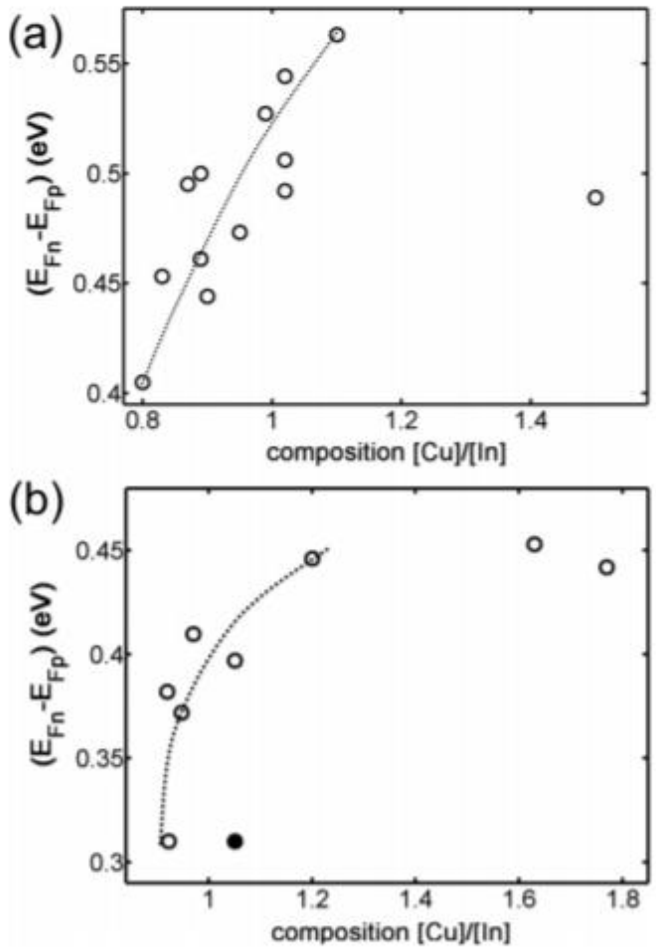

FIG. 1. Splitting of the quasi-Fermi levels as a function of the composition for the epitaxial (a) and the polycrystalline (b) sample series; the lines are a guide to the eye.

S. Siebentritt. et al, *Sol. Energy Mater. Sol. Cells*, 2013.

薄膜形貌表征

ΔP=0 MPa

ΔP=0.06 MPa

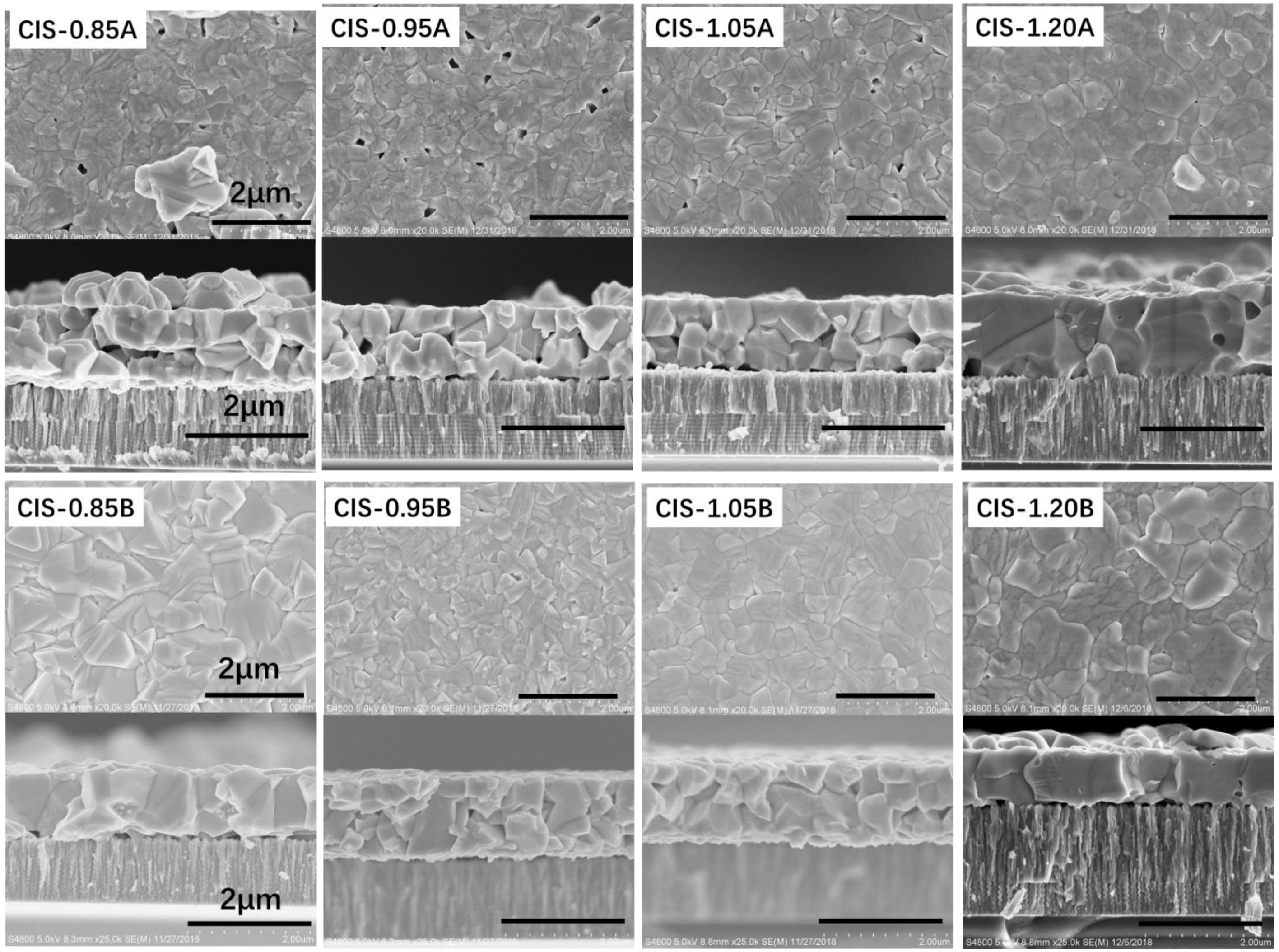

常压：晶粒排布松散　　　　加压：晶粒排布致密

With $(NH_4)_2S$ etching, $Cu_{2-x}Se$ on surface can be removed

ΔP=0 MPa

ΔP=0.06 MPa

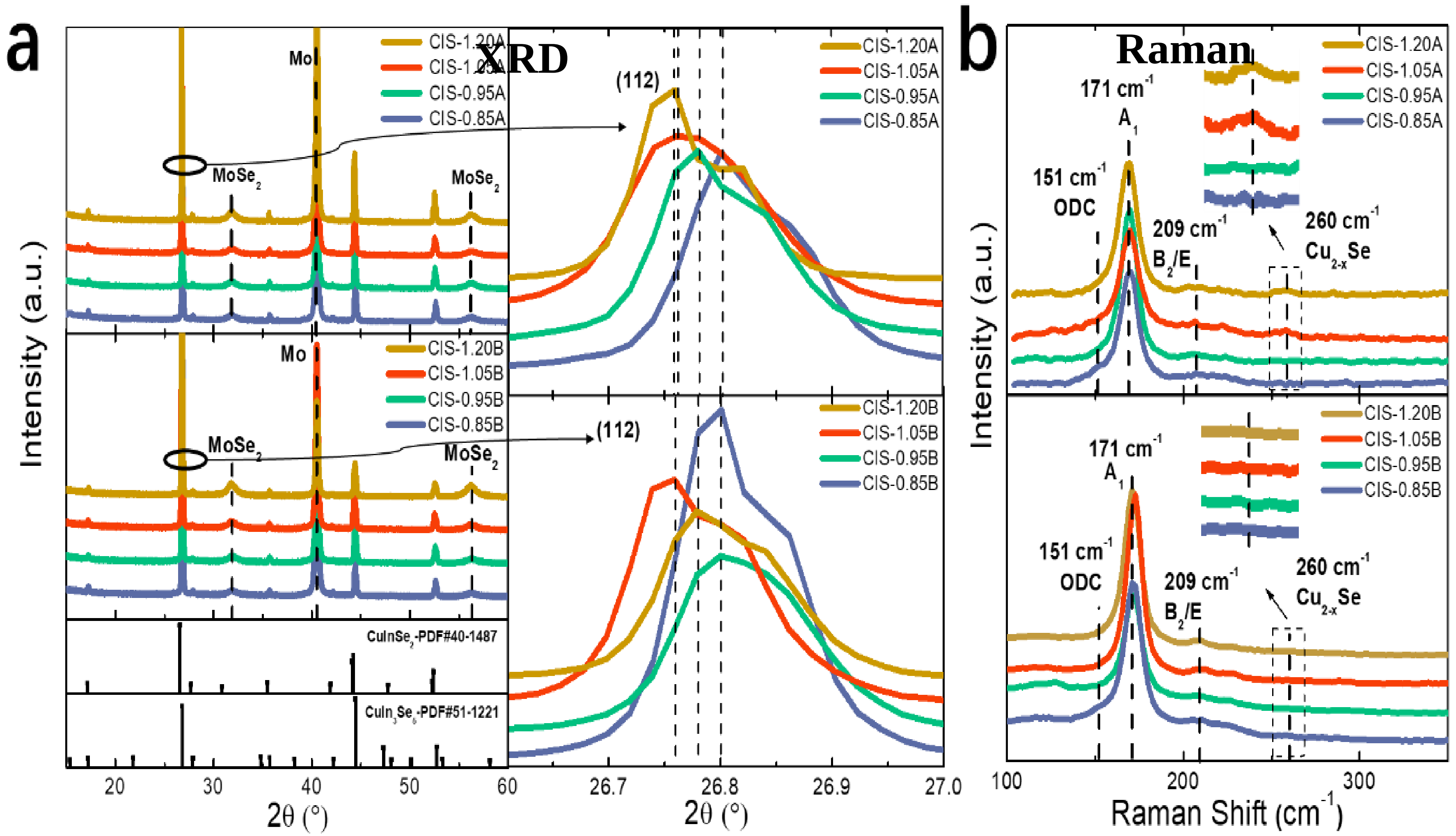

$Cu_{2-x}Se$ exits in Cu-rich films

$Cu_{2-x}Se$ free

Nano Energy, 2020,104438.

Cu-rich CIS: Optoelectronic Properties

GDEOS

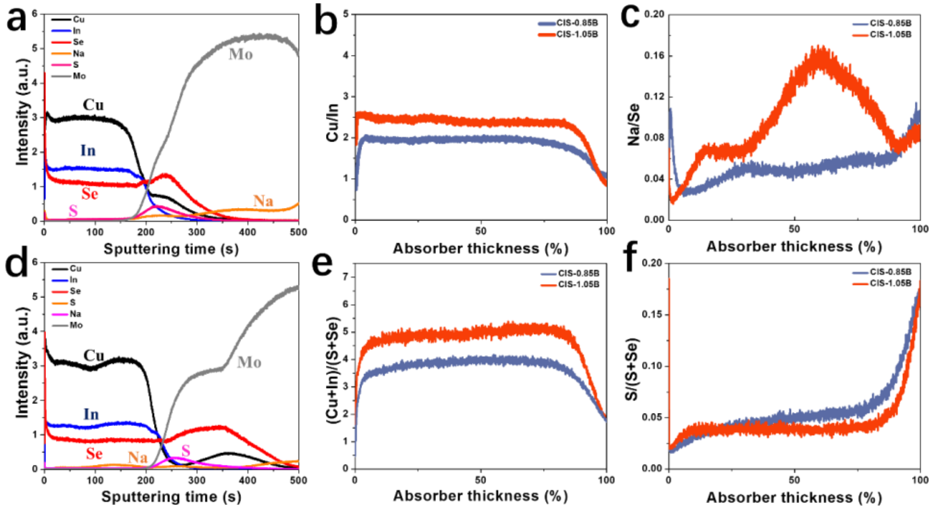

c-AFM

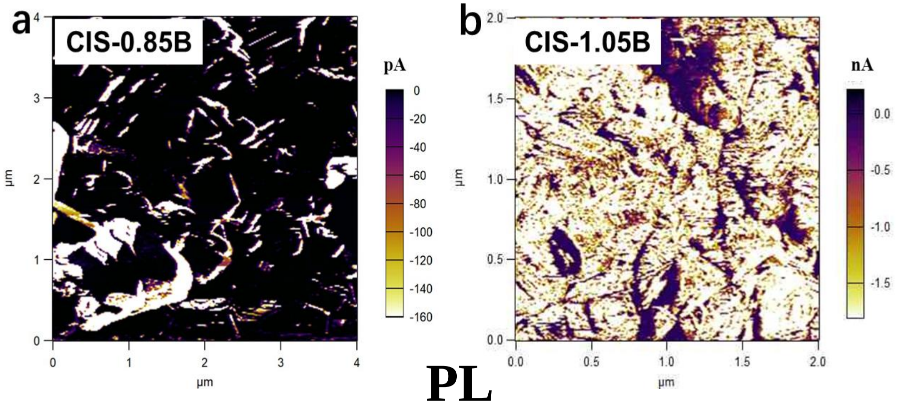

PL

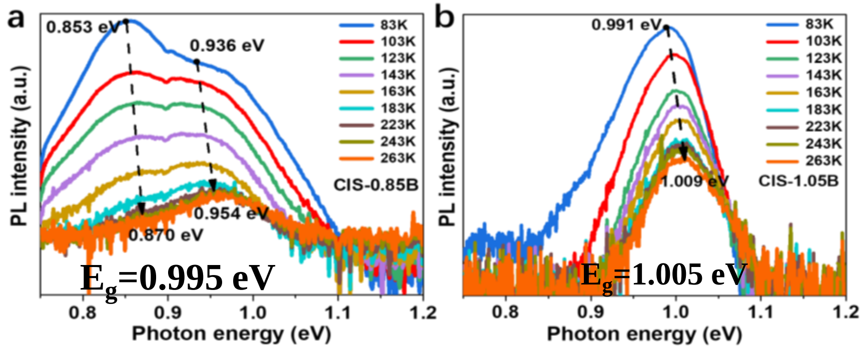

TEM

EDX

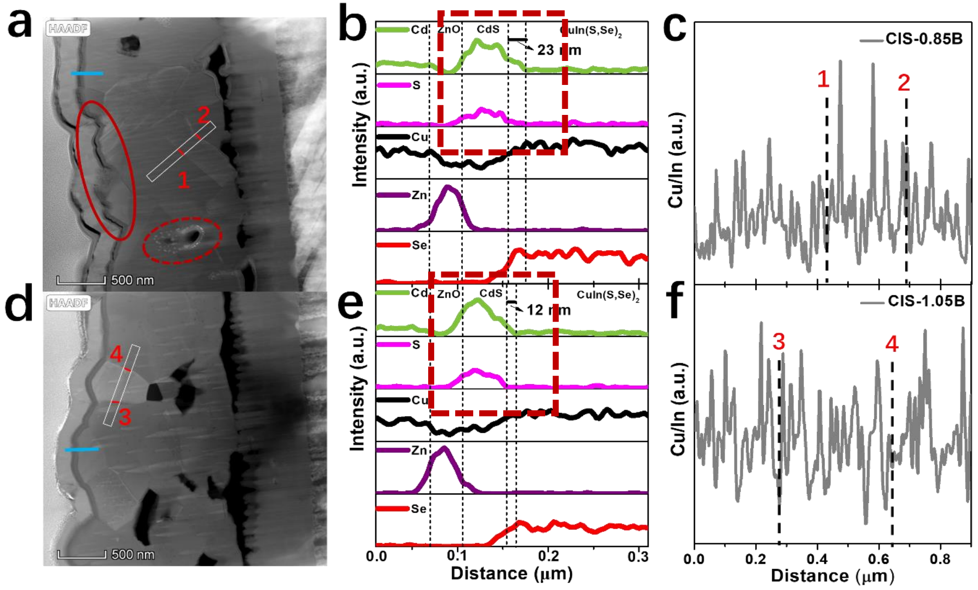

- Cu-rich composition
- Shorter Cd diffusion into absorber
- Epitaxial like interface
- Higher and more uniform conductivity
- Higher PL peak position

Nano Energy, 2020,104438.

Cu-rich Absorber：Band Tailing

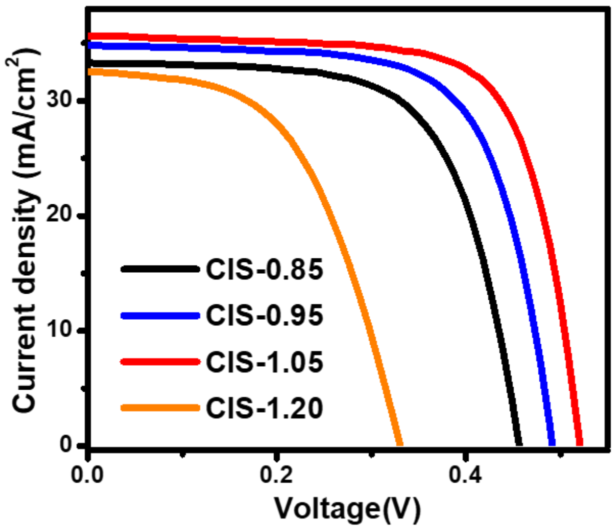

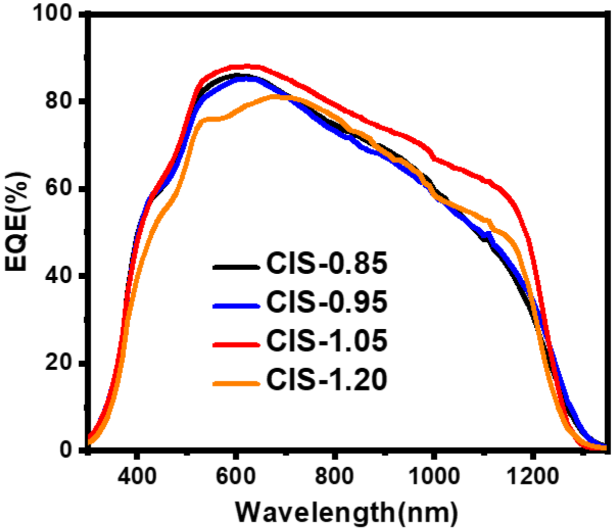

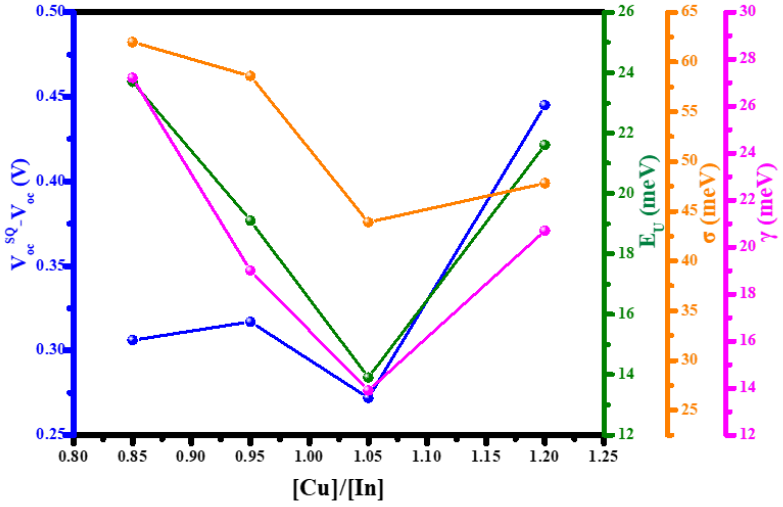

Device	Cu/In	E_g(eV)	J_{sc}(mA/cm^2)	V_{oc}(V)	FF (%)	PCE_{ave}	PCE_{max}	E_U(meV)	σ_g (meV)	Γ_{opt}(meV)	J_0(mA·cm^{-2})	*n*	R_s(Ω cm^2)	R_{sh}(Ω cm^2)
CIS-0.85	0.85	0.995	33.46±1.33	0.453±0.002	65.27±0.64	9.89±0.34	9.96	23.7	62.0	27.2	6.57×10^{-7}	1.58	1.7±0.1	458±274
CIS-0.95	0.95	0.998	34.07±1.78	0.477±0.013	65.56±2.17	10.65±0.60	11.66	19.1	58.6	19.0	1.76×10^{-7}	1.41	1.7±0.1	1357±236
CIS-1.05	1.05	1.005	34.66±1.46	0.516±0.004	70.50±0.60	12.61±0.80	13.29	13.9	43.9	13.9	5.61×10^{-8}	1.44	1.5±0.1	869±386
CIS-1.20	1.06	1.011	29.42±2.33	0.324±0.008	51.06±1.98	4.87±0.59	5.62	21.6	47.8	20.7	8.63×10^{-5}	1.60	3.1±0.6	663±631

Unpublished data.

Champion Cu-rich CIS/CIGS Device from DMF Solution

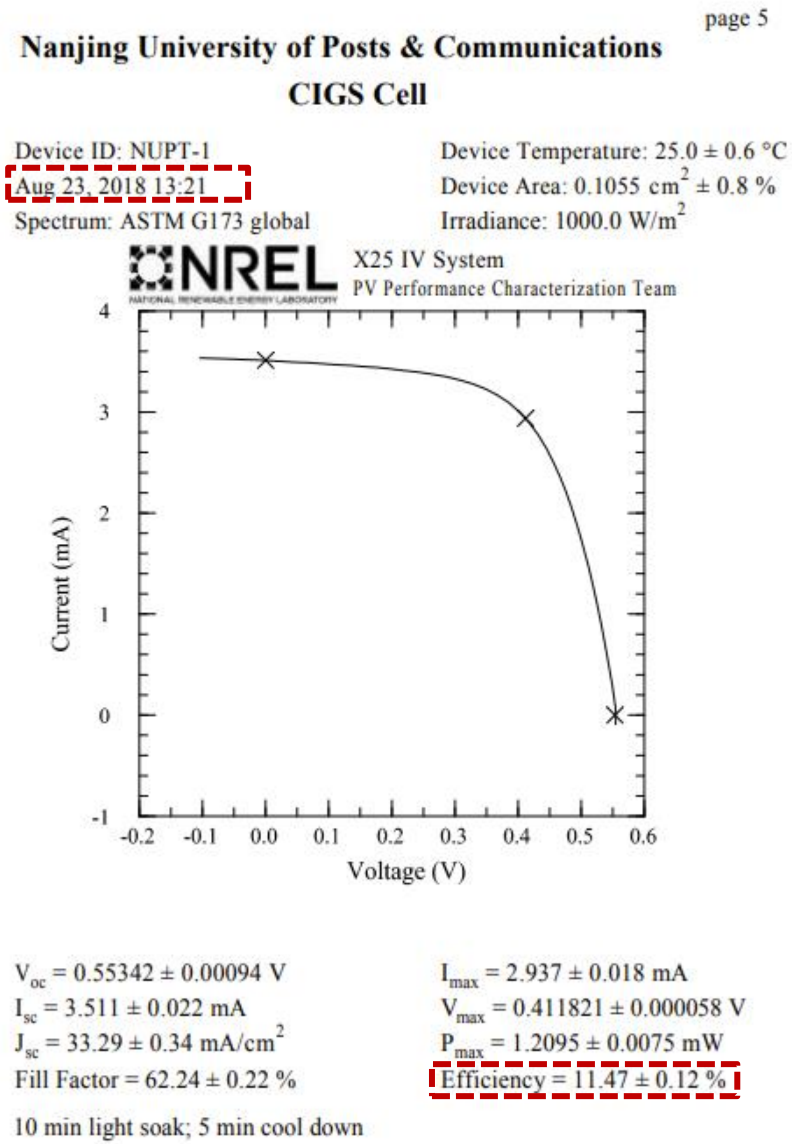
page 5

Nanjing University of Posts & Communications

CIGS Cell

Device ID: NUPT-1
Aug 23, 2018 13:21
Spectrum: ASTM G173 global

Device Temperature: 25.0 ± 0.6 °C
Device Area: 0.1055 cm^2 ± 0.8 %
Irradiance: 1000.0 W/m^2

NREL X25 IV System
PV Performance Characterization Team

V_{oc} = 0.55342 ± 0.00094 V
I_{sc} = 3.511 ± 0.022 mA
J_{sc} = 33.29 ± 0.34 mA/cm^2
Fill Factor = 62.24 ± 0.22 %

I_{max} = 2.937 ± 0.018 mA
V_{max} = 0.411821 ± 0.000058 V
P_{max} = 1.2095 ± 0.0075 mW
Efficiency = 11.47 ± 0.12 %

10 min light soak; 5 min cool down

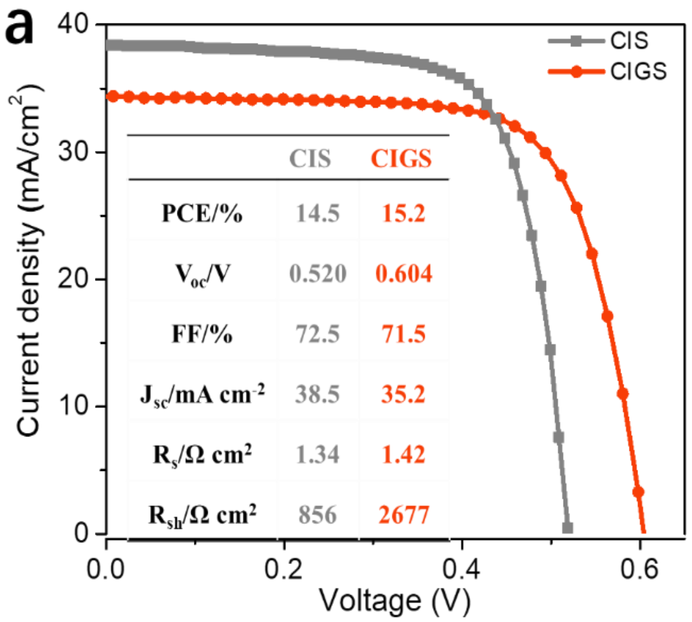

	CIS	CIGS
PCE/%	14.5	15.2
V_{oc}/V	0.520	0.604
FF/%	72.5	71.5
J_{sc}/mA cm^{-2}	38.5	35.2
R_s/Ω cm^2	1.34	1.42
R_{sh}/Ω cm^2	856	2677

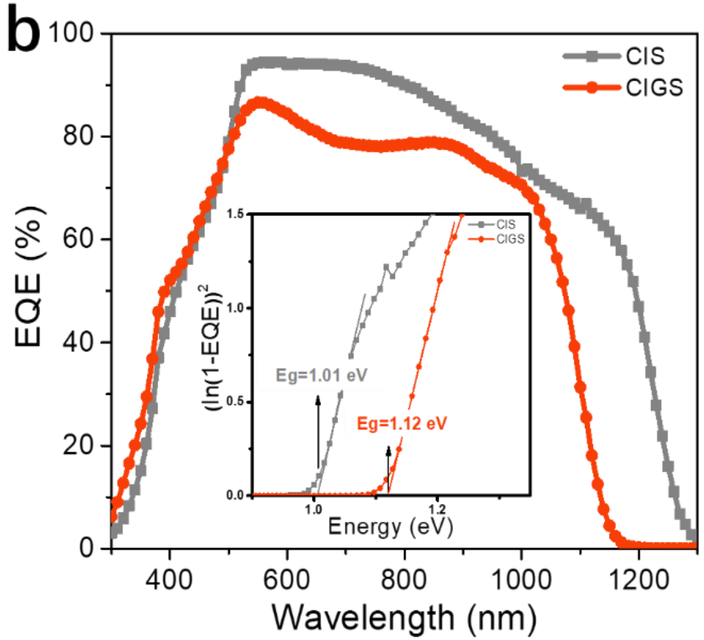

PCE=14.5%
V_{oc}=520 mV
J_{sc}=38.5 mA/cm^2
FF=72.5%
$V_{oc,def}$=0.235V
V_{oc}/V_{oc}^{SQ}=67%

PCE=15.2%
V_{oc}=604 mV
J_{sc}=35.2 mA/cm^2
FF=71.51%
$V_{oc,def}$=0.273 V
V_{oc}/V_{oc}^{SQ}=69%

Nano Energy, 2020,104438.

2. 3 水溶液：配合物前驱体的使用

- **Challenges: Hydrolysis, Impurities originating from starting materials, Oxidation**

12.3% CIS

$Cu(TU)_3Cl$

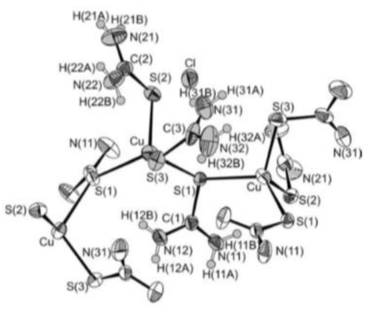

P. Bombicz et al. Inorg.Chim. Acta 357 (2004) 513.

$In(TU)_3Cl$

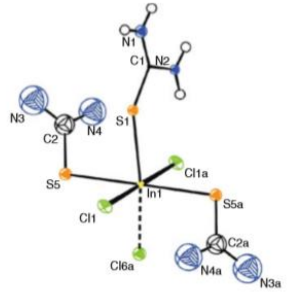

J Therm Anal Calorim (2011) 83.

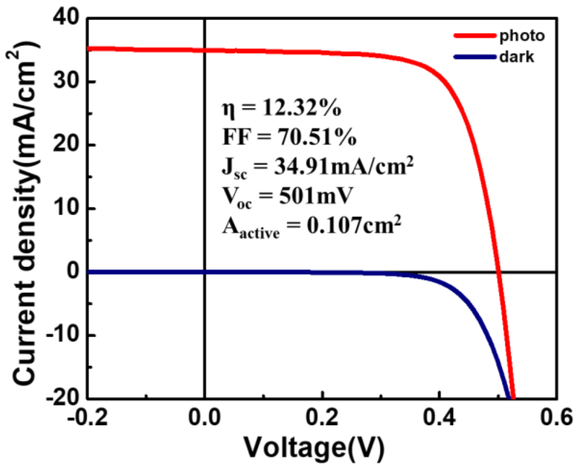

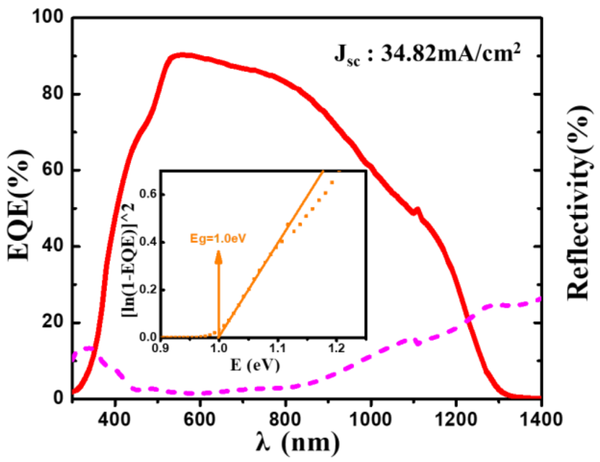

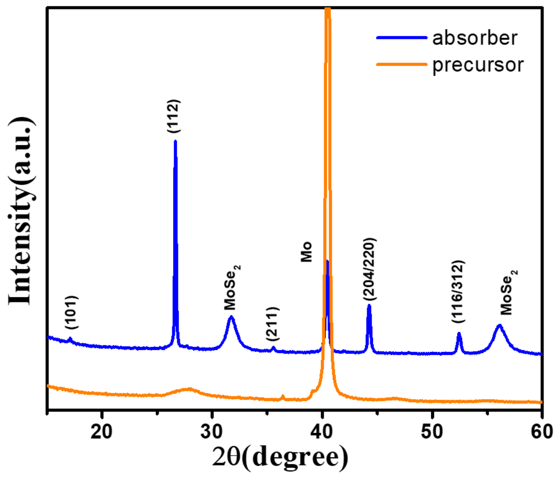

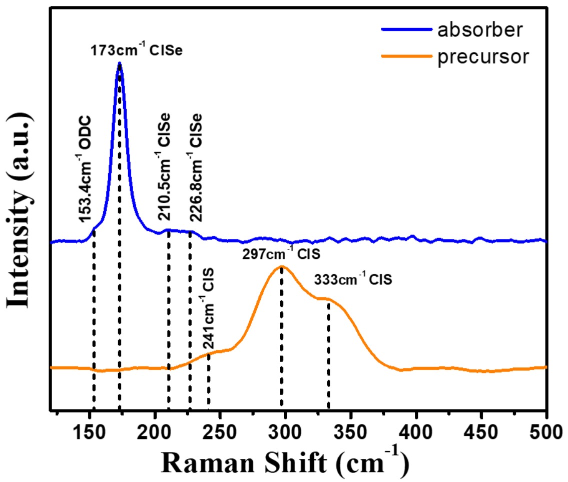

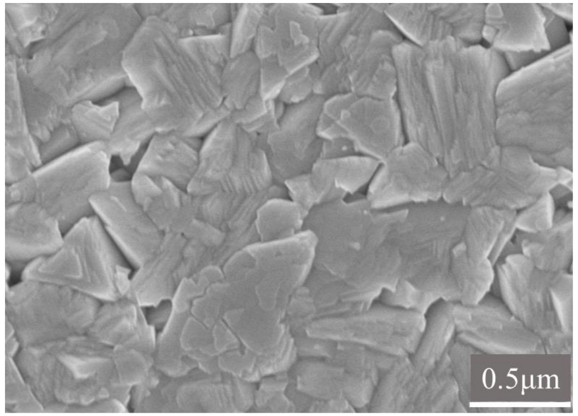

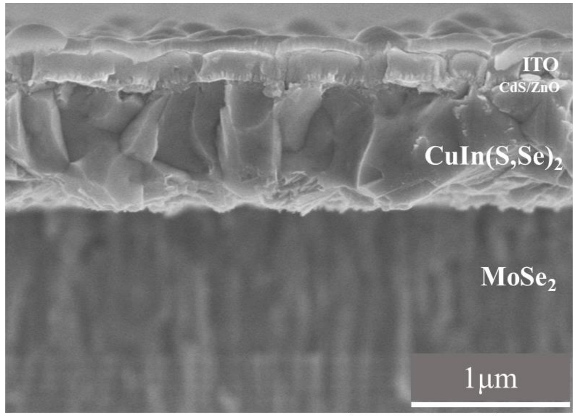

Nano Energy, 2019, 818.

Chemistry in Aqueous Solution

All the solutions prepared by mixing TU and $InCl_3$ became unclear.

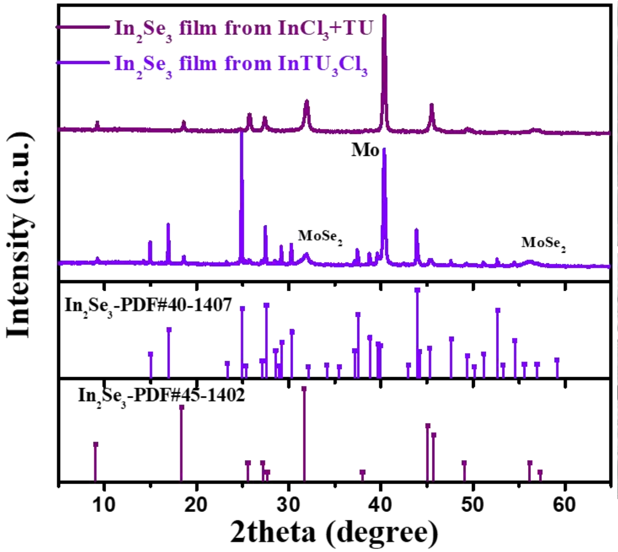

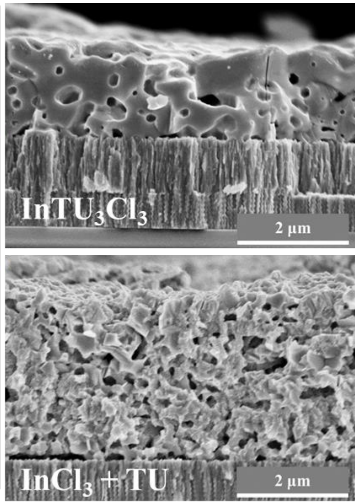

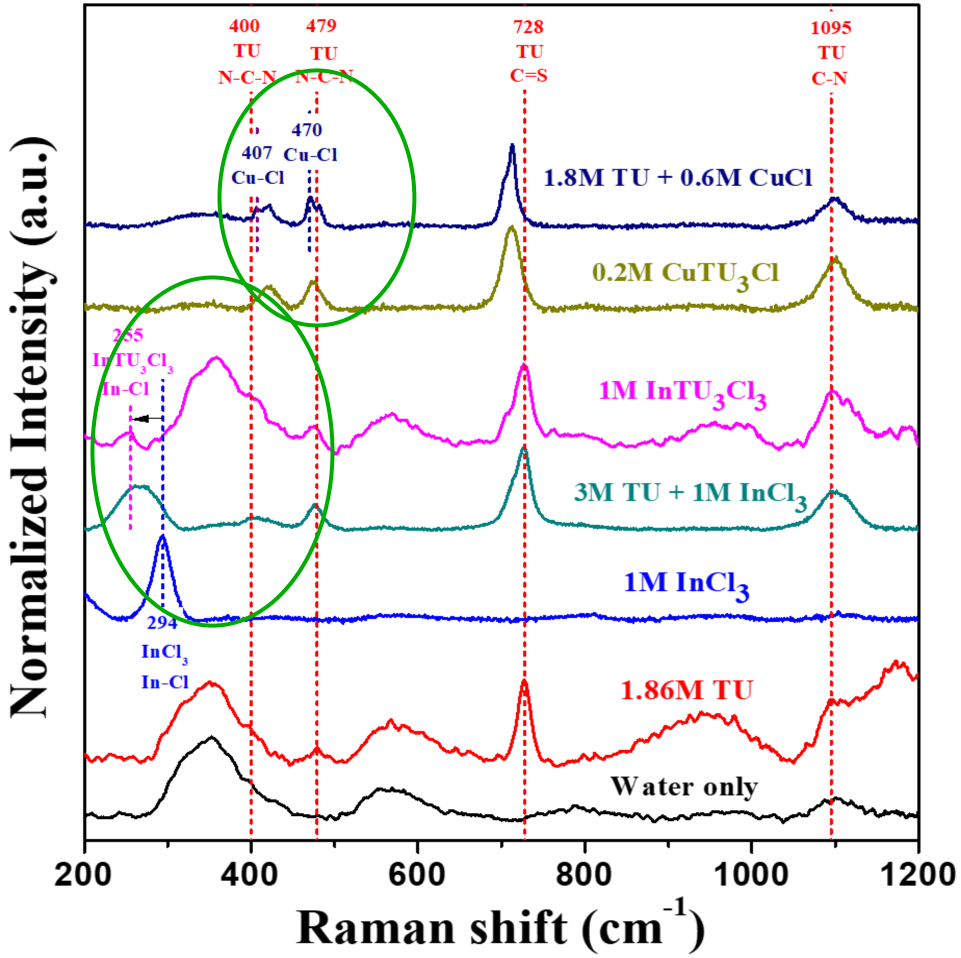

The direct bonding of all metal ions with sulfur in the precursor solution is the key for high quality absorber film.

Nano Energy, 2019, 818.

2.3 NMP溶液：空气与惰性氛围退火

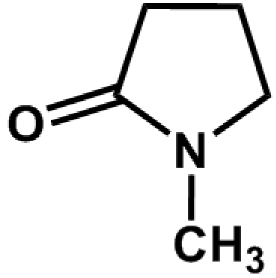

- 安全、低毒、环境友好
- 来源广、成本低
- 各行业广泛应用
- 溶液稳定，可长期保存
- 在薄膜中残留较少或无残留

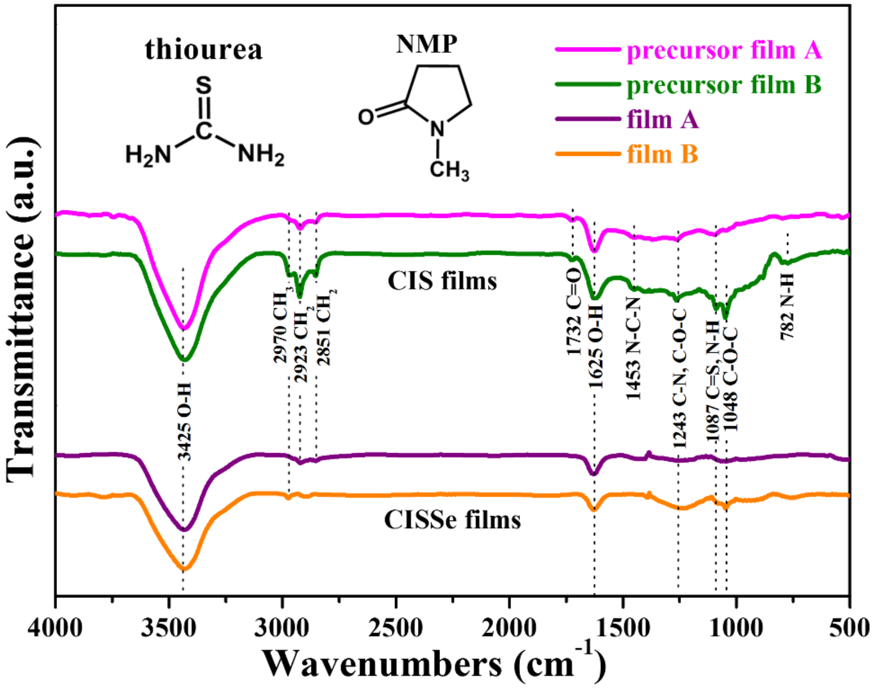

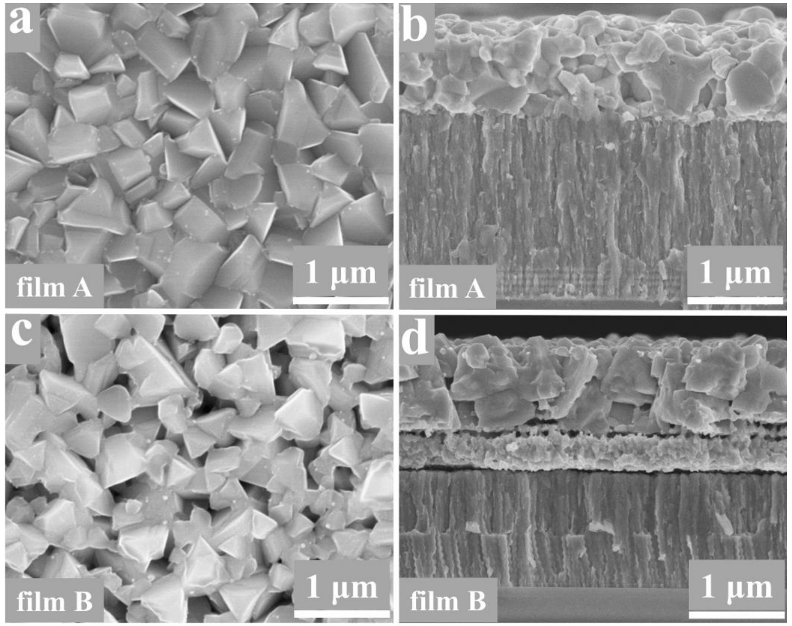

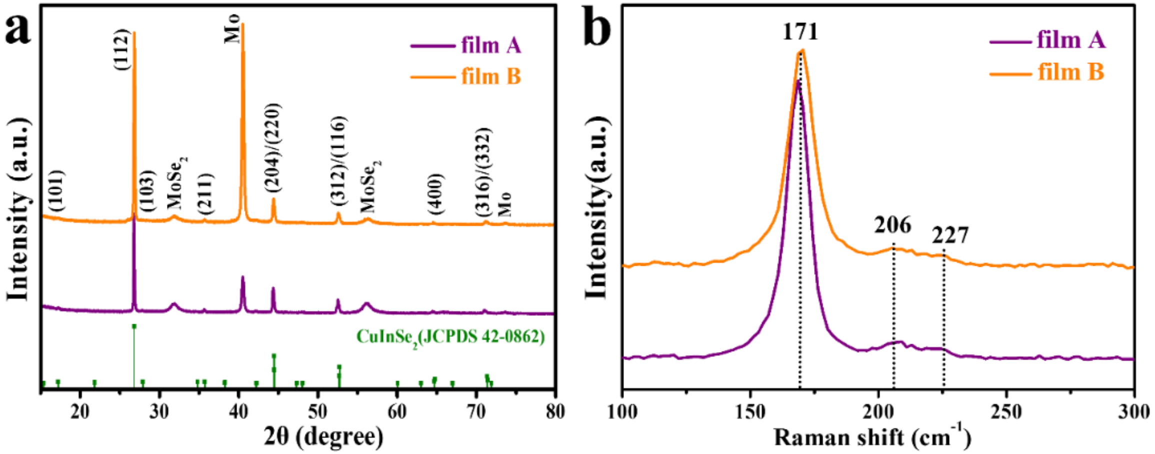

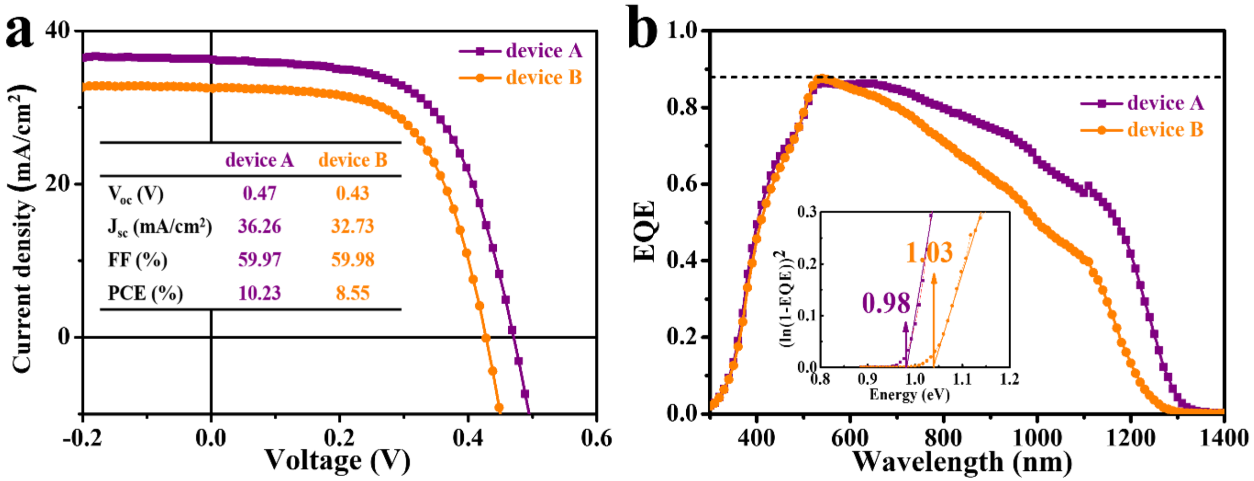

Solar RRL, **2019**, 3, 1900052.

Vacuum Based CIGS: Grain Growth Mechanism

Three-step evaporation: liquid $Cu_{2-x}S$ assisted grain growth

CIS

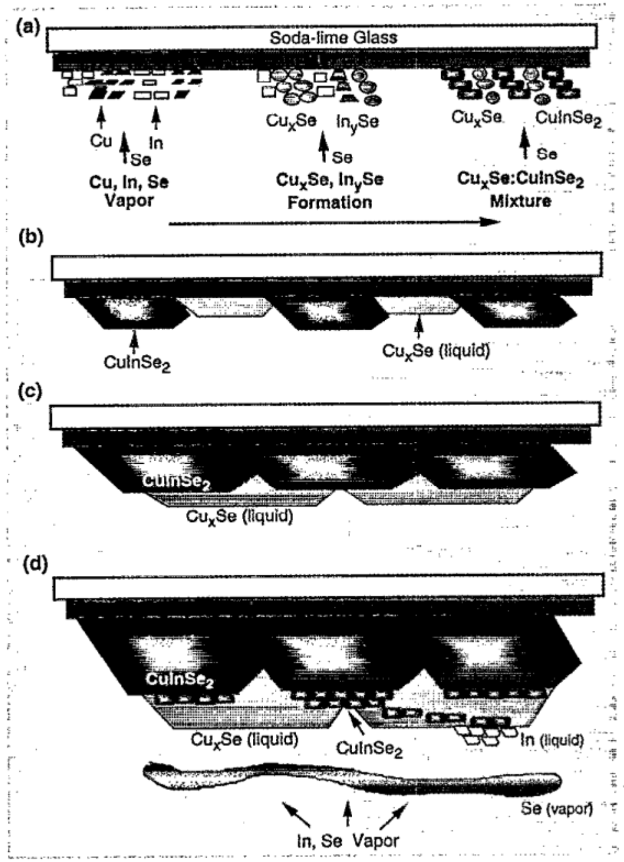

FIG. 11. Pictorial representation of thin-film $CuInSe_2$ growth model: (a) Initial atomistic accommodation, reaction, and nucleation, (b) $CuInSe_2$ and Cu_xSe island formation, (3) $CuInSe_2$ coalescence with vertical phase separation, and (4) Cu_xSe conversion and local epitaxial growth.

J. R. Tuttle, et al., J. Appl. Phys., 1995, 77, 153.

$$Cu_{2-x}Se + (In,Ga)_2Se_3 \rightarrow Cu(In,Ga)Se_2$$

Large grain
Cu-poor composition
KCN etching

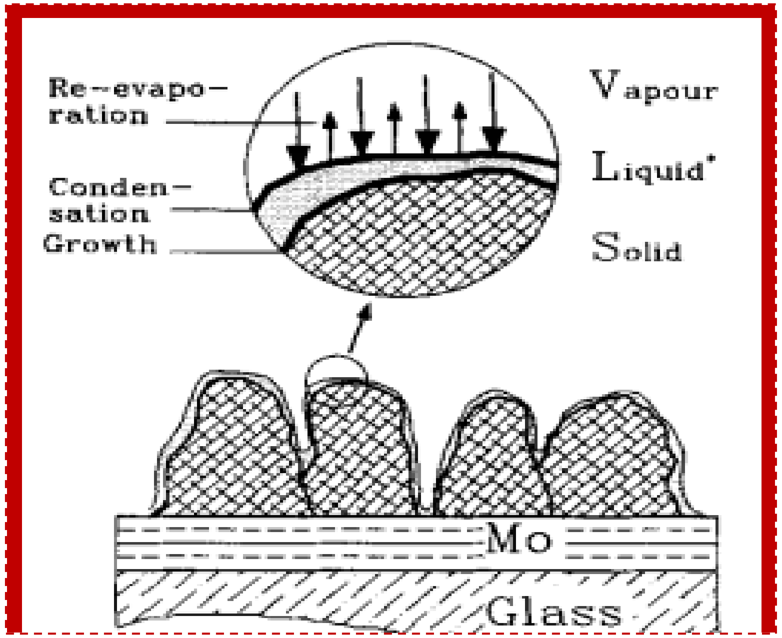

R. Klenk, et al., *Adv. Mater.*, 1993, 5, 114.

CIGS

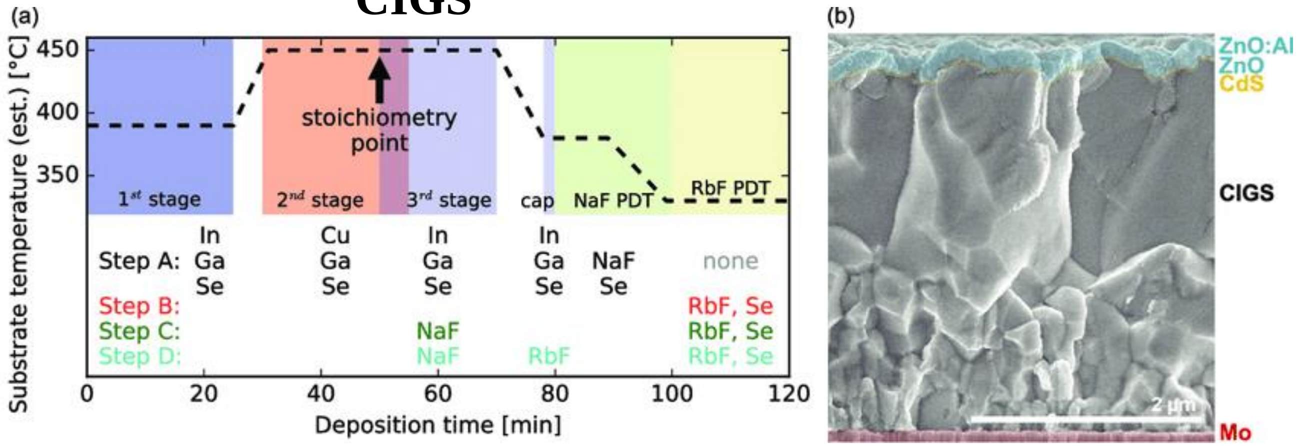

R. Carron, Adv. Energy Mater. 2019, 9, 1900408.

3.溶液法CIS/CIGS晶粒生长机制

$Cu(Tu)Cl_3 + In(TU)_3Cl \rightarrow CuInS_2$ (precursor film)

Cu-rich absorber (CGI = ~1) better performance

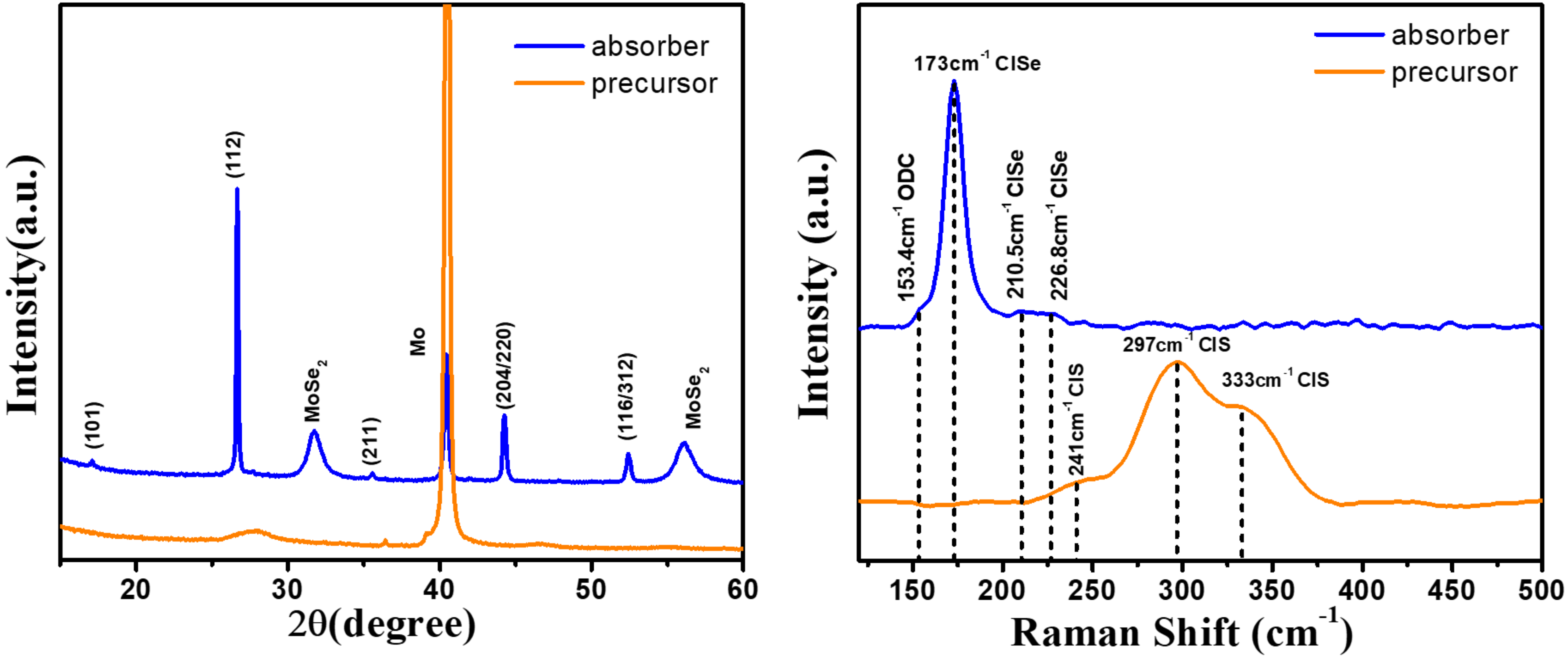

Grain Growth of Solution Processed CIS absorber

Selenization profile

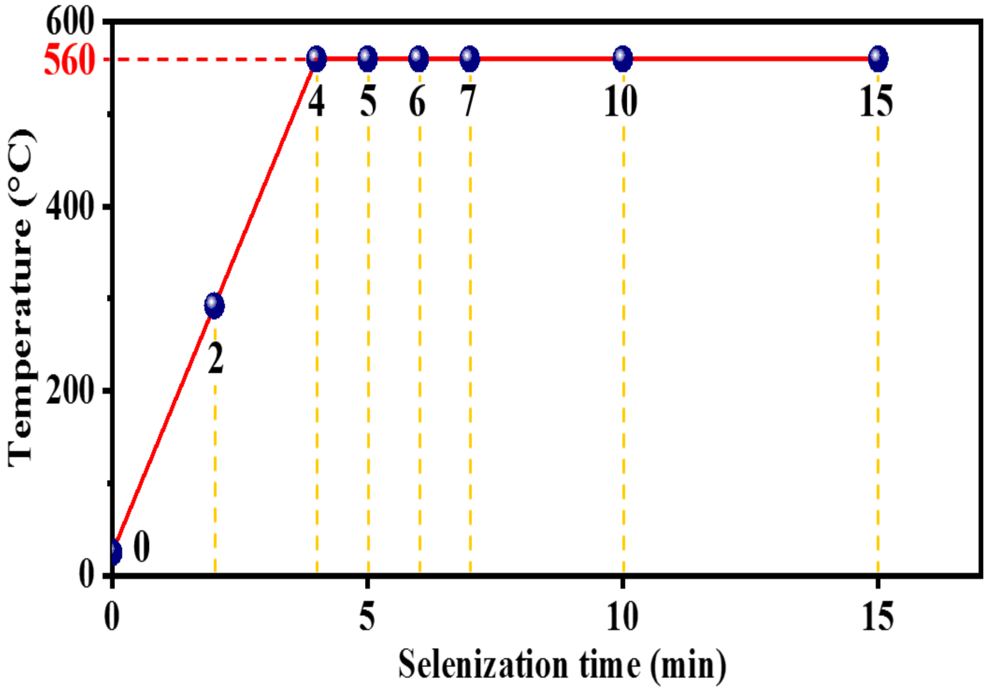

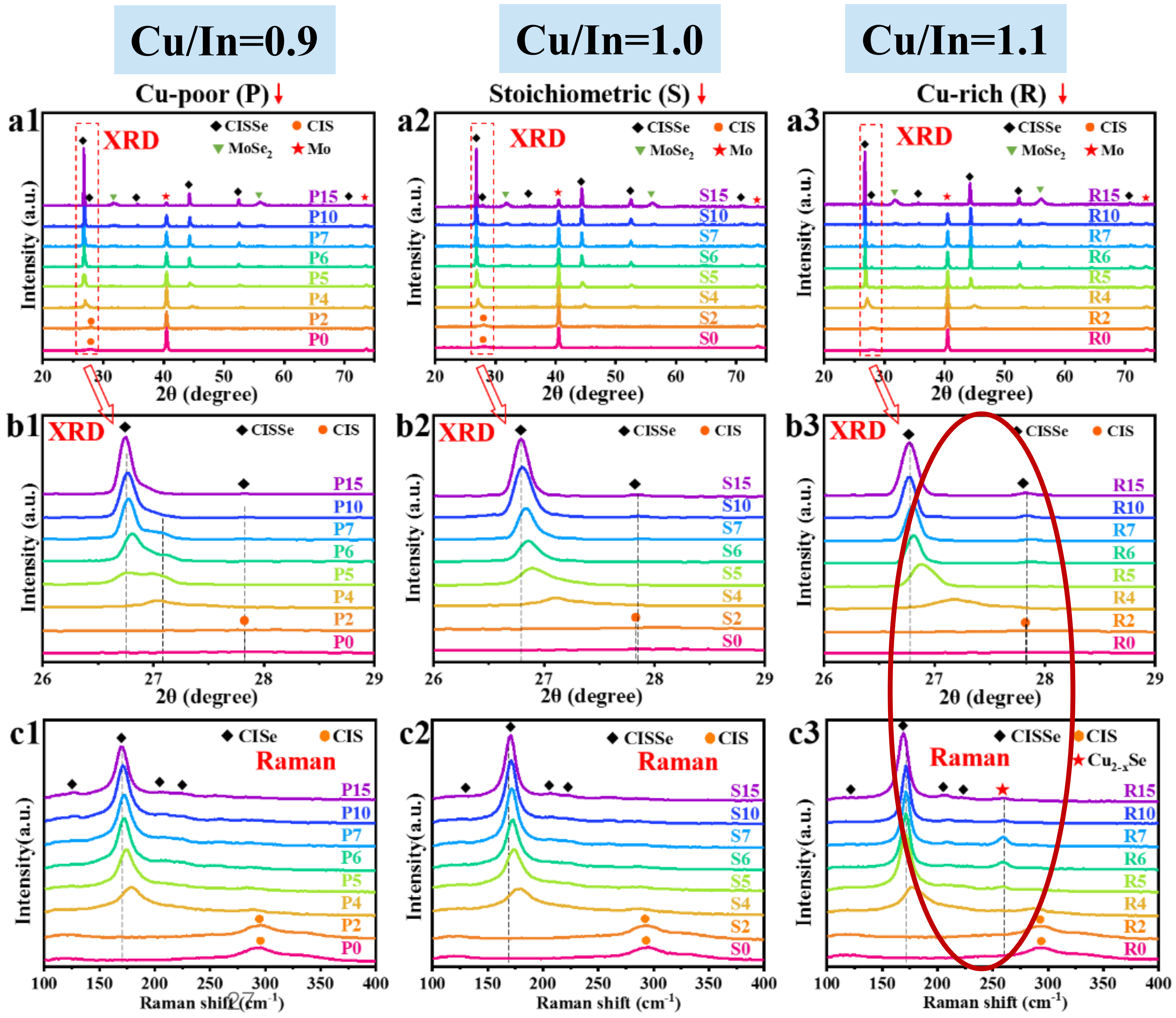

- ➢ $CuInS_2$+Se → $CuIn(S,Se)_2$
- ➢ 贫铜、化学计量比均无Cu_{2-x}Se
- ➢ 富铜存在Cu_{2-x}Se

Grain Growth of Solution Processed CIS absorber

Cu/In=0.9

Cu/In=1.0

Cu/In=1.1

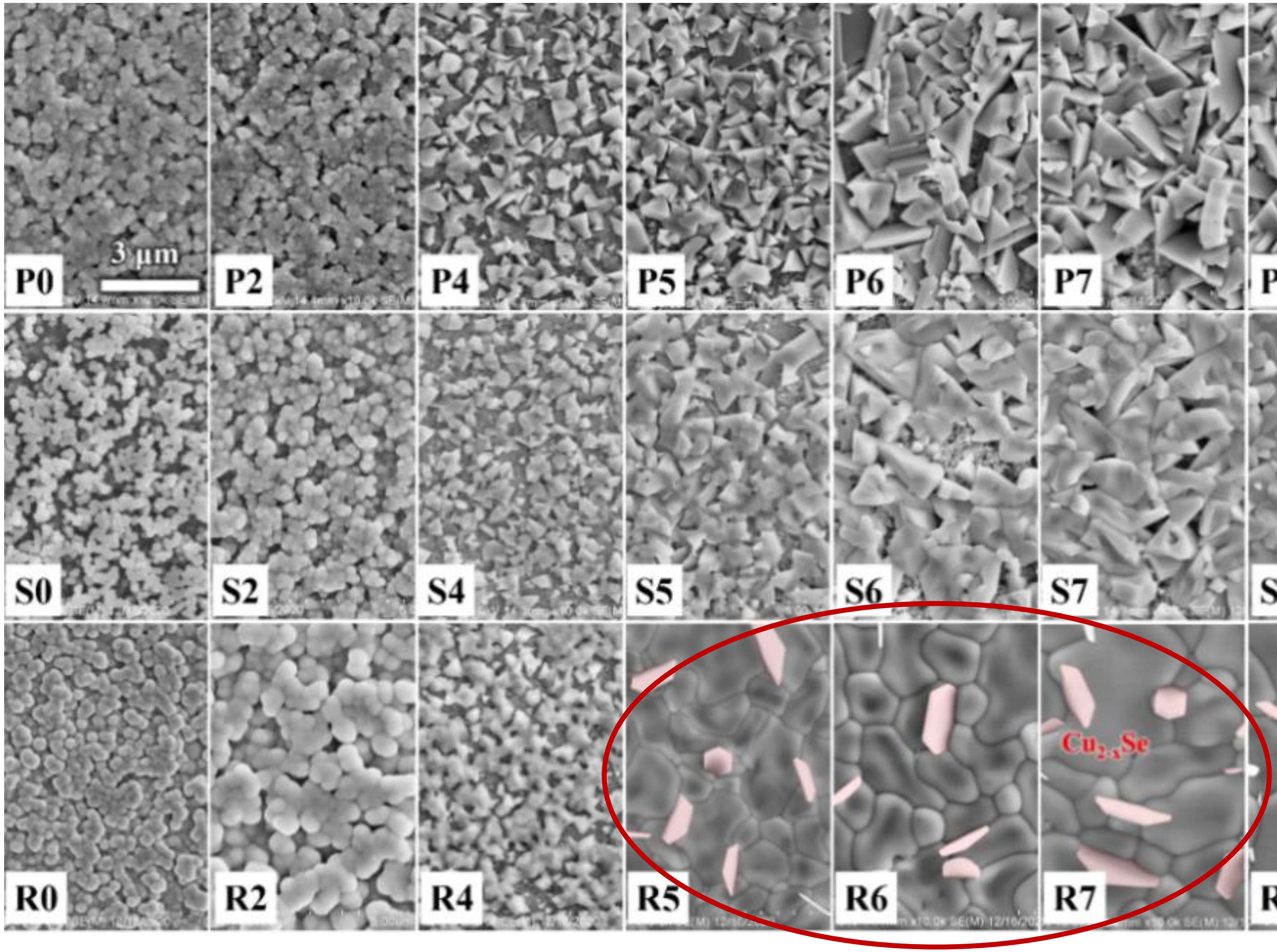

Grain Growth of Solution Processed CIS absorber

Cu/In=0.9

Cu/In=1.0

Cu/In=1.1

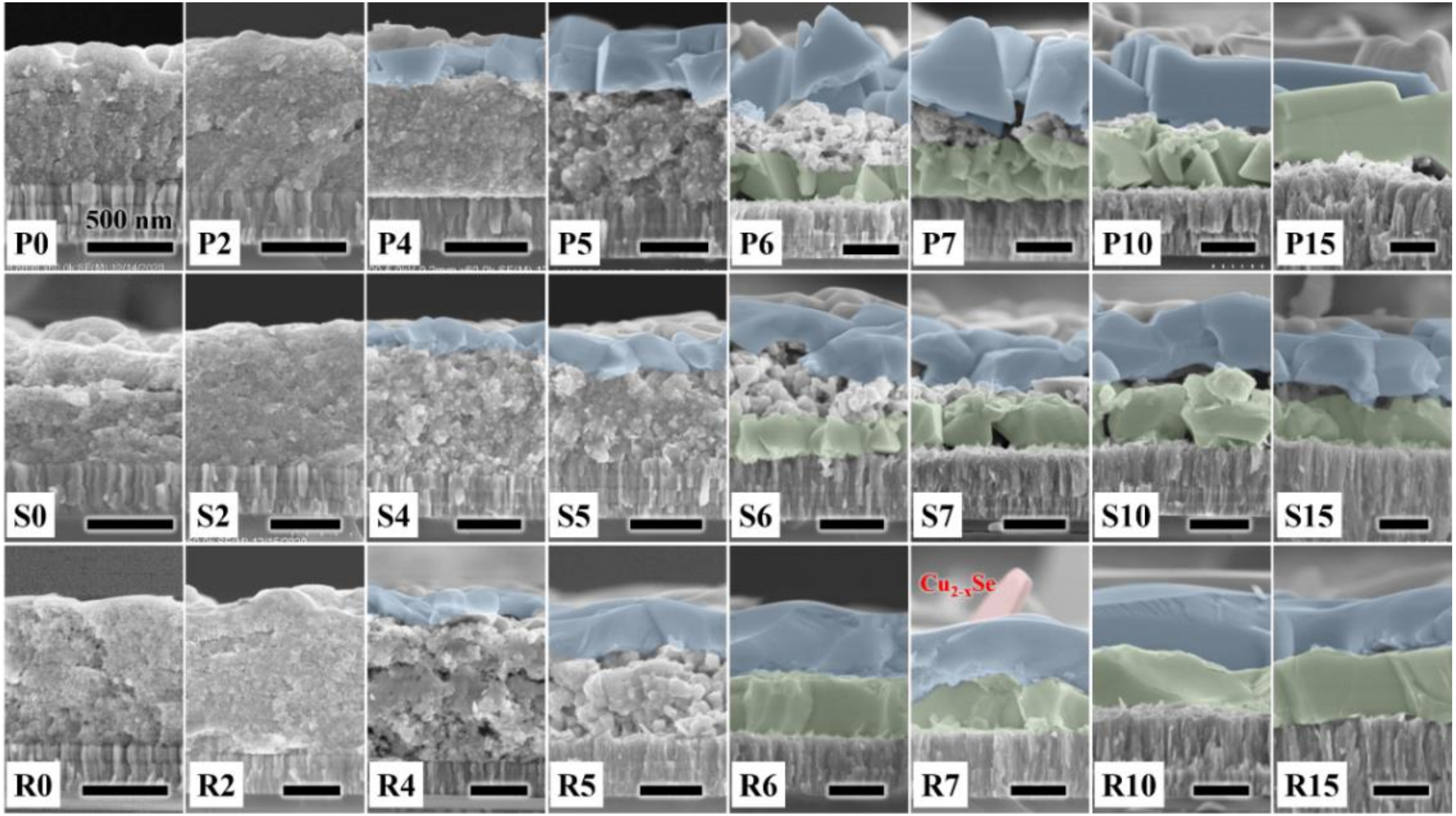

- ➢ 双向生长（双层结构）；
- ➢ 薄膜生长速度：富铜＞化学计量比＞贫铜。

Grain Growth of Solution Processed CIS absorber

Direct phase transformation grain growth: $CuInS_2$+Se → $CuIn(S,Se)_2$

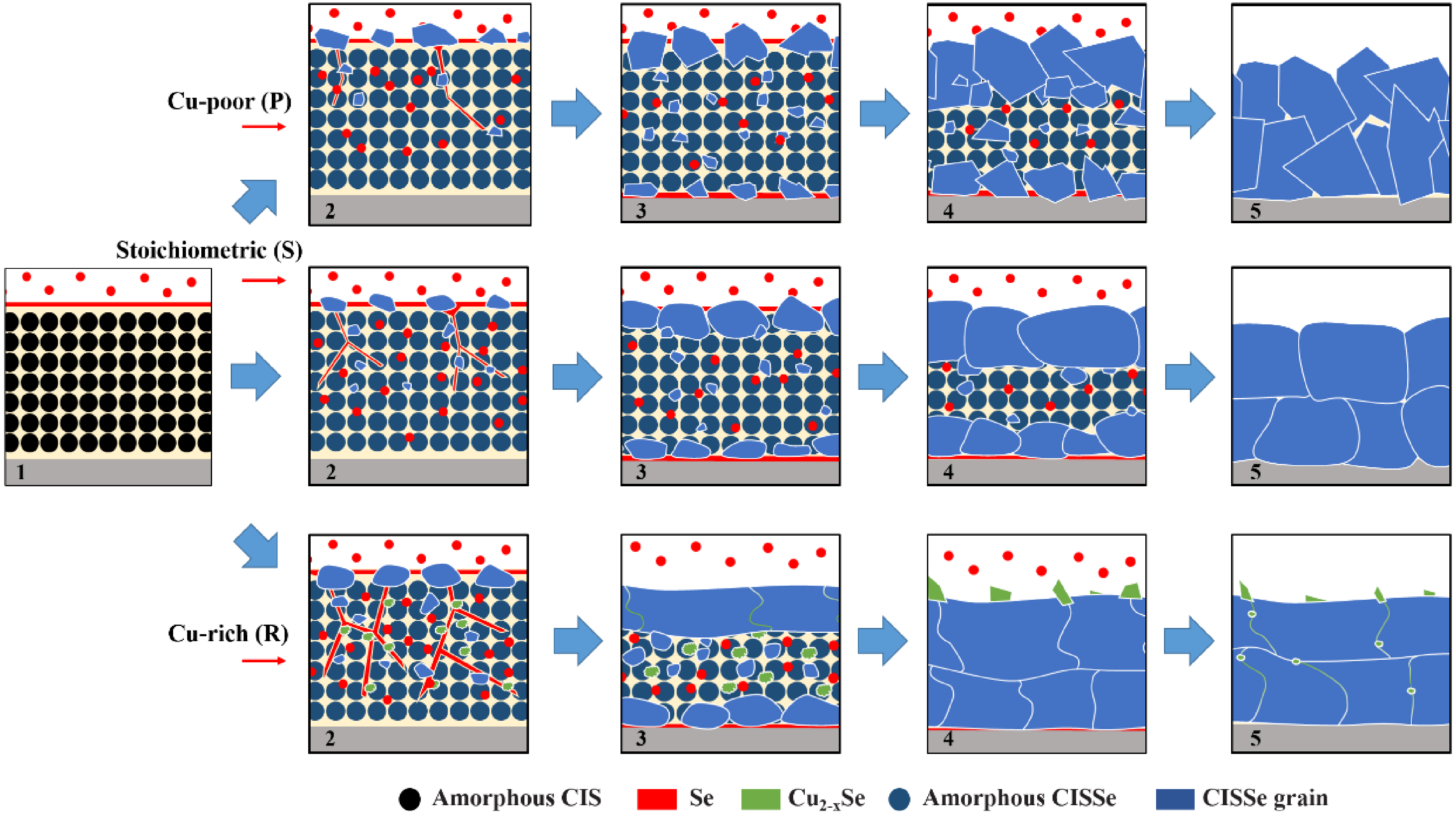

Adv. Energy Mater., **2022**, 12, 2103644.

Device Performance: the Effect of Cu/In Ratios

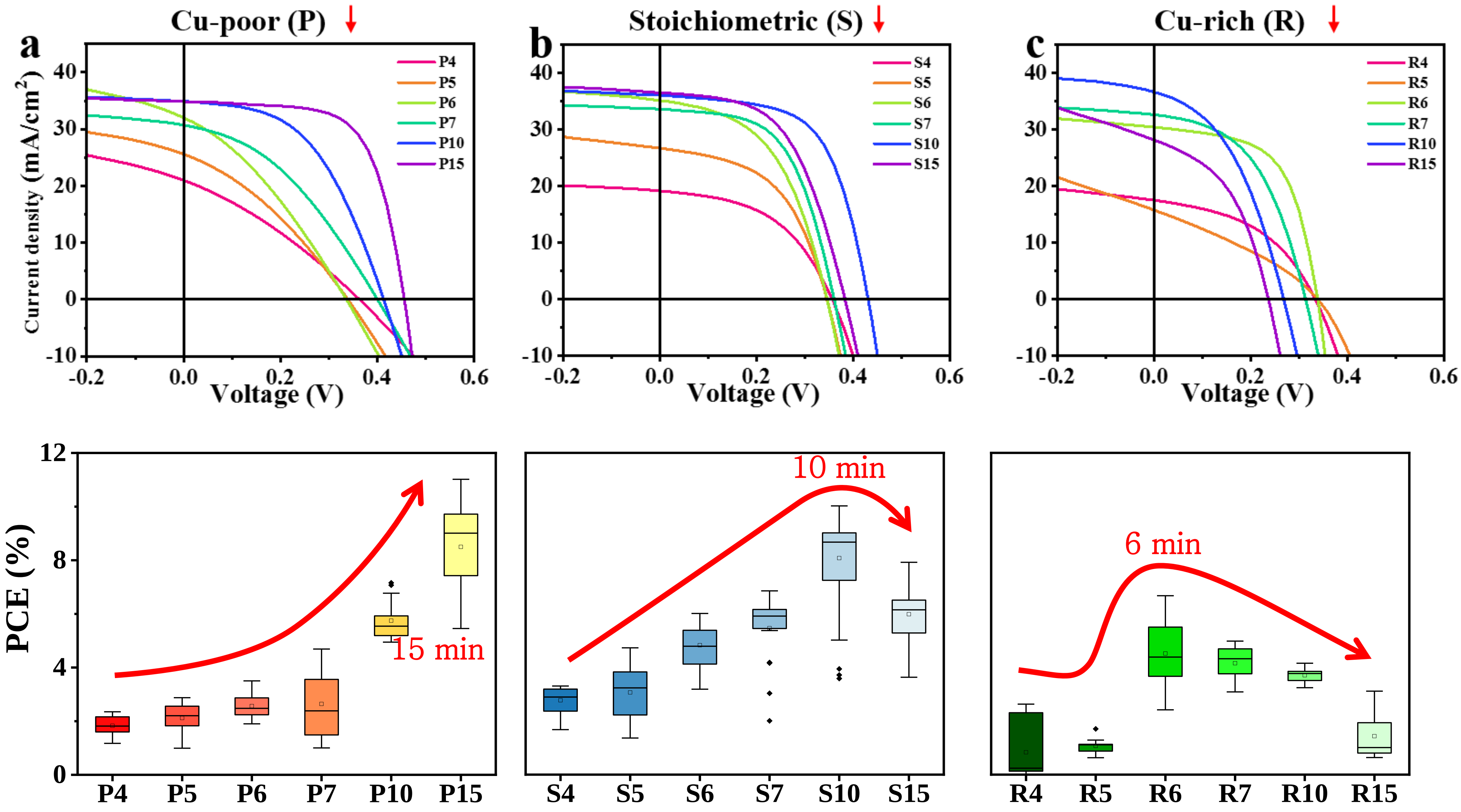

Adv. Energy Mater., **2022**, 12, 2103644.

High Tolerance to Composition Near Stoichiometry

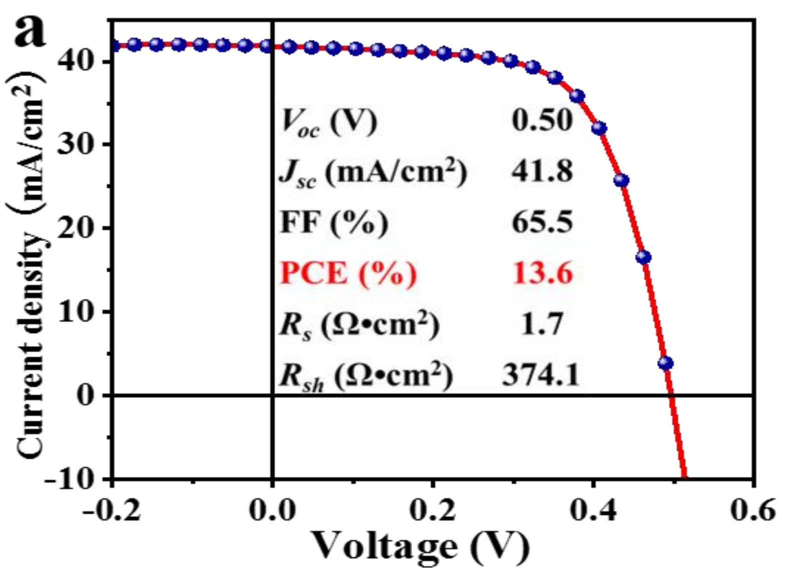

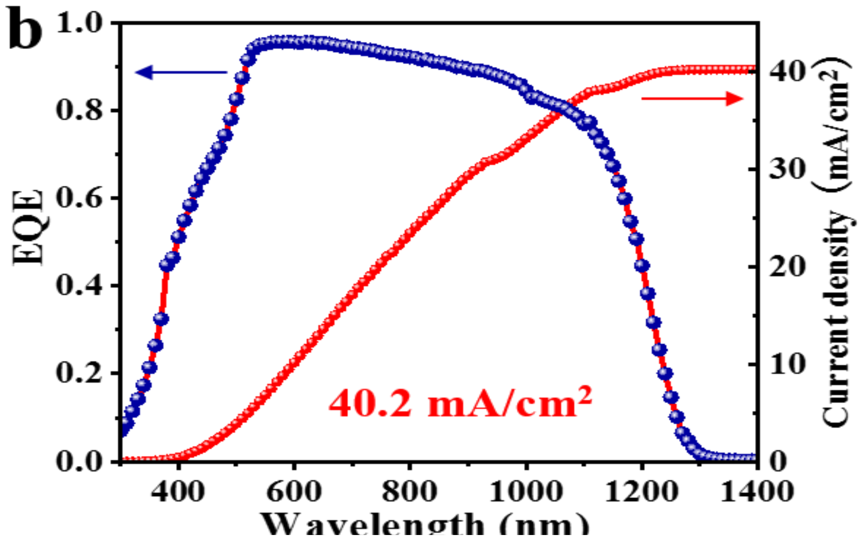

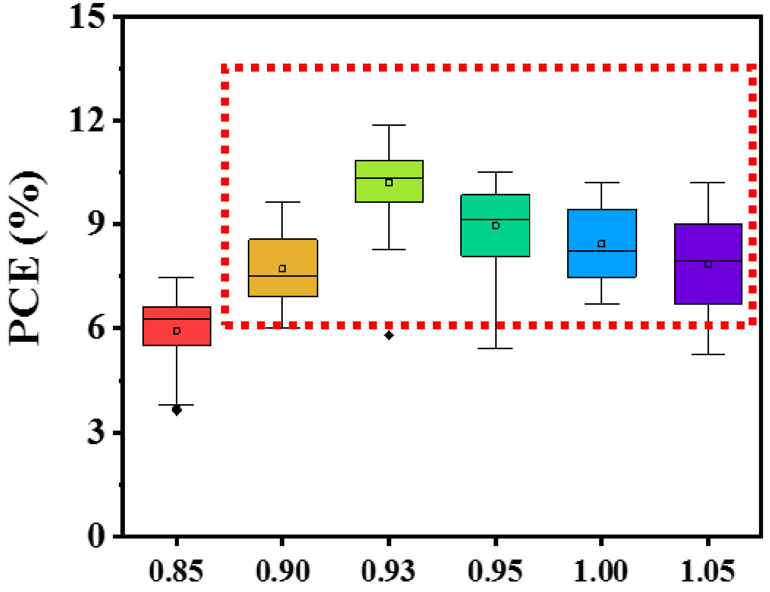

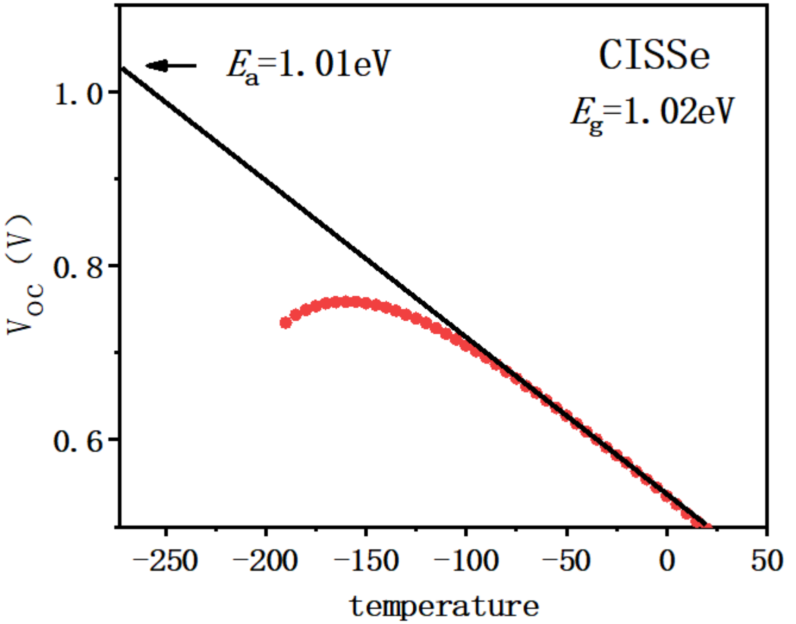

直接相变机制：组分有较宽的缓冲范围

CIS Solar Cell via Doctor-blading

DMF
溶液

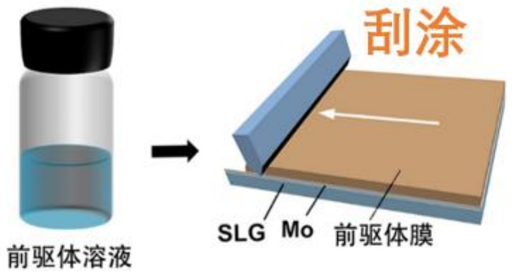

C_{Cu+In}=0.9/1.3/1.7 mol/L

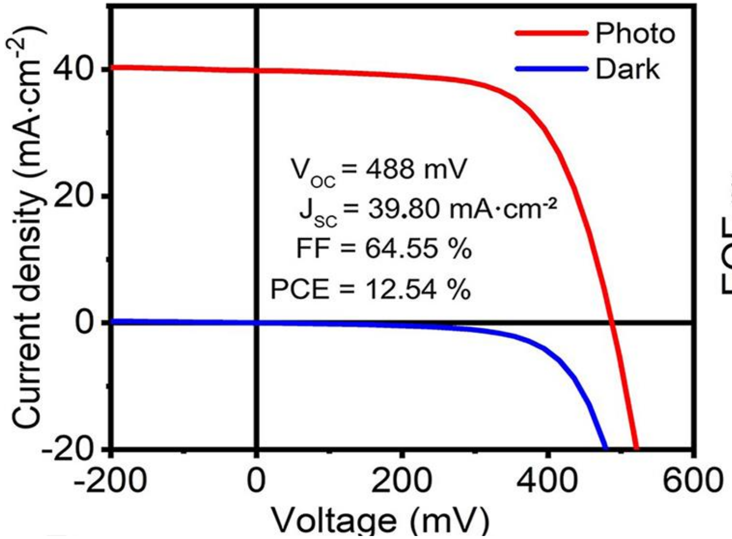

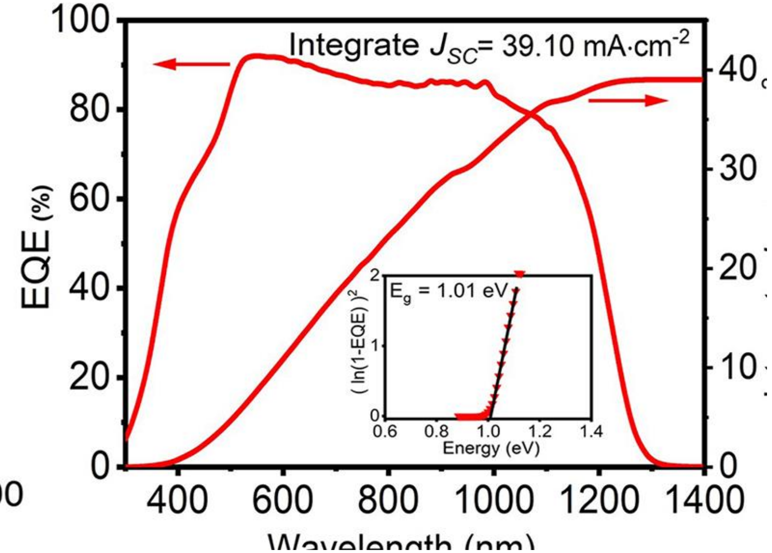

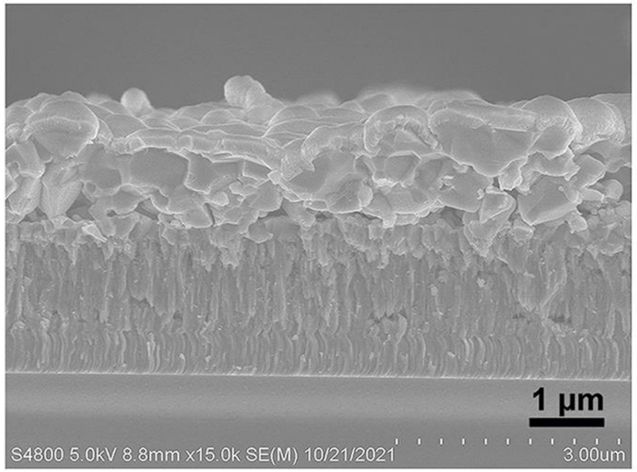

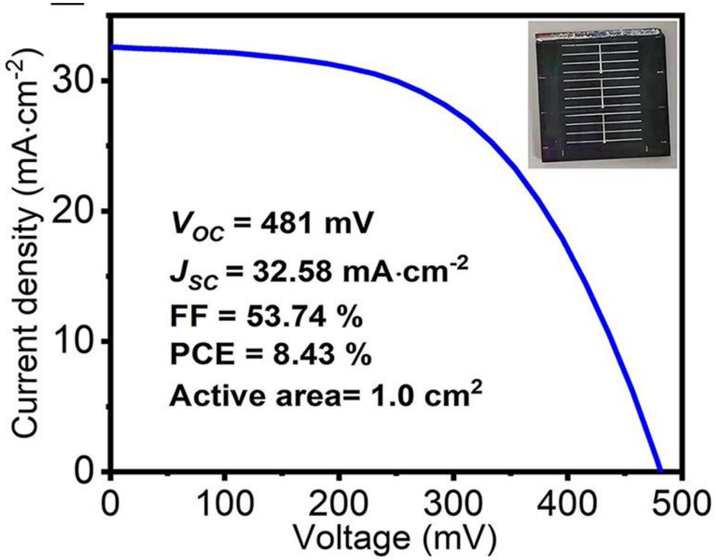

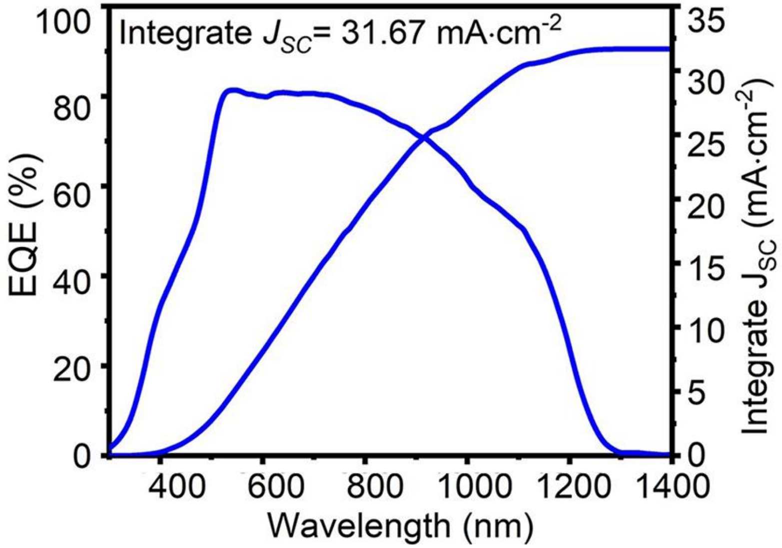

器件的效率：12.54% (0.1 cm^2)，8.43% (1 cm^2)

4. 总结与展望

- 前驱体溶液路径直接生成黄铜矿结构薄膜，直接相变薄膜生长机制
- 实现高效富铜CIGS电池效率 （15.5%）
- 硒化条件的优化是提高溶液法CIGS电池效率关键
- 高质量体相和异质结性质（$n=1.44$, $J_0= 5.61\times10^{-8}$mA·cm^{-2}, E_U＜14meV, $E_a\approx E_g$）
- 溶液法效率提高策略：背界面，组分梯度和碱金属等

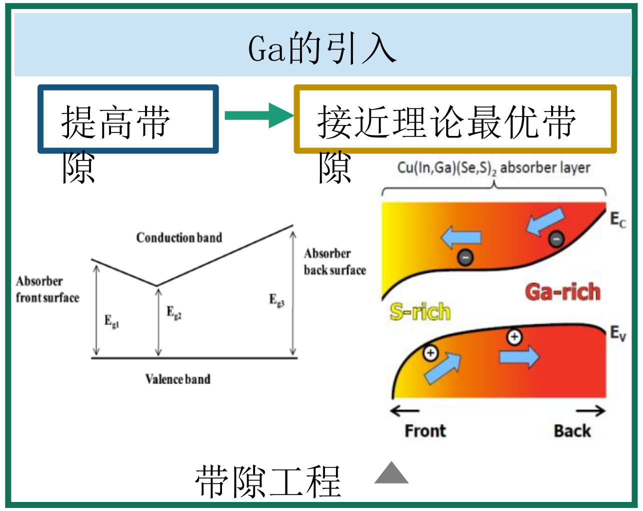

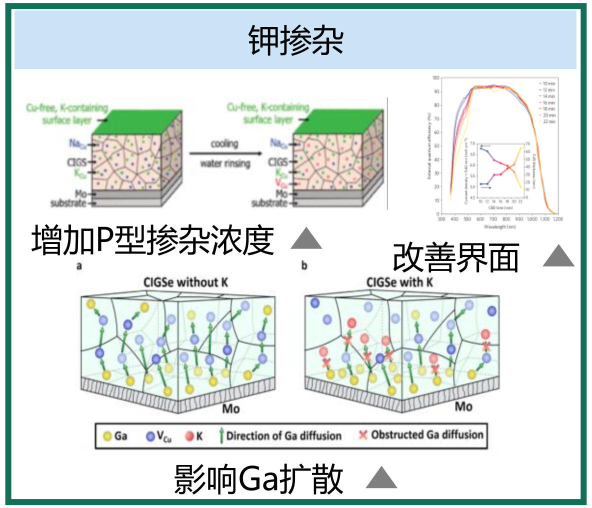

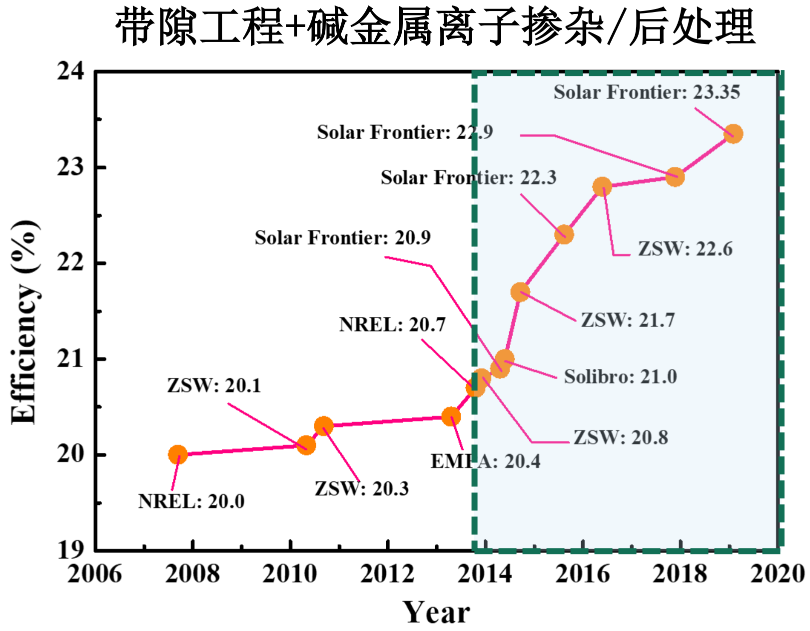

纲要

I. 铜铟镓硒薄膜太阳能电池

1. CIGS薄膜太阳能电池简介
2. 真空法CIGS薄膜太阳能电池
3. 溶液法CIGS薄膜太阳能电池
4. 总结与展望

II. 铜锌锡硫薄膜太阳能电池

1. CZTS薄膜太阳能电池优势及挑战
2. 吸收层缺陷与调控
3. 异质结界面缺陷与调控
4. 总结与展望

III. 致谢

1. CZTS的优势与挑战

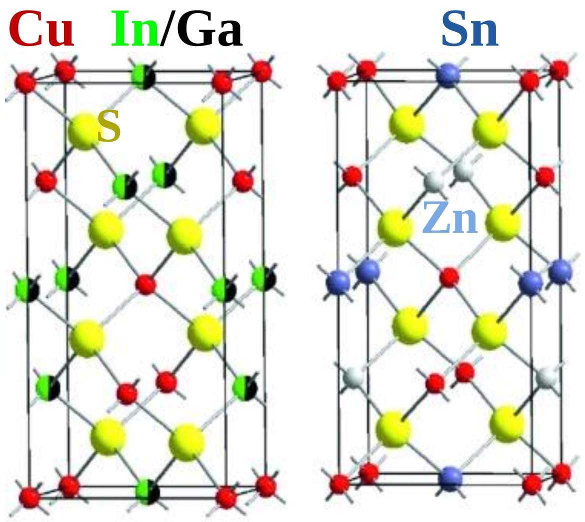

CIGS CZTS (Kesterite)

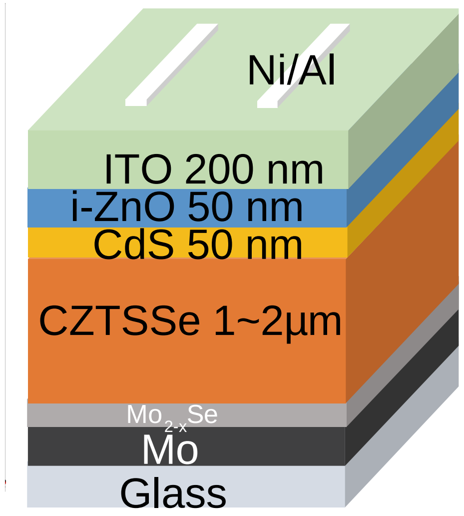

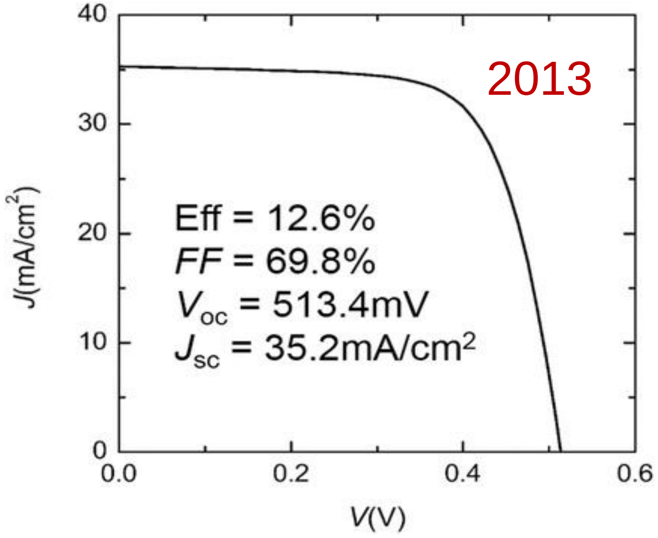

- **Similar crystal structure to CIGS**
- **High theoretical efficiency (32-33%)**
- **Direct band gap materials, high absorption coefficient, less materials required (0.5-2μm)**
- **Ideal and tunable band gap: 0.95-1.5 eV (fro pure Se to pure S)**

- **Use earth abundant materials**
- **Less toxic than CdTe**
- **Might be the solution for low cost and green thin film PV**

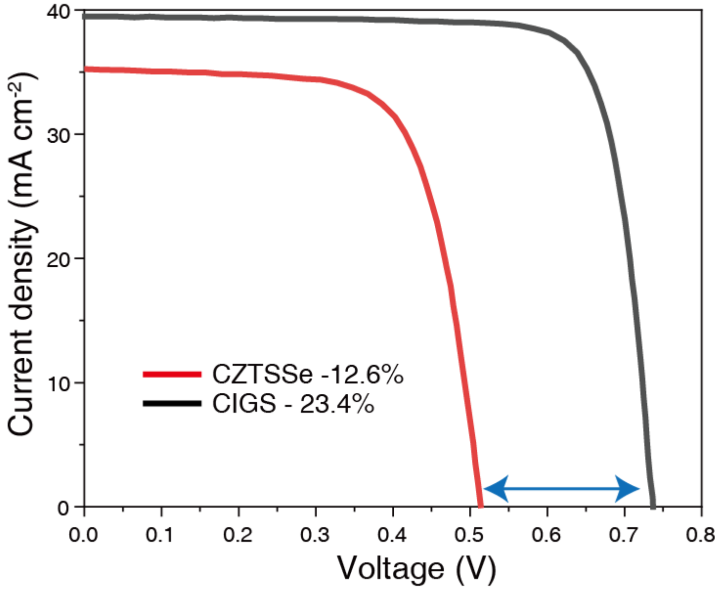

Large V_{oc} deficit

$V_{oc,def} = V_{oc}^{SQ} – V_{oc}$

V_{oc}/V_{oc}^{SQ}

	CZTS	CIGS
$V_{oc,def}$:	0.373 V,	0.106 V
V_{oc}/V_{oc}^{SQ}:	0.57,	0.87

Mitzi, et al. *Adv. Energy Mater.* 2013. Nakamura, et al. IEEE J. Photovoltaics, 2019.

Possible Reasons for Large $V_{oc\text{-}def}$

Absorber Fabrication

precursor film→ absorber film

Secondary phases

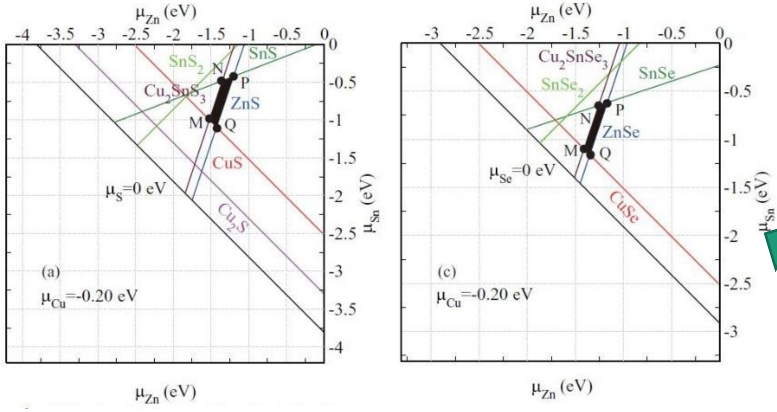

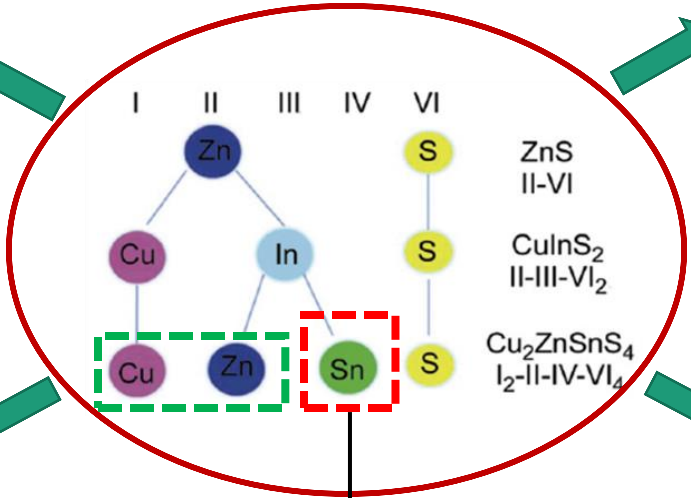

Sn: two oxidation state

Deep defects

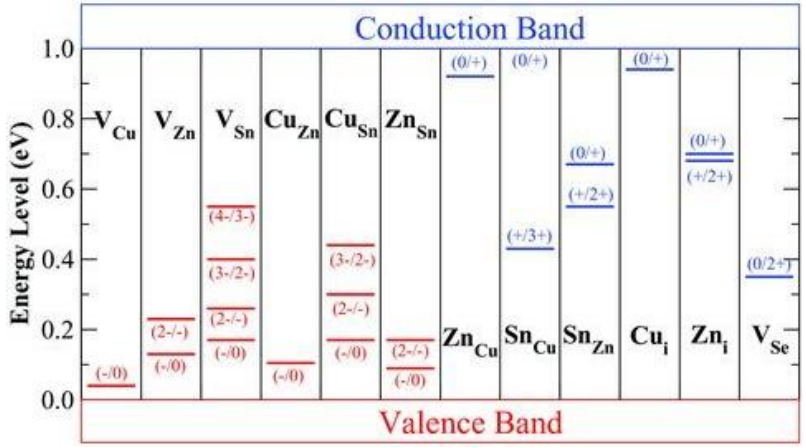

Band tailing

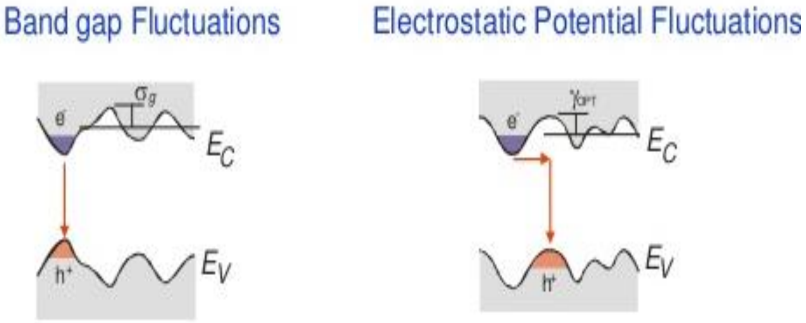

Causes : Competition between kesterite and stannite phase, secondary phases, non-uniform S/(S+Se), non-uniform strain

Causes : Charged defects

Cu_{Zn}^+, V_{Cu}^+, Zn_{Cu}^-, Sn_{Zn}^{2-}

Cu-Zn disorder

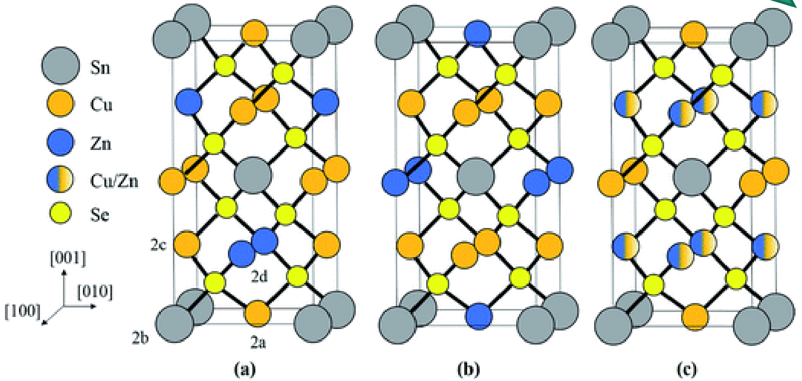

Chen, et al, *Adv. Mater.* 2013, 25, 1522, *Chem. Mater.*, 2013, 25, 3162. *Sol. Mater. Sol. Cell* 2015, 132, 363. *J. Mater. Chem. A*, 2018, 6, 189.

Recombination Locations: Absorber and Interface

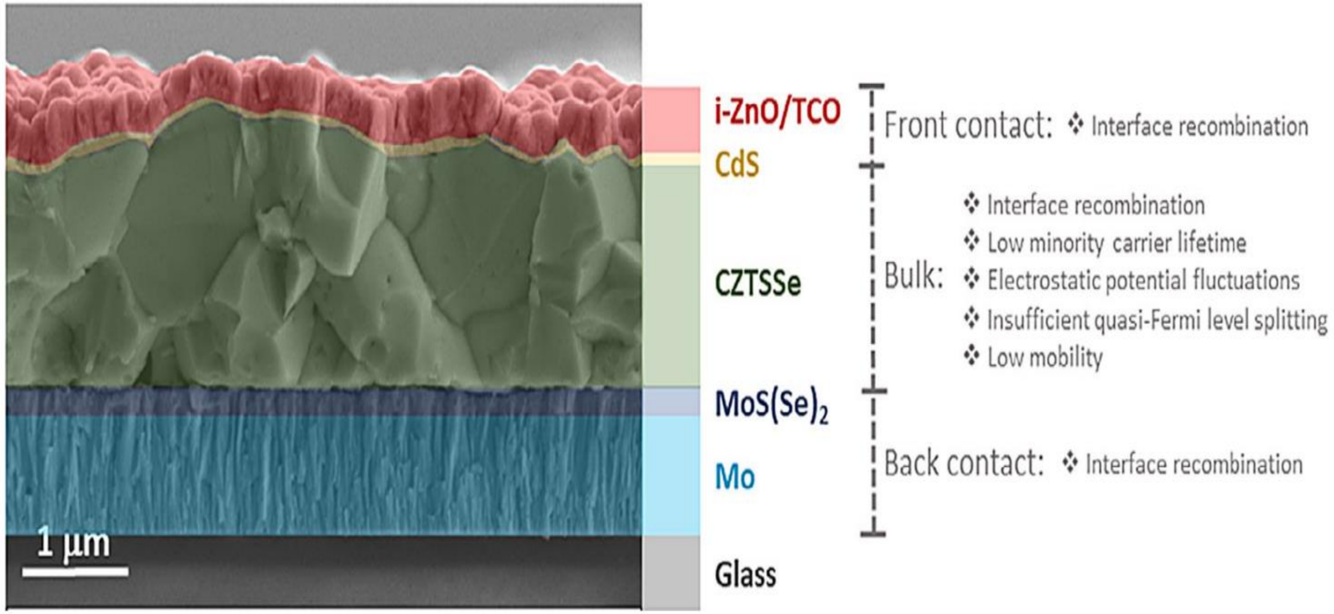

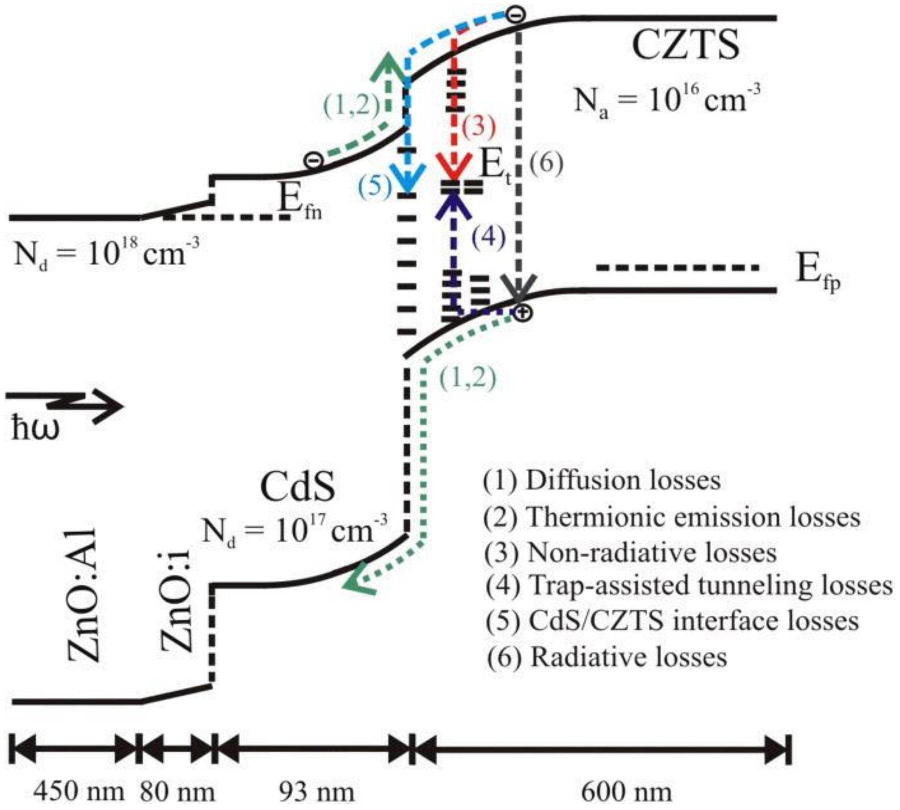

Giraldo, et al, Advanced Micro- and Nanomaterials for Photovoltaics. Elsevier. 2019: 93-120.

Chen, et al, *Adv. Mater.* 2013, 25, 1522

Vacuum Approach-Physical Deposition

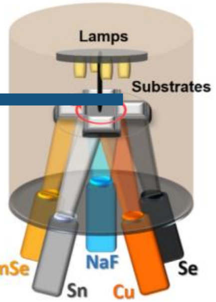

Precursors: Metal (Cu/Zn/Sn), sulfide/selenide (SnS, ZnS)

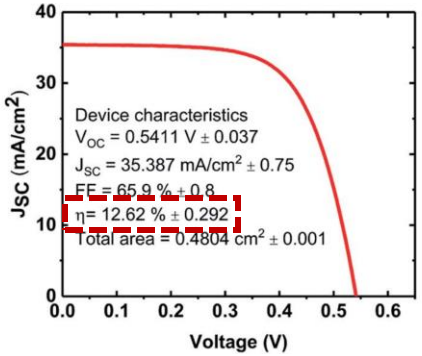

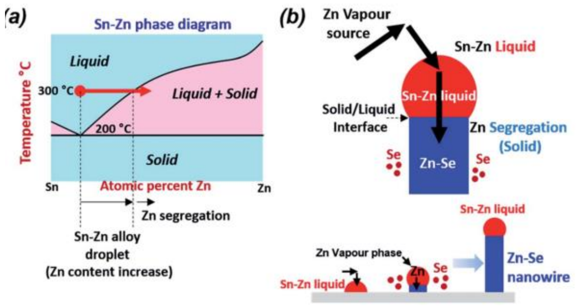

- The 12.62% record efficiency by vacuum process.[1]
- H_2S gas is introduced into selenization to suppress the volatilization of Zn.
- Precise **optimization of the selenization process**

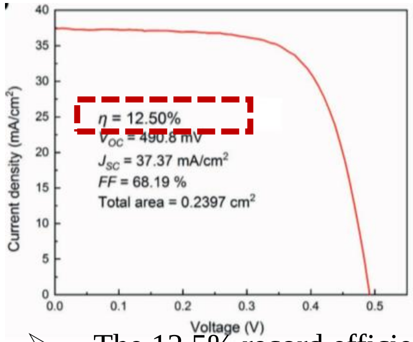

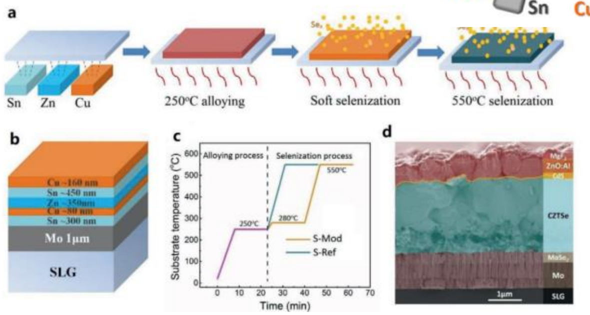

- The 12.5% record efficiency of pure-selenide $Cu_2ZnSnSe_4$ cells.[2]
- The **soft-selenization process** employed to prepare a local chemical environment for the formation of CZTSe.

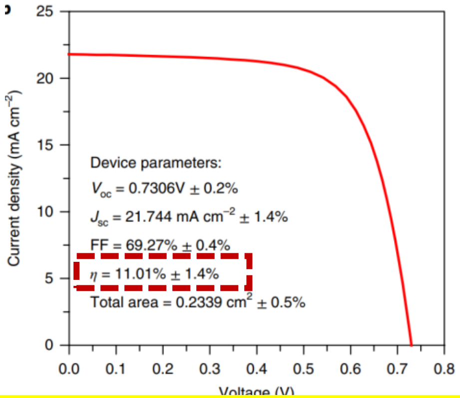

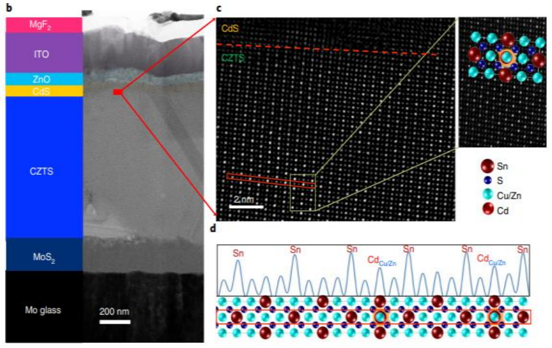

- The 11.0% record efficiency of pure-sulfide Cu_2ZnSnS_4 cells.[3]
- By employing **post-heat treatment for the heterojunction**.

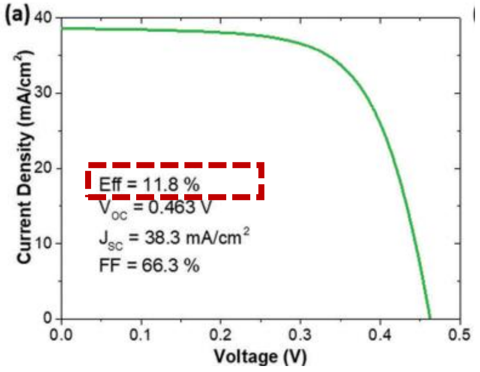

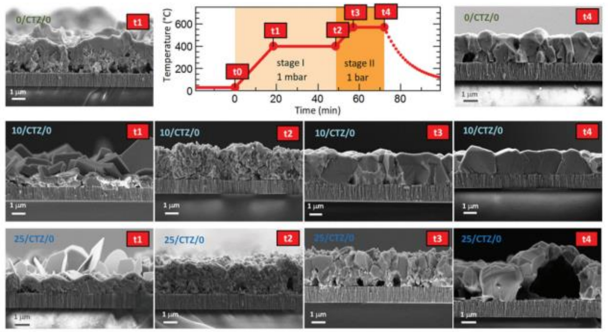

- **Introduce Ge layer to avoid Sn loss.**[4]
- Ge change the evolution of phases during selenization.

[1] Son D H, Kim S H, Kim S Y, et al. Journal of Materials Chemistry A, 2019, 7, 25279.
[2] Li J, Huang Y, Huang J, et al. Advanced Materials, 2020, 32, 2005268.
[3]Yan C, Huang J, Sun K, et al. Nature Energy, 2018, 3, 764.
[4]Giraldo S, Saucedo E, Neuschitzer M, et al. Energy & Environmental Science, 2018, 11, 582.

Solution Approach-Molecular Level Mixture

Precursors: metal, metal oxides, metal salts + S source (thiourea)

2-methoxyethanol

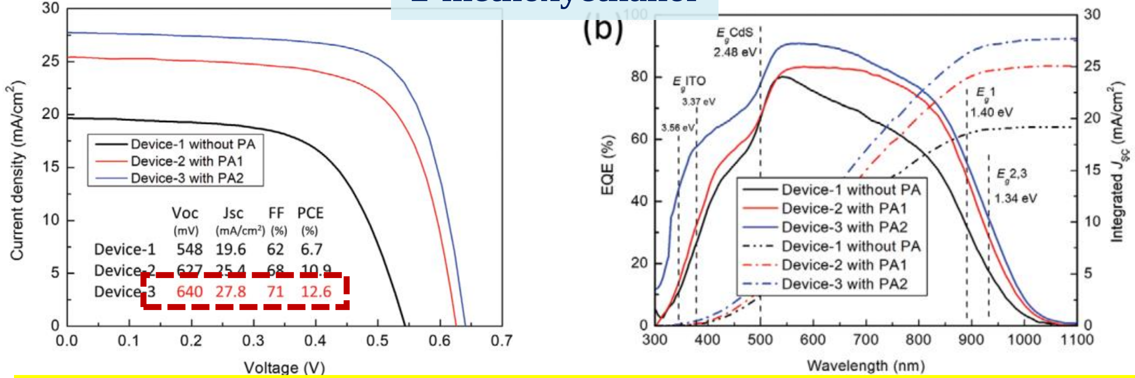

- Over 12% efficient solution processed Cd-alloyed CZTS cell.[1]
- **A post annealing procedure is proposed to complete device** to decreased non-radiative recombination.

DMSO

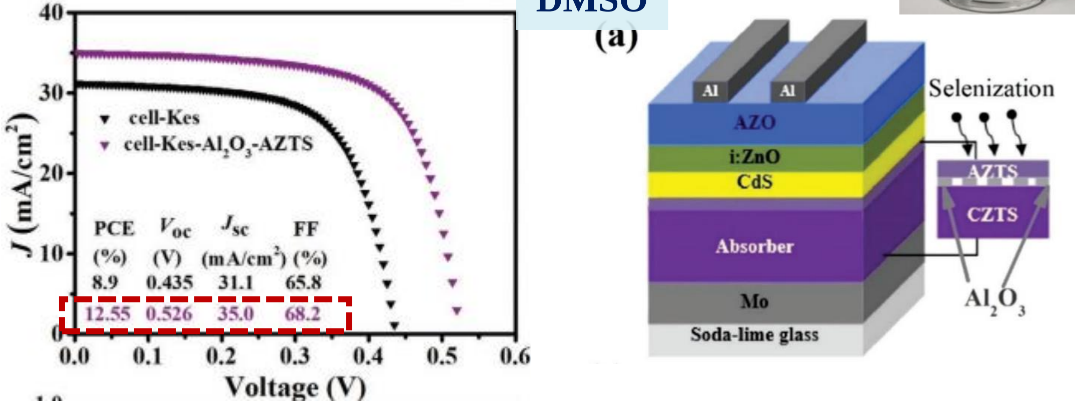

- **N-type surface design** for p-type CZTSSe Thin Film with 12.55% efficiency. [2]

TGA-ammonia

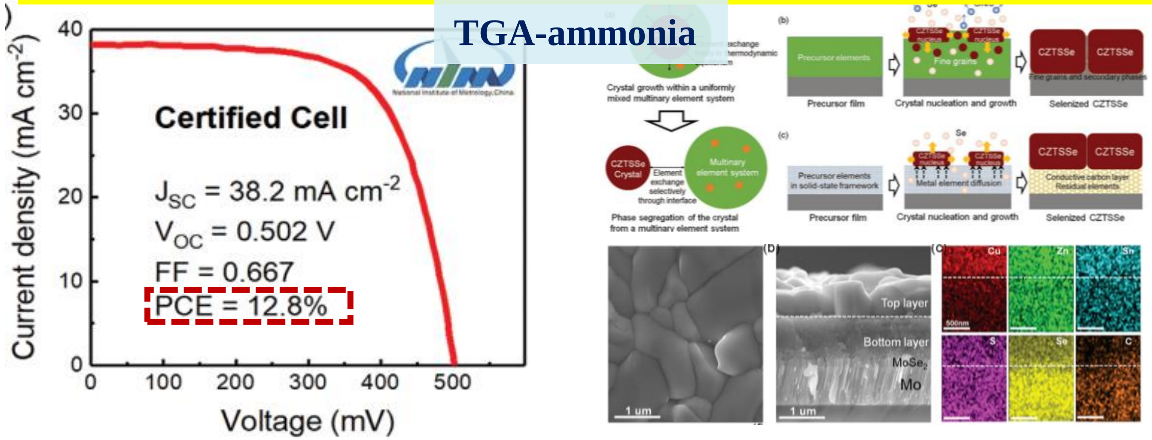

- A certified active-area PCE of 12.8% for CZTSSe cell.[3]
- The device efficiency has a high tolerance to composition due a conductive carbon framework.

amine−thiol

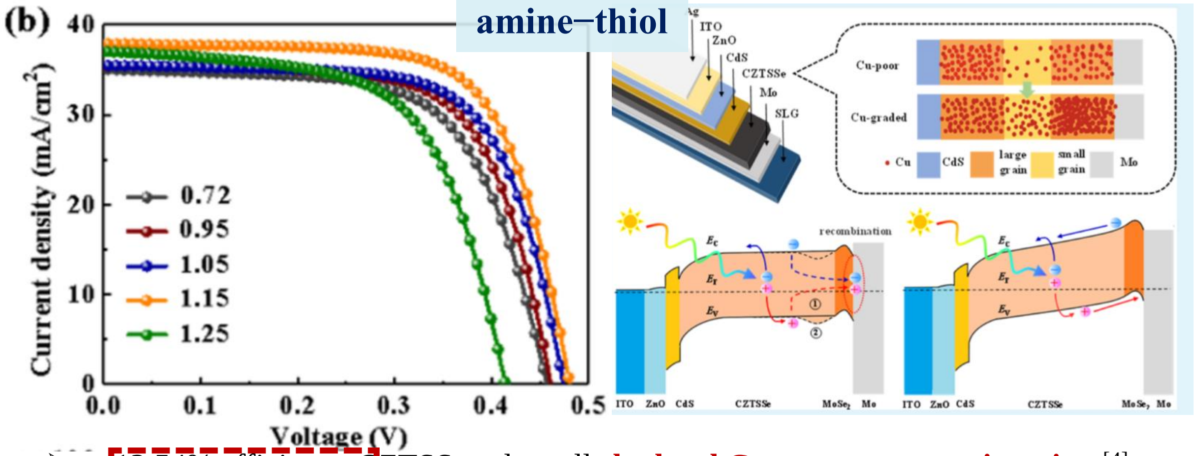

- 12.54% efficiency CZTSSe solar cells **by local Cu component engineering**.[4]

[1] Su Z, Liang G, Fan P, et al. Advanced Materials, 2020, 32(32): 2000121.
[2] Sun Y, Qiu P, Yu W, et al. Advanced Materials, 2021: 2104330.
[3] Xu X, Guo L, Zhou J, et al. Advanced Energy Materials, 2021, 11(40): 2102298.
[4] Zhao Y, Zhao X, Kou D, et al. ACS Applied Materials & Interfaces, 2021, 13(1): 795-805.

2. 吸收层缺陷与调控

2.1 缺陷与前驱体化合物锡的价态（Sn^{2+} vs Sn^{4+}）
2.2 V_{OC} 损失与晶粒生长机制
2.3 Cu-Zn无序与带尾态及银合金化

2.1 缺陷与前驱体化合物锡的价态（Sn^{2+} vs Sn^{4+}）

DMSO Molecular Precursor Solution Approach

$Cu(OAc)_2 \cdot H_2O$
$ZnCl_2$
$SnCl_2 \cdot 2H_2O$
$SC(NH_2)_2$ (Tu)

DMSO

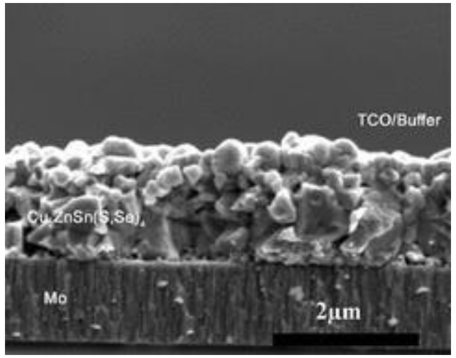

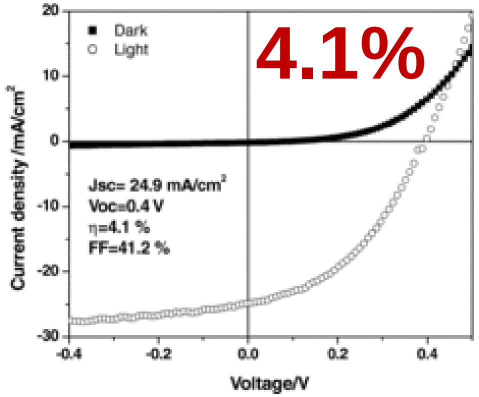

Ki and Hillhouse, *Adv. Energy Mater.* 2011, 732.

+I +II +IV

Cu_2ZnSnS_4

$2Cu^{2+}+Sn^{2+} \rightleftharpoons 2Cu^{+}+Sn^{4+}$

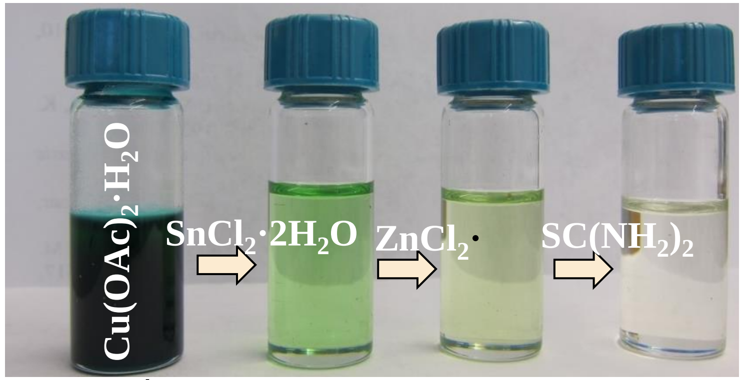

Adv. Energy Mater. 2014, 1301823

Control the redox reaction

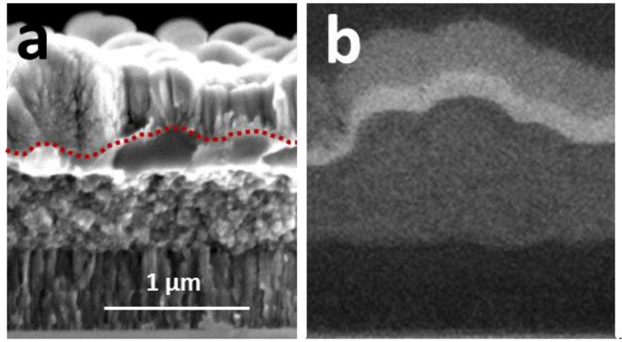

$V_{oc,def}$: 0.424 V
V_{oc}/V_{oc}^{SQ} : 0.51

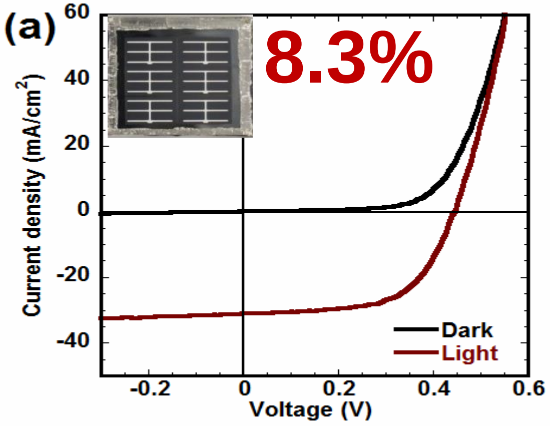

Sn^{2+} vs Sn^{4+} Precursor

+I +II +IV

Cu_2ZnSnS_4

$Cu^+ + Sn^{2+}$

CuCl, $ZnCl_2$, **$SnCl_2 \cdot 2H_2O$,** Tu

$Cu^+ + Sn^{4+}$

CuCl, $Zn(OAc)_2$, **$SnCl_4$,** Tu

IEEE 7th WCPEC, 2018

Sn^{2+} vs Sn^{4+}: Effect on V_{oc}

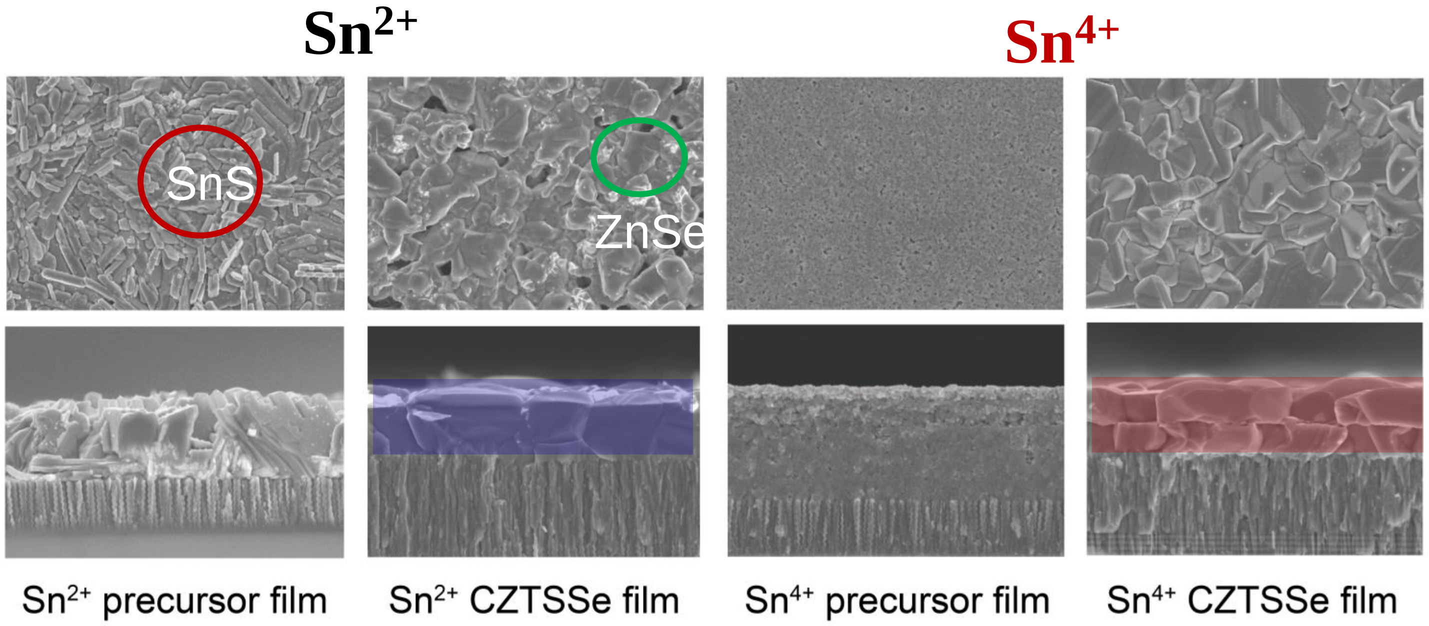

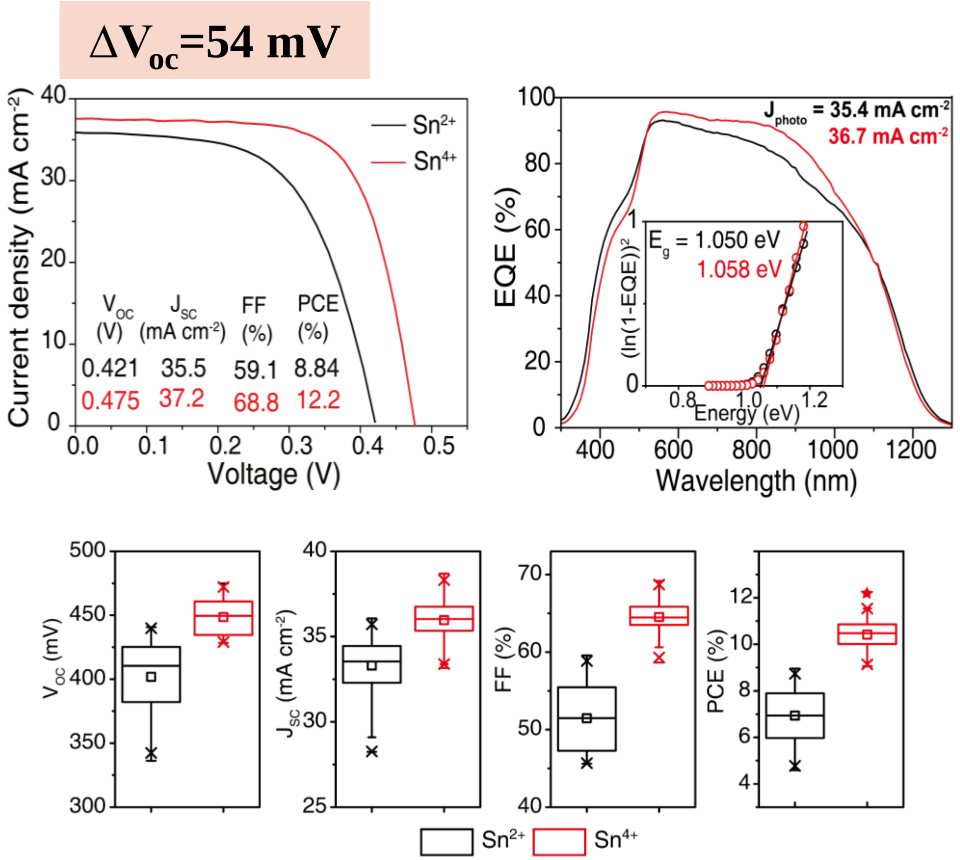

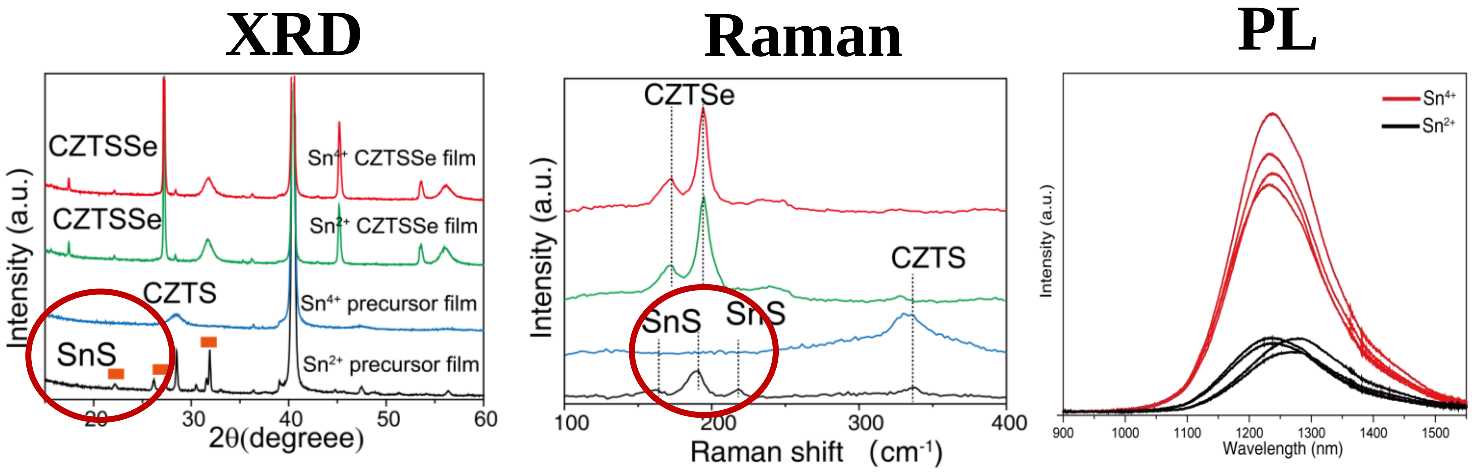

- ➢ Dramatic difference in composition and morphology of the precursor films
- ➢ Sn^{4+} shows high uniformity
- ➢ Sn^{4+} device has much high V_{oc} and FF

SCI. CHINA Mater., 2021, 1, 52.

Sn^{2+} vs Sn^{4+}: Response to Junction Heat Treatment (JHT)

JHT (200ºC/20 h, vaccum)

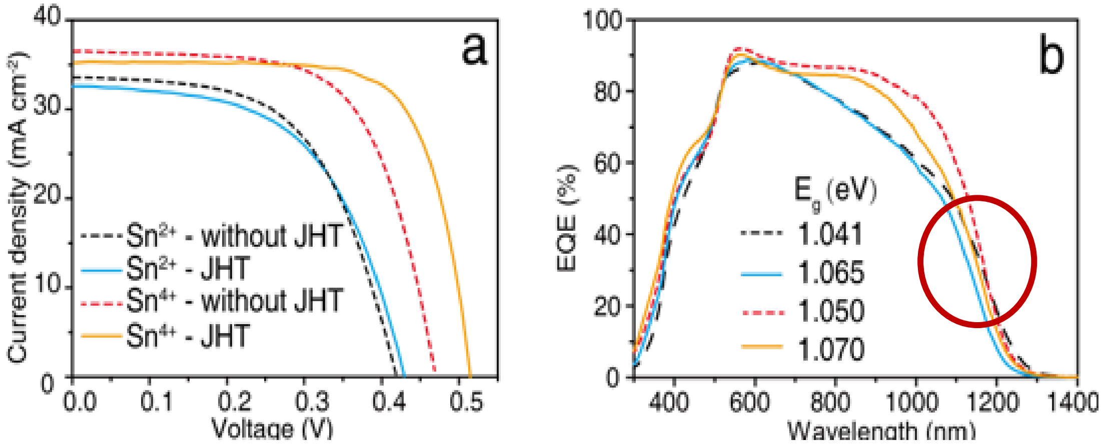

Sn^{2+}
E_g: increase 24 meV
J_{sc}: decrease
V_{oc}: no obvious change
FF: no obvious change

Sn^{4+}
E_g: increase 20 meV
J_{sc}: decrease
V_{oc}: enhance 50 mV
FF: increase

Raman **GDOES**

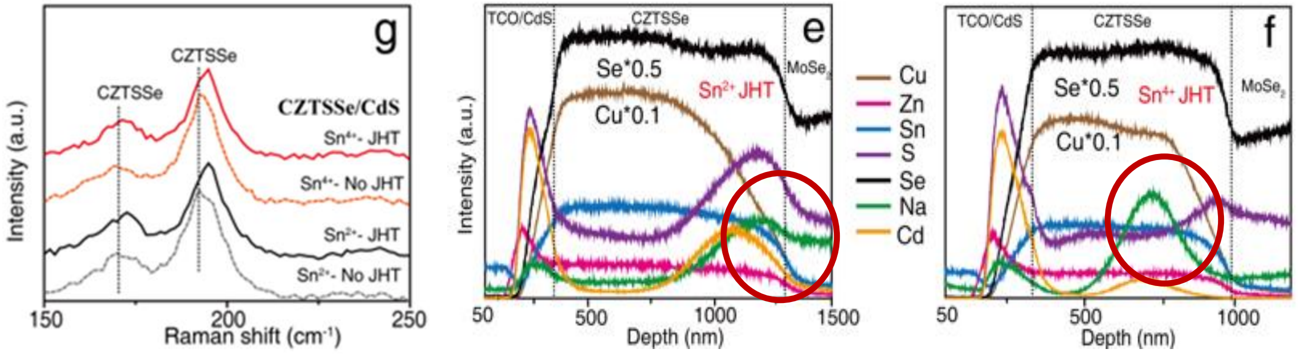

Top Sn^{4+} **Top Sn^{2+}**

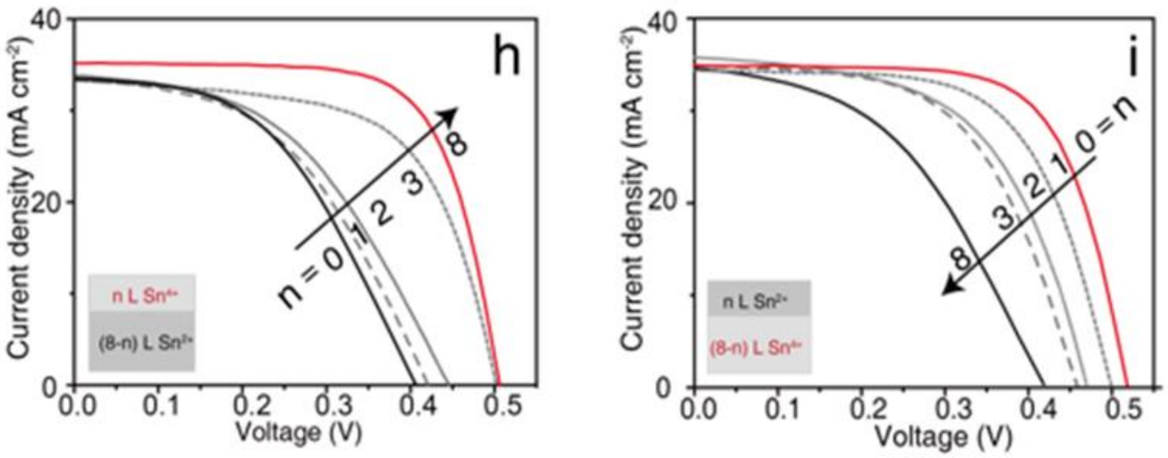

V_{oc} directly related to the oxidation state of the Sn precursor

- ➢ **Order level similarly improved upon JHT**
- ➢ **Large Cd and S diffuse into film**
- ➢ **Surface property is more important**

SCI. CHINA Mater., 2021, 1, 52.

Champion CZTSSe Device from Sn^{4+} DMSO Solution

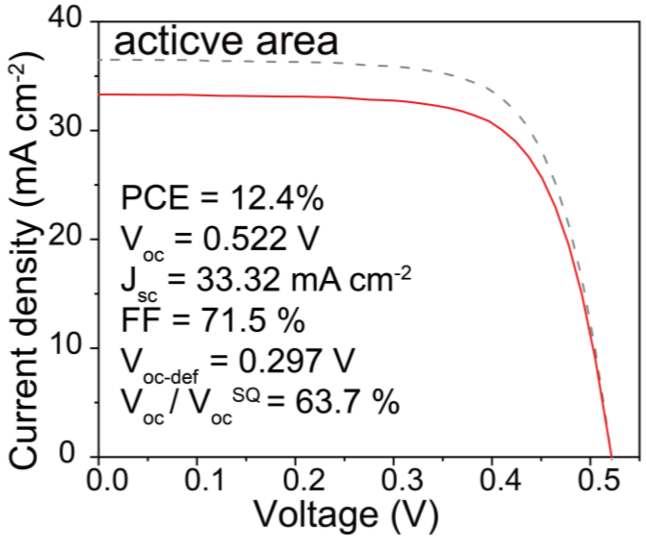

Total area: 12.4%
Active area: 13.6%

$V_{oc,def}$: 0.297 V
V_{oc}/V_{oc}^{SQ} : 63.7%

SCIENCE CHINA Materials — ARTICLES

mater.scichina.com link.springer.com
Published online 29 July 2020 | https://doi.org/10.1007/s40843-020-1408-x

CrossMark

Sn^{4+} precursor enables 12.4% efficient kesterite solar cell from DMSO solution with open circuit voltage deficit below 0.30 V

Yuancai Gong[1], Yifan Zhang[1], Erin Jedlicka[2], Rajiv Giridharagopal[2], James A. Clark[3], Weibo Yan[1], Chuanyou Niu[1], Ruichan Qiu[1], Jingjing Jiang[1], Shaotang Yu[1], Sanping Wu[1], Hugh W. Hillhouse[3], David S. Ginger[2], Wei Huang[1] and Hao Xin[1*]

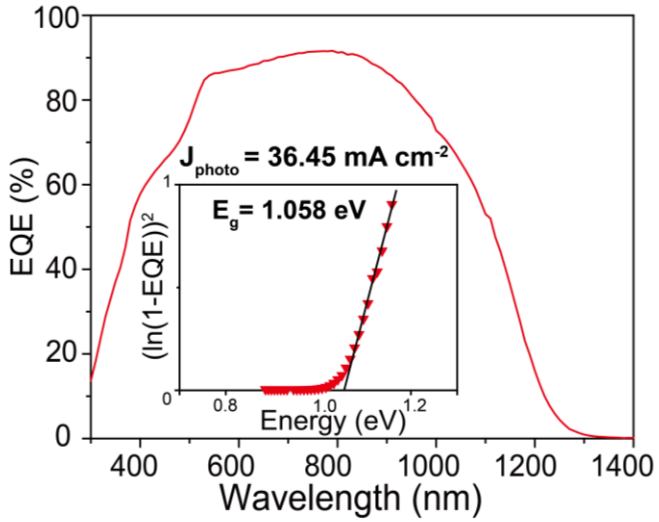

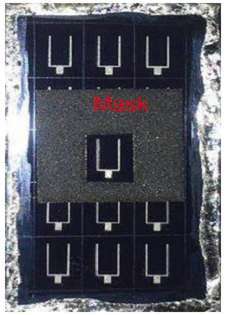

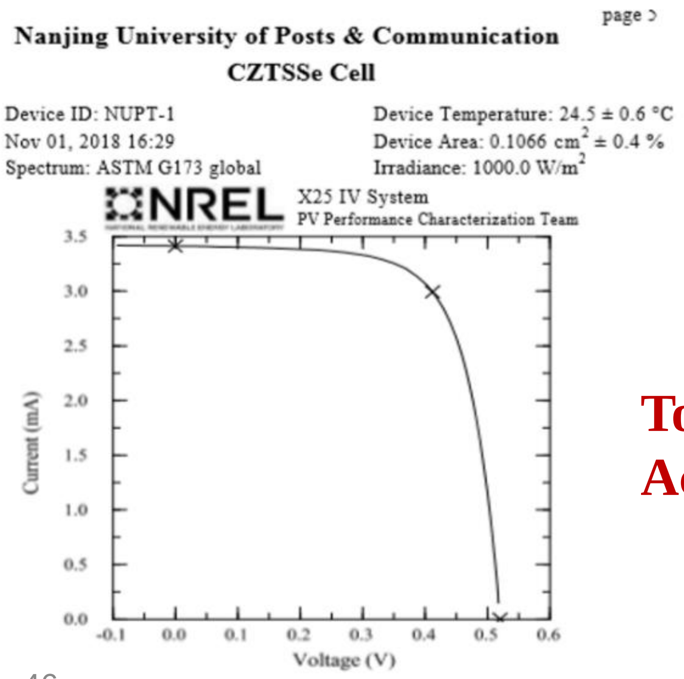

Total area: 11.56%
Active area: 13.22%

2.2 V_{OC} 损失与晶粒生长机制

Energy & Environmental Science

ROYAL SOCIETY OF CHEMISTRY

PAPER

View Article Online
View Journal | View Issue

Check for updates

Cite this: *Energy Environ. Sci.*, 2021, 14, 2369

Identifying the origin of the V_{oc} deficit of kesterite solar cells from the two grain growth mechanisms induced by Sn^{2+} and Sn^{4+} precursors in DMSO solution†

Reaction of each precursor in the DMSO solution with Tu		Reaction from solution to solid film
$CuCl + 3Tu = Cu(Tu)_3Cl$ (1)		$Cu_{2-x}S$
$ZnCl_2 + 2Tu = Zn(Tu)_2Cl_2$ (2)		ZnS
$Zn(OAc)_2 + 2Tu = Zn(Tu)_2(OAc)_2$ (3)	$\xrightarrow{\triangle}$	ZnS
$SnCl_2 + 2Tu = Sn(Tu)_2Cl_2$ (4)		SnS (strong Sn-S bond)
$SnCl_4 + 2DMSO = Sn(DMSO)_2Cl_4$ (5)		**Nothing** (weak Sn-O bond)

Reaction Path from Solution to Precursor film

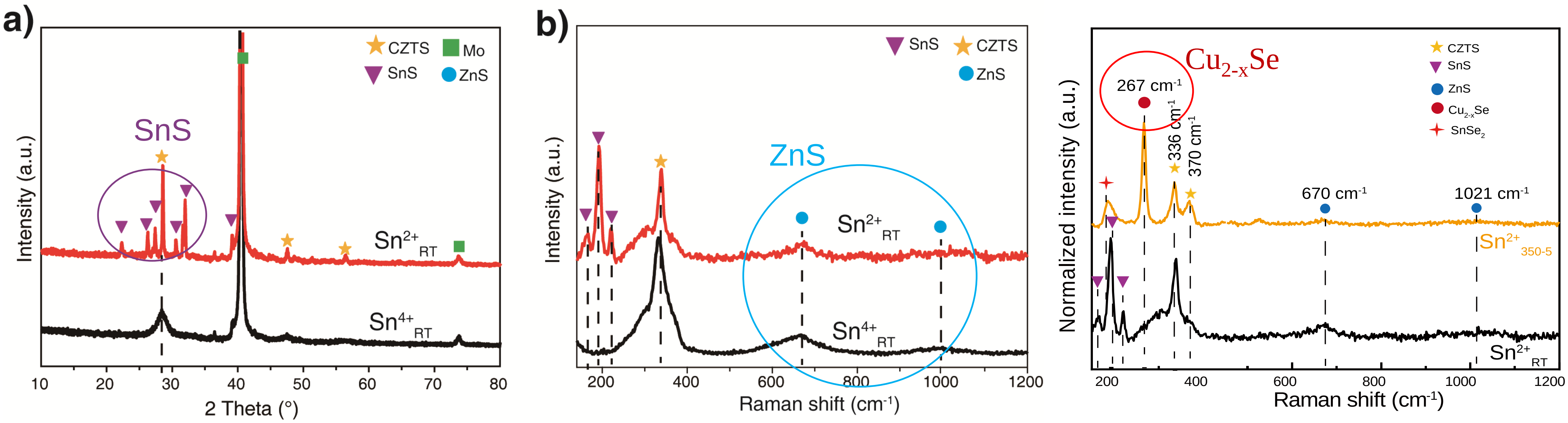

Sn^{2+} solution

$Sn(Tu)_xCl_2$ $\rightarrow$ SnS

$Zn(Tu)_2Cl_2 \rightarrow ZnS$

$Cu(Tu)_3Cl \rightarrow Cu_{2-x}S$

$Cu(Tu)_3Cl$+$Zn(Tu)_2Cl_2$+**$Sn(Tu)_xCl_2$** $\rightarrow Cu_2ZnSnS_4$

Sn^{4+} solution

$Zn(Tu)_2(OAc)_2 \rightarrow$ ZnS (10) (trace)

$Cu(Tu)_3Cl$+$Zn(Tu)_2(OAc)_2$+**$Sn(DMSO)_2Cl_4$** $\rightarrow Cu_2ZnSnS_4$

Grain Growth from Precursor Film to Absorber

Selenization profile

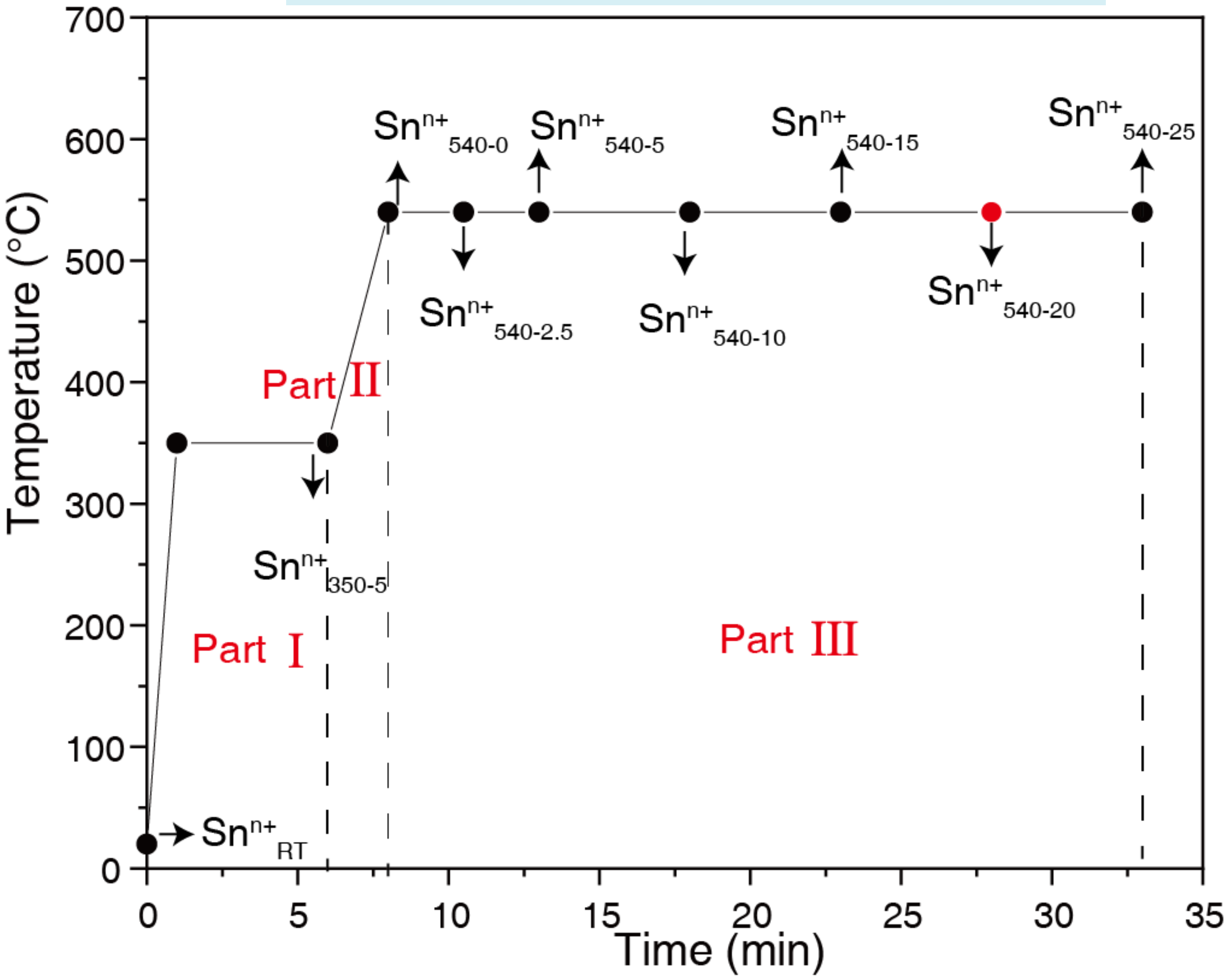

Grain Growth from Precursor Film to Absorber

Sn^{2+}

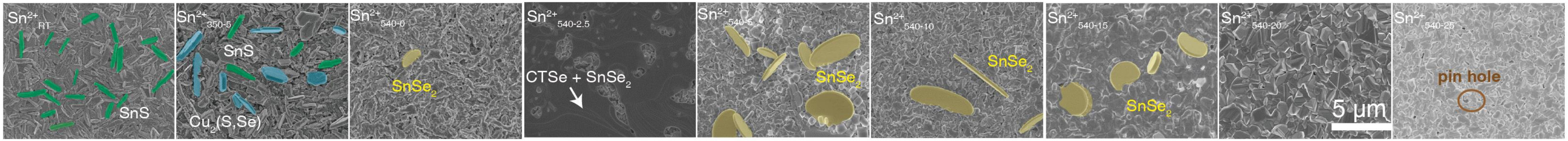

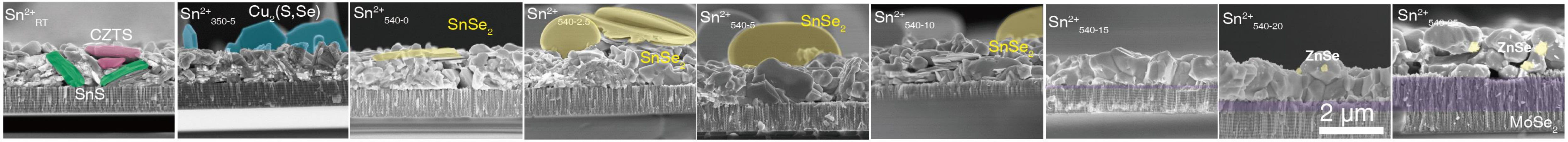

Sn^{4+}

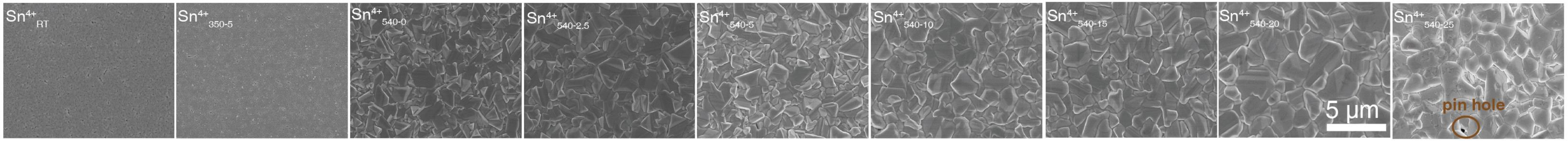

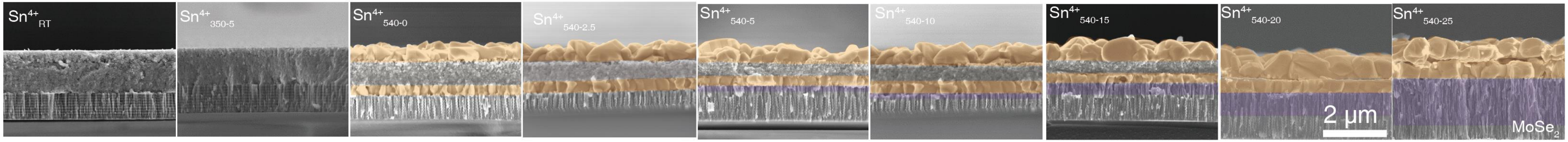

Grain Growth from Precursor Film to Absorber

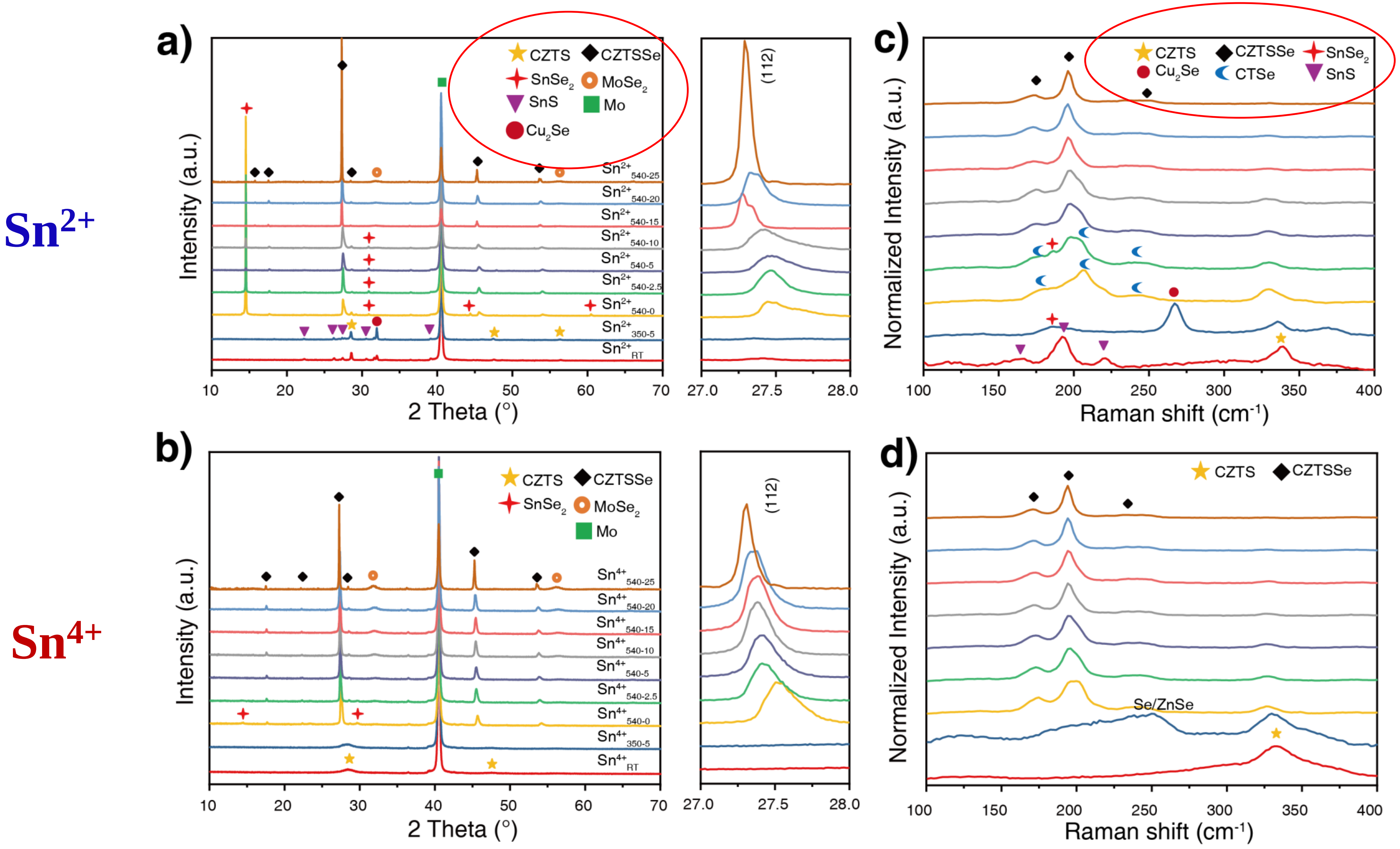

Reaction Path to Absorber

Sn^{2+}: multi-phase fusion

Part I

$Cu_2S + Se \rightarrow Cu_2Se$ (7)

$SnS + Se \rightarrow SnSe_2$ (8)

$ZnS + Se \rightarrow ZnSe$ (9)

Part II

$SnS + Se \rightarrow SnSe_2$ (10)

$Cu_2Se + SnSe_2 \rightarrow Cu_2SnSe_3$ (11)

$Cu_2ZnSnS_4 + Se \rightarrow Cu_2ZnSn(S,Se)_4$ (12)

Part III:

$Cu_2ZnSnS_4 + Se \rightarrow Cu_2ZnSn(S,Se)_4$ (12)

$Cu_2SnSe_3 + ZnSe \rightarrow Cu_2ZnSnSe_4$ (13)

$Cu_2Se + SnSe_2 + ZnSe \rightarrow Cu_2ZnSnSe_4$ (14)

$Mo + Se \rightarrow MoSe_2$ (15)

Sn^{4+}: direct phase transformation

Part I

$ZnS + Se \rightarrow ZnSe$ (9)

Part II

$Cu_2ZnSnS_4 + Se \rightarrow Cu_2ZnSn(S,Se)_4$ (12)

Part III:

$Cu_2ZnSnS_4 + Se \rightarrow Cu_2ZnSn(S,Se)_4$ (12)

$Mo + Se \rightarrow MoSe_2$ (15)

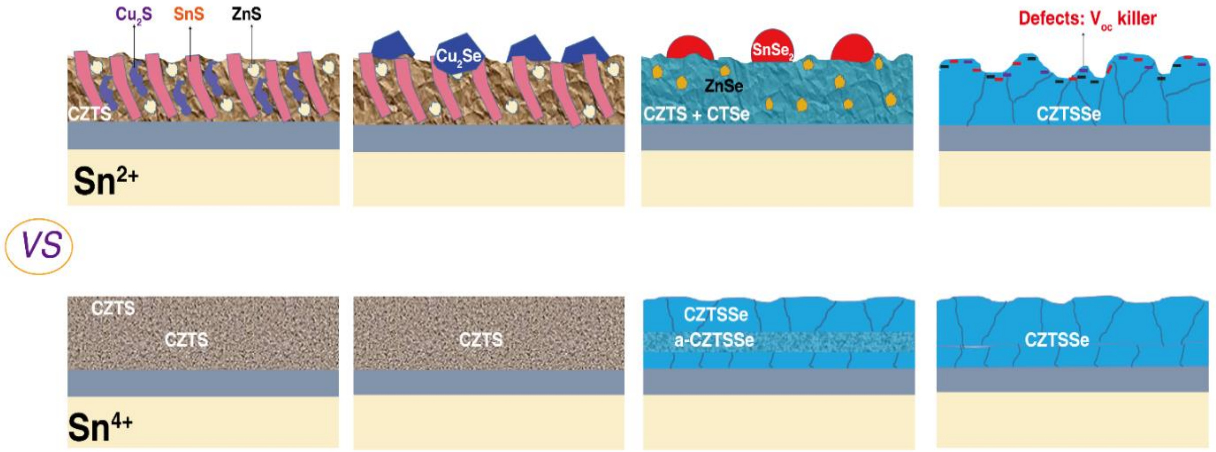

Energy Environ. Sci. 2021, 14, 2369.

JHT on the Electronic Property of the Absorbers

ΔV_{oc}= ~80 mV

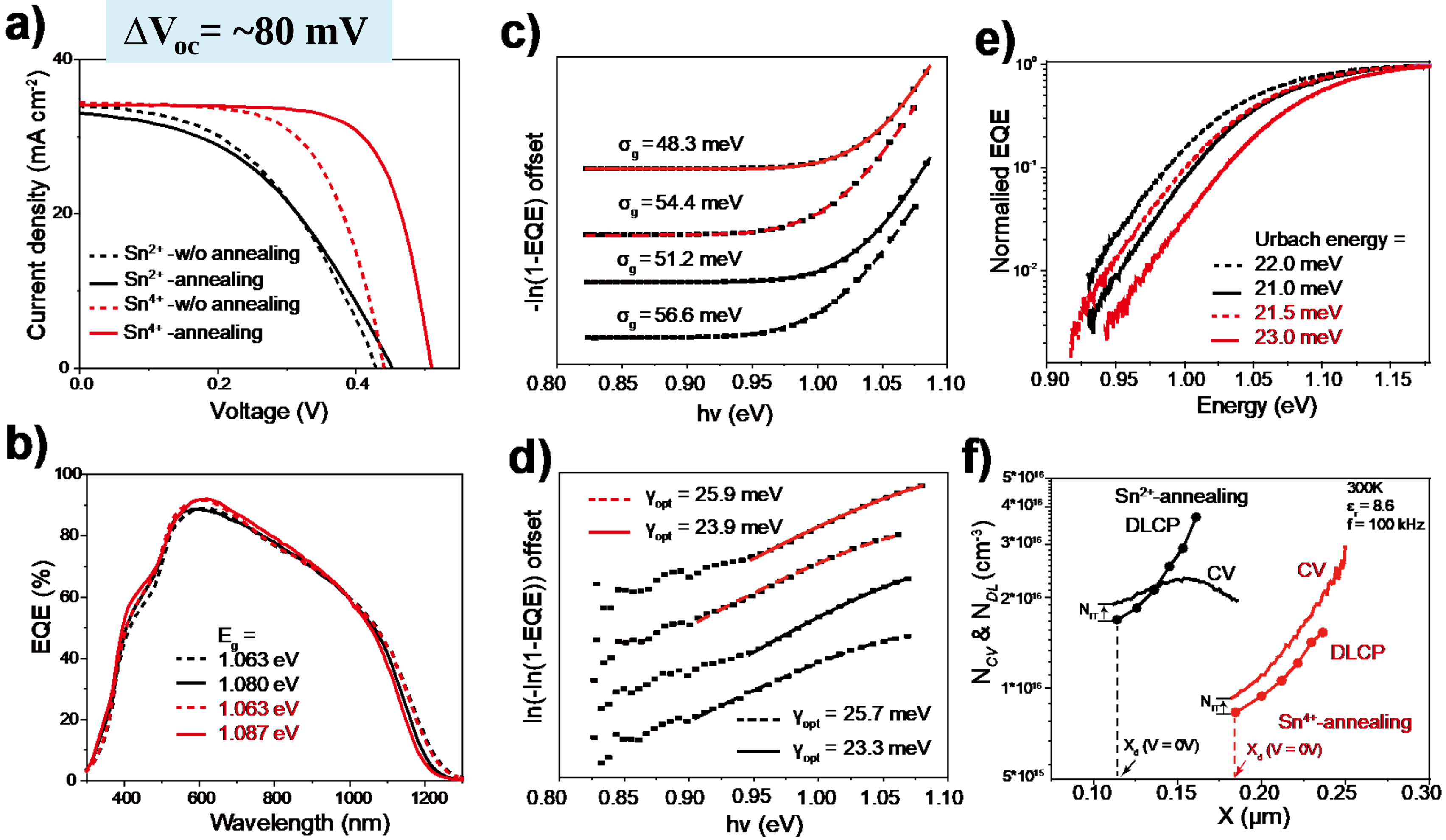

V_{oc}/V_{oc}^{SQ} = 63.7%
FF/FF^{SQ} = 84.1%

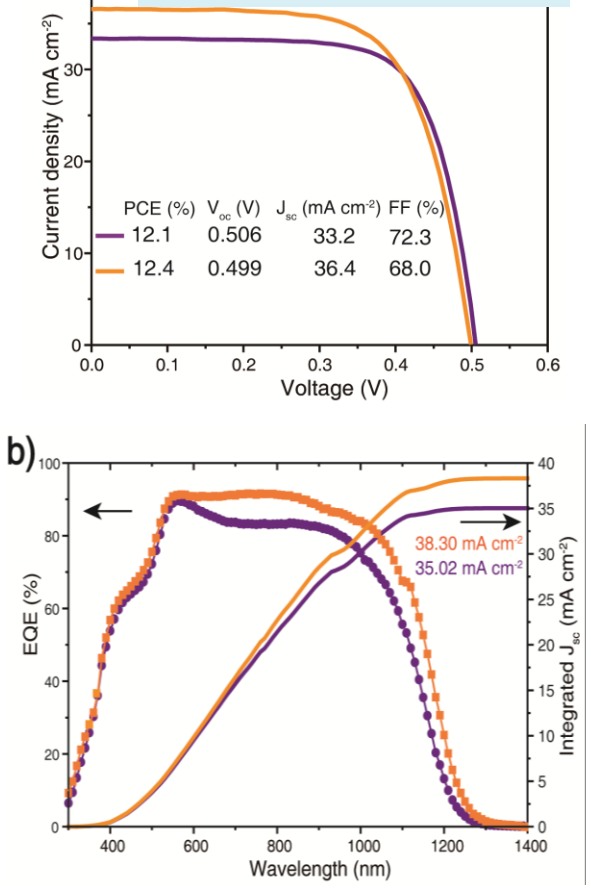

- Band gap (order level) similarly improved upon JHT
- Band tailing (E_U) does not show correlation to V_{oc}
- Charge carrier concentration (especially surface defects) significantly reduced

Same Reaction Path from DMF Solution

$SnCl_4 + 2DMF = Sn(DMF)_2Cl_4$

$Cu(Tu)_3Cl + Zn(Tu)_2(OAc)_2 + Sn(DMF)_2Cl_4 \rightarrow Cu_2ZnSnS_4$

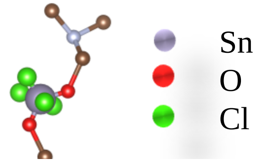

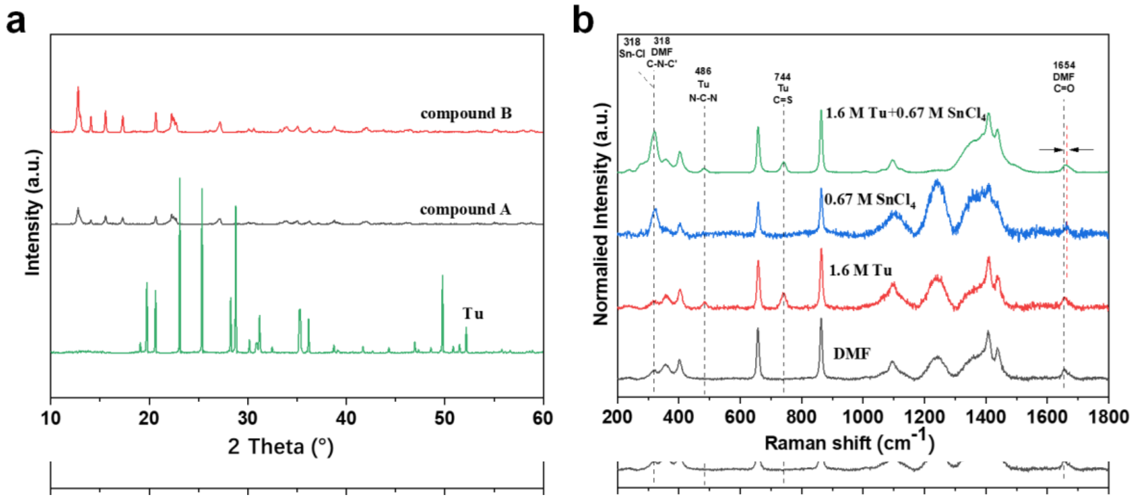

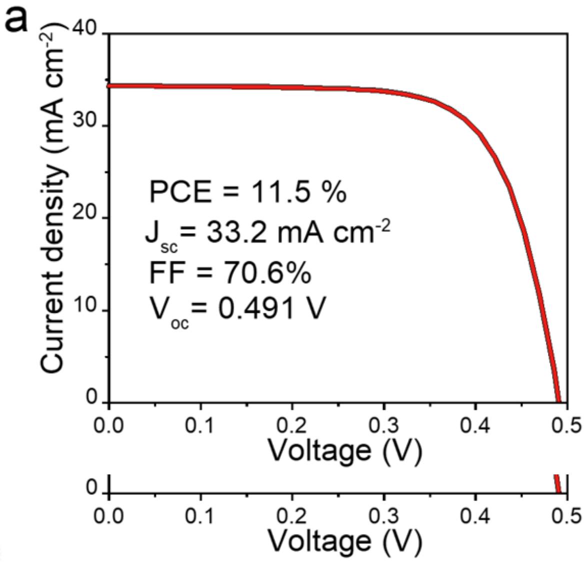

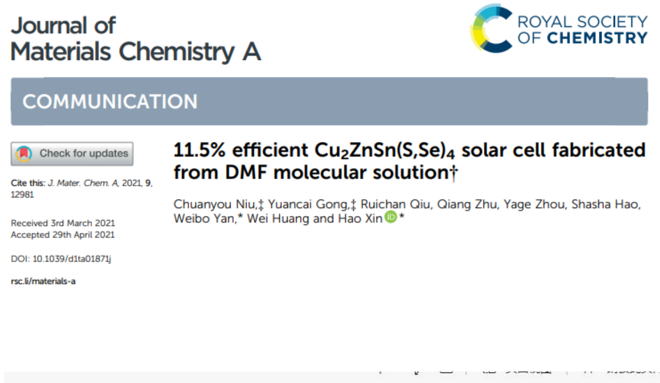
Journal of Materials Chemistry A

ROYAL SOCIETY OF CHEMISTRY

COMMUNICATION

Check for updates

Cite this: J. Mater. Chem. A, 2021, 9, 12981

Received 3rd March 2021
Accepted 29th April 2021

DOI: 10.1039/d1ta01871j

rsc.li/materials-a

11.5% efficient $Cu_2ZnSn(S,Se)_4$ solar cell fabricated from DMF molecular solution†

Chuanyou Niu,‡ Yuancai Gong,‡ Ruichan Qiu, Qiang Zhu, Yage Zhou, Shasha Hao, Weibo Yan,* Wei Huang and Hao Xin*

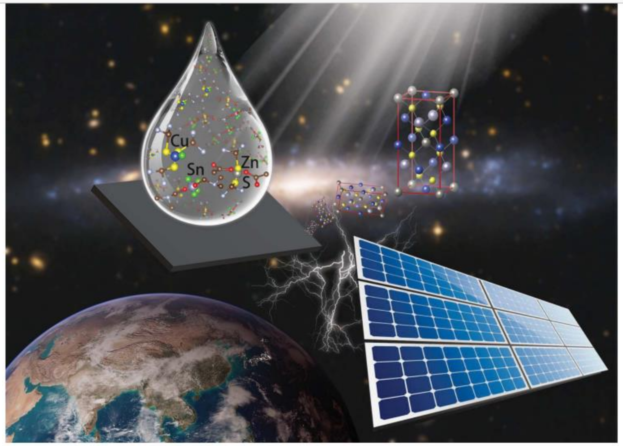

Highlighting a study on a solution processed kesterite solar cell by Prof. Hao Xin's group from Nanjing University of Posts and Telecommunications.

11.5% efficient $Cu_2ZnSn(S,Se)_4$ solar cell fabricated from DMF molecular solution

Efficient CZTSSe thin film solar cells are fabricated from N, N-dimethylformamide (DMF) solution. Studies of chemical reactions of precursors CuCl, $Zn(OAc)_2$, $SnCl_4$, and Thiourea (Tu) in the DMF solution and the reaction path from solution to CZTSSe absorber material show a kesterite structured CZTS precursor film was formed due to the coordination of $SnCl_4$ with DMF, which enables direct phase transformation grain growth mechanism and thus high quality CZTSSe absorber materials. A champion device with an efficiency of 11.5%, a V_{oc} of 0.491 V, and a FF of 70.6% has been achieved, the highest performance of CZTSSe solar cells fabricated from DMF molecular solution.

As featured in:

See Weibo Yan, Hao Xin et al., J. Mater. Chem. A, 2021, 9, 12981.

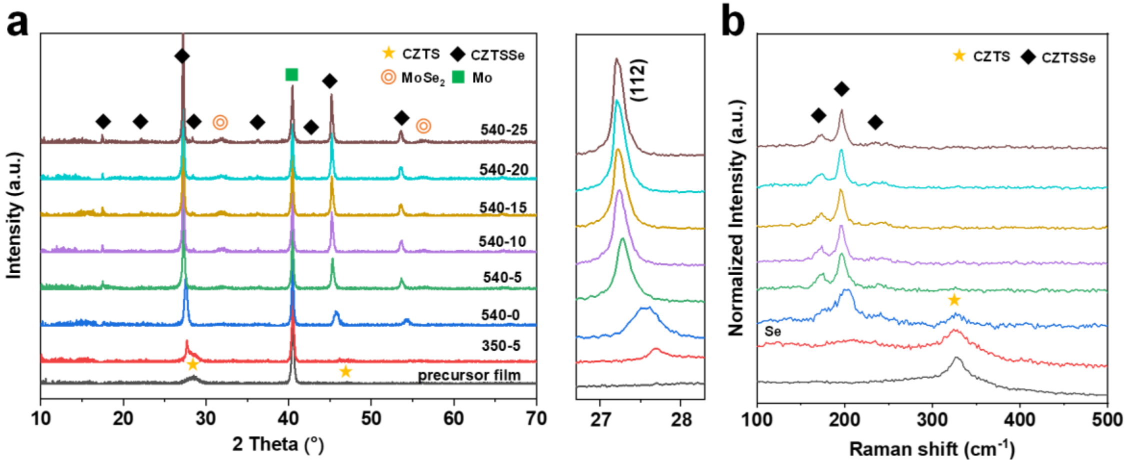

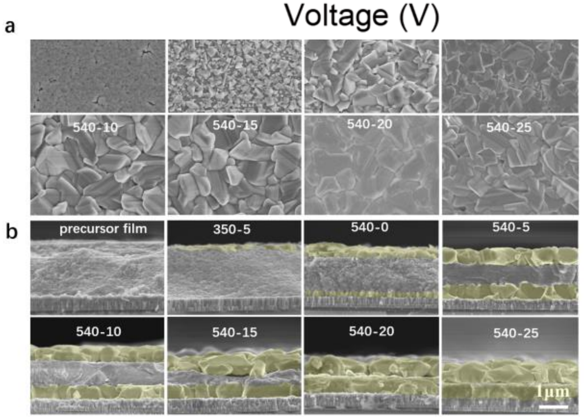

Direct phase transformation grain growth is a universal strategy for achieving high quality kesterite absorber.

2.3 Cu-Zn无序与带尾态及银合金化

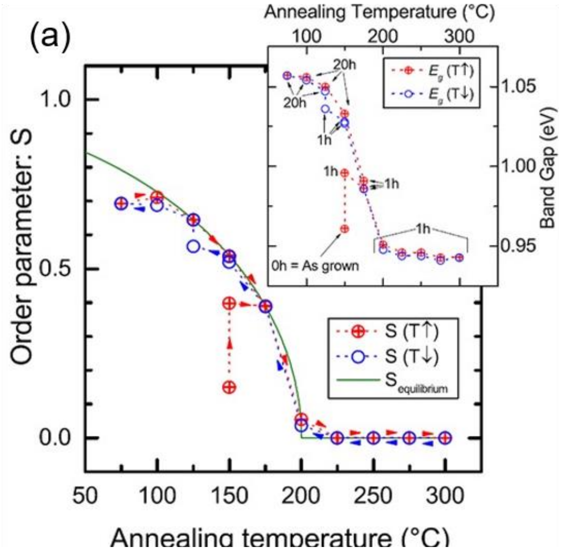

Rey et al. *Appl. Phys. Lett.* **2014,** *105*, 112106.

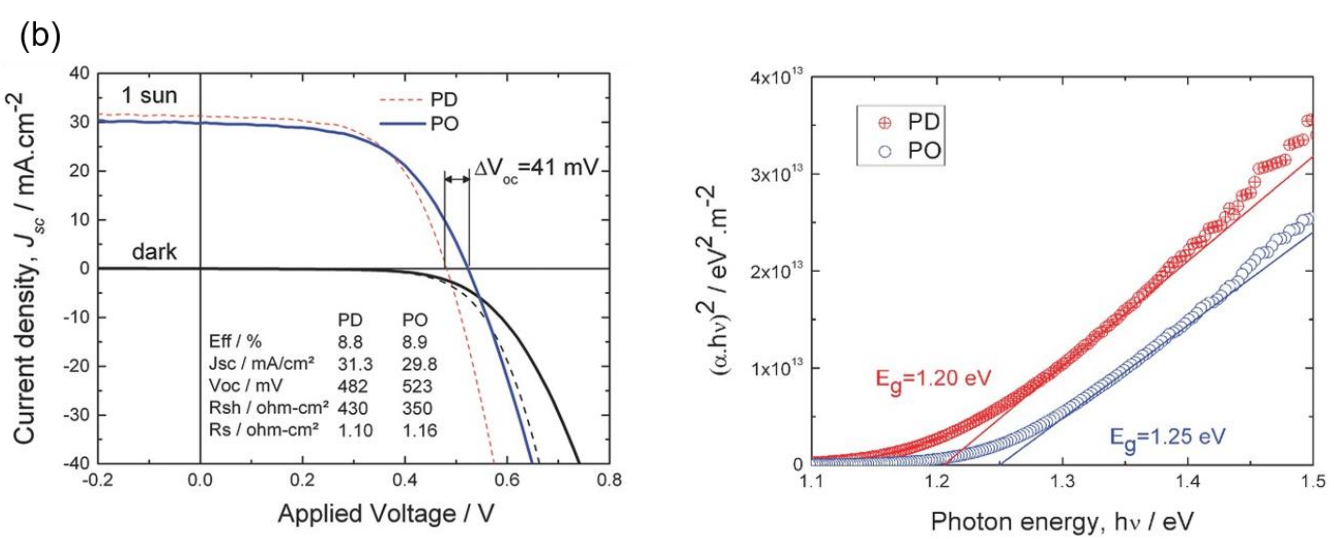

Bourdais, et al. *Adv. Energy Mater.* **2016,** *6*, 1502276.

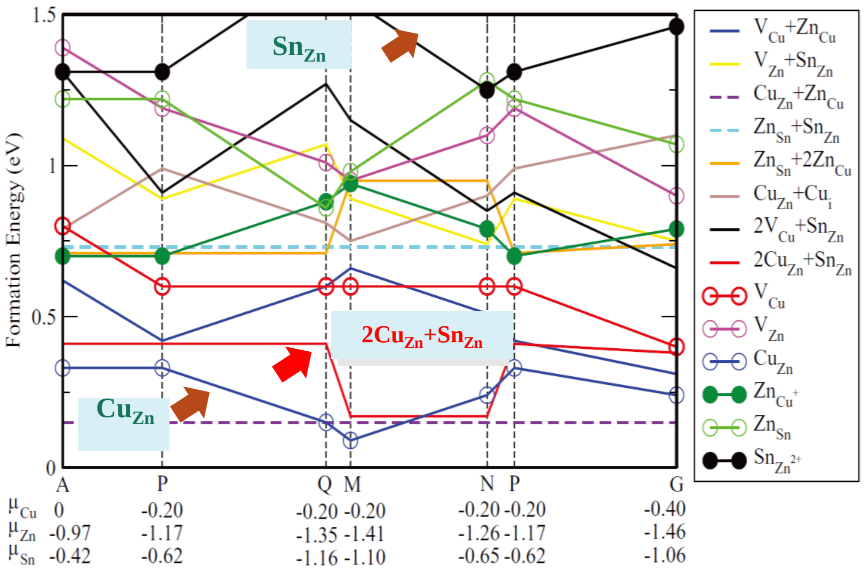

Chen et al. *Adv. Mater. 2013, 25, 1522* .

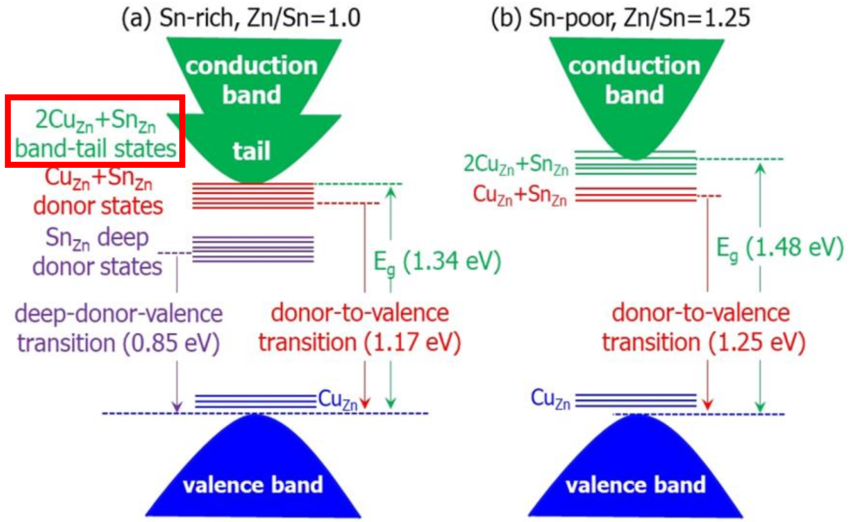

Ma et al. *J. Phys. Chem. Lett 2019 10, 7929.*

Ag Alloying via Direct Phase Transformation Grain Growth

RESEARCH ARTICLE

Ag Incorporation with Controlled Grain Growth Enables 12.5% Efficient Kesterite Solar Cell with Open Circuit Voltage Reached 64.2% Shockley–Queisser Limit

Yuancai Gong, Ruichan Qiu, Chuanyou Niu, Junjie Fu, Erin Jedlicka, Rajiv Giridharagopal, Qiang Zhu, Yage Zhou, Weibo Yan, Shaotang Yu, Jingjing Jiang, Sixin Wu, David S. Ginger,* Wei Huang,* and Hao Xin**

$CuCl + 3Tu = Cu(Tu)_3Cl$

$Zn(OAc)_2 + 2Tu = Zn(Tu)_2(OAc)_2$

$SnCl_4 + 2DMSO = Sn(DMSO)_2Cl_4$

→ Cu_2ZnSnS_4

$AgNO_3 + 3Tu = Ag(Tu)_3NO_3$

→ **$(Ag,Cu)_2ZnSnS_4$**

Ag^+ coordinates with Tu as Cu^+

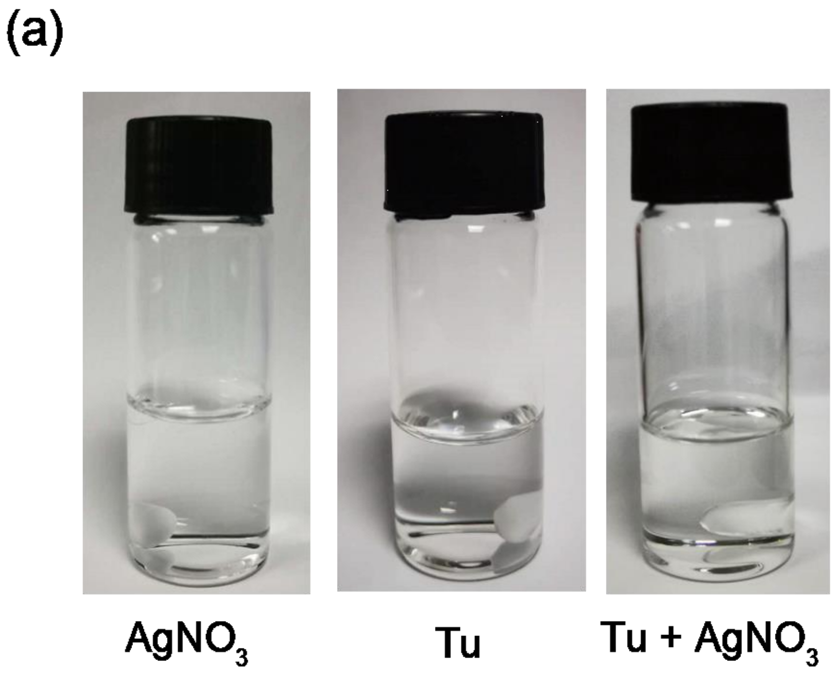

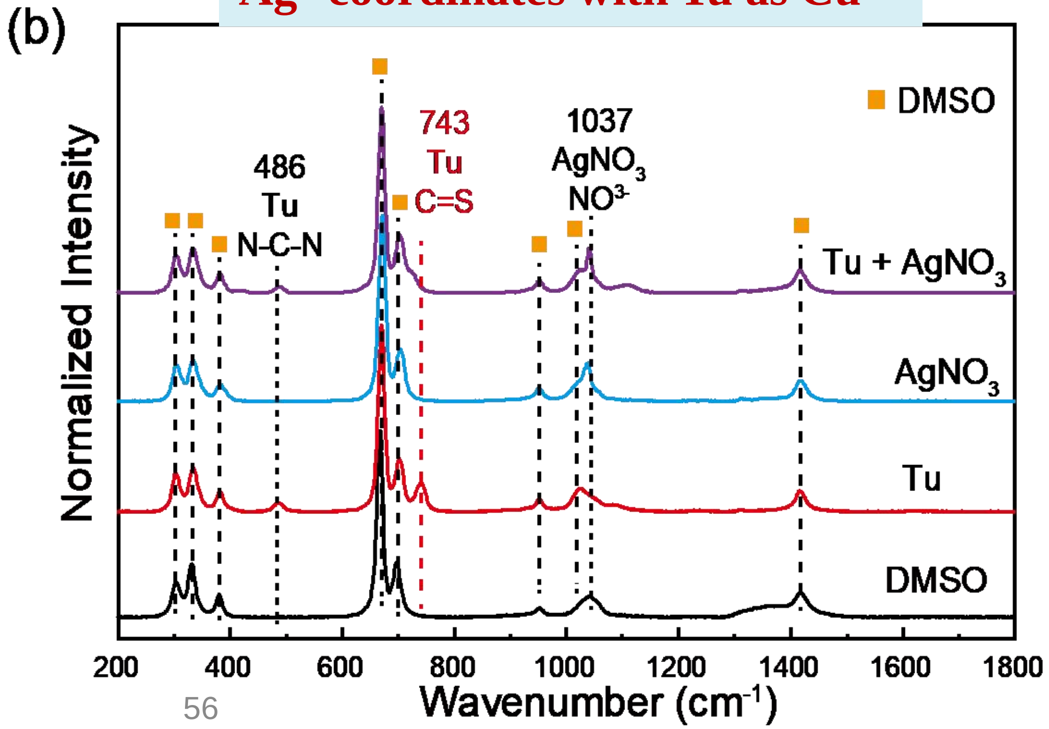

Ag Incorporation Through DMSO Solution

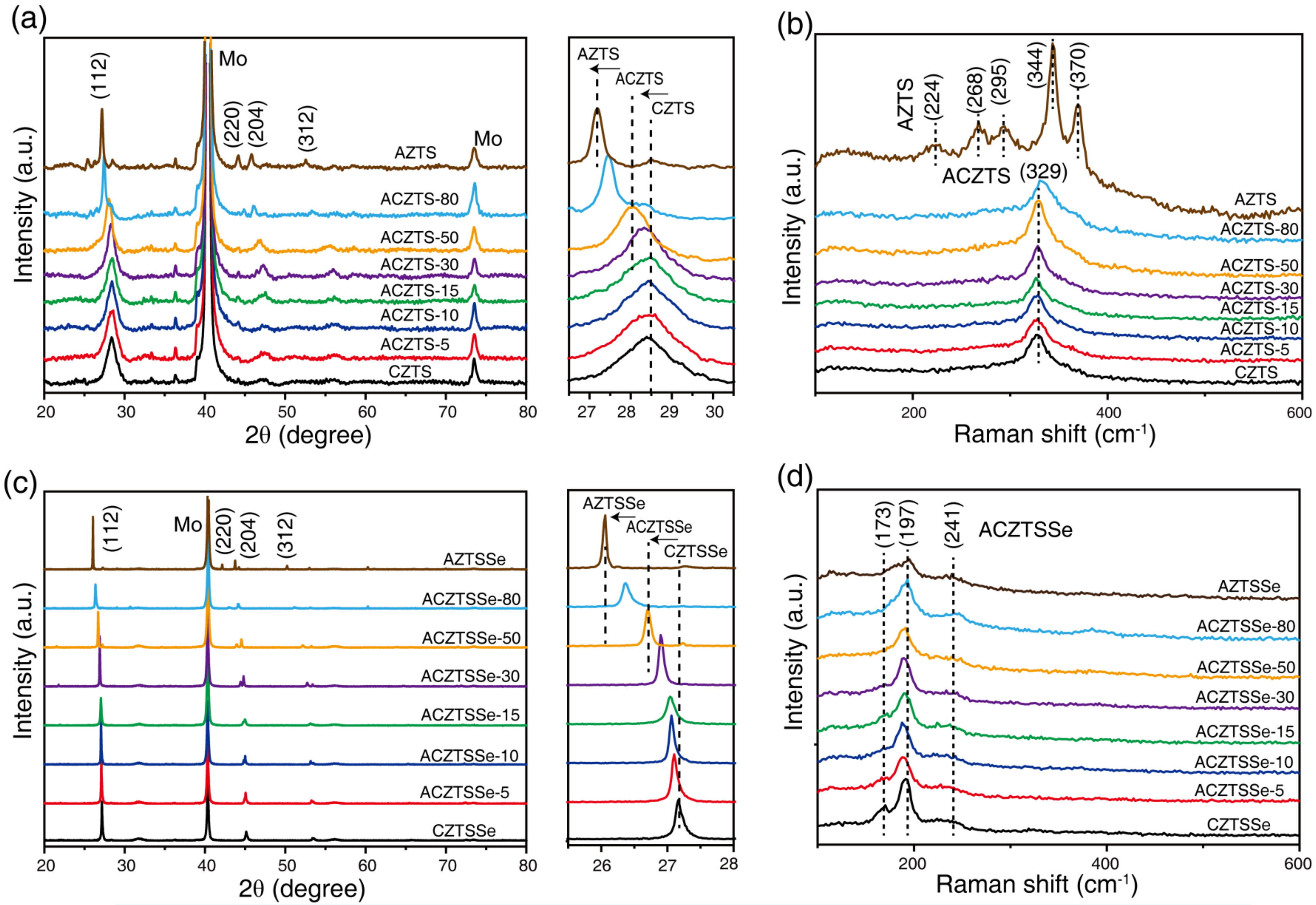

$(Ag_x,Cu_{1-x})_2ZnSnS_4$ (X=0-1) successfully fabricated.

New Ag Alloying Strategy Mitigates Band Tailing

JHT (200ºC/20 h, vaccum)

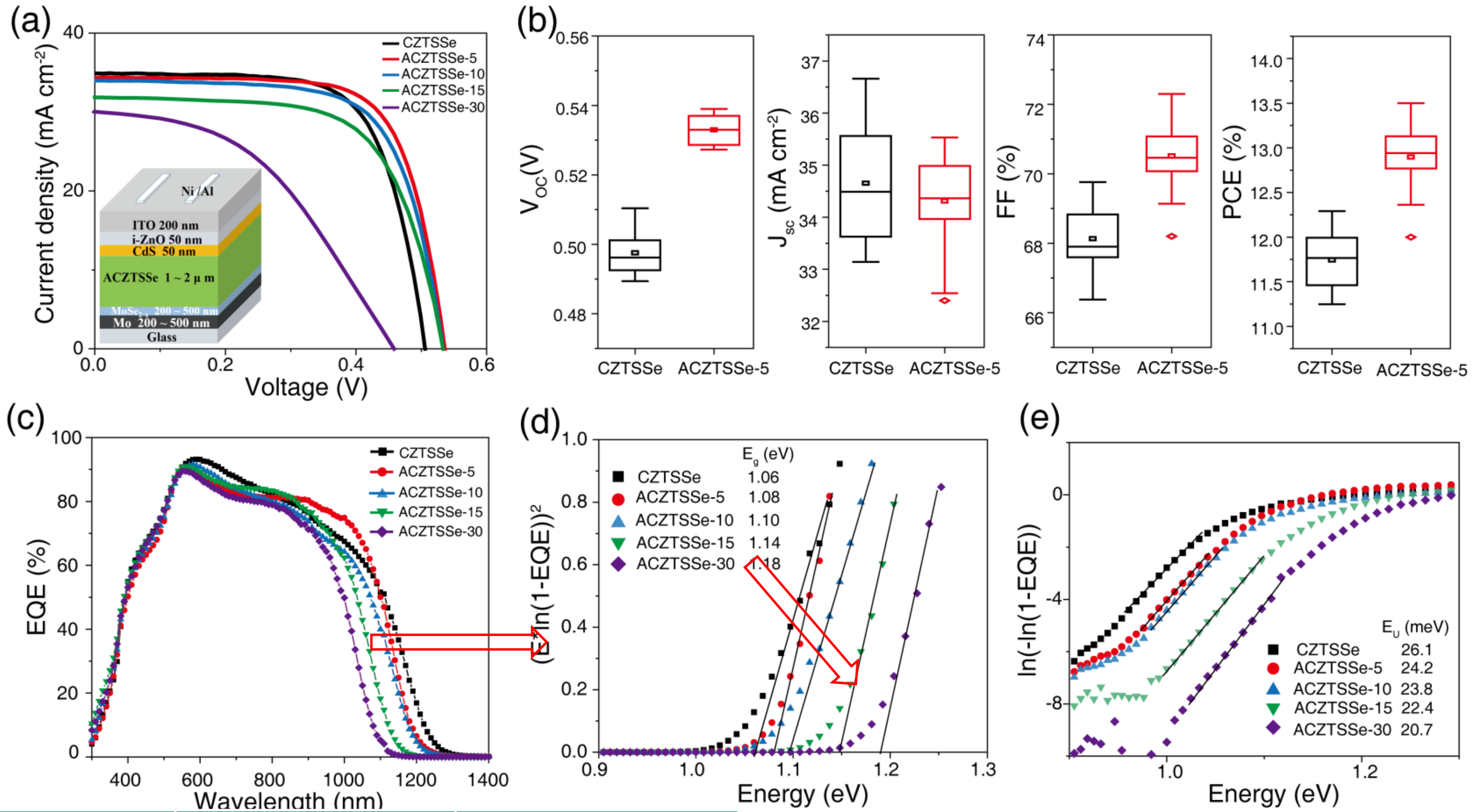

Device	V_{oc} (V)	J_{sc} (mA cm^{-2})	FF (%)	PCE (%)
CZTSSe	0.497±0.006	34.65±1.10	68.1±0.91	11.7±0.31
ACZTSSe-5	0.533±0.004	34.3±0.80	70.5±0.88	12.9±0.33
ACZTSSe-10	0.536±0.006	33.7±1.23	65.8±0.91	11.9±0.52
ACZTSSe-15	0.529±0.007	31.86±0.83	59.7±3.85	10.07±0.86
ACZTSSe-30	0.401±0.070	30.04±1.81	39.35±4.79	4.86±1.42

- **Band gap increases with Ag concentration increases**
- **E_U decreases with Ag concentration increases**
- **High efficiency with 5-10% Ag**

Ag (5%) Alloying on Defect Property

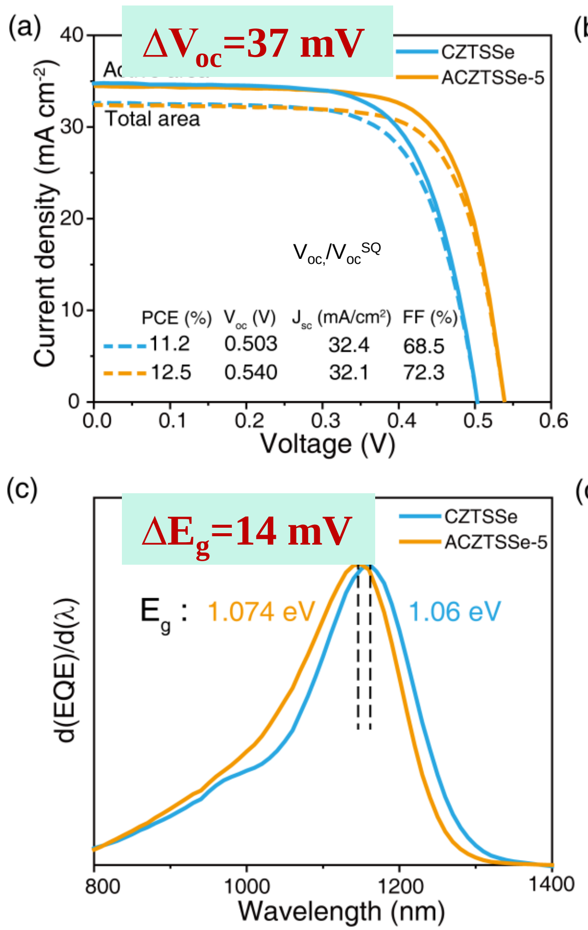

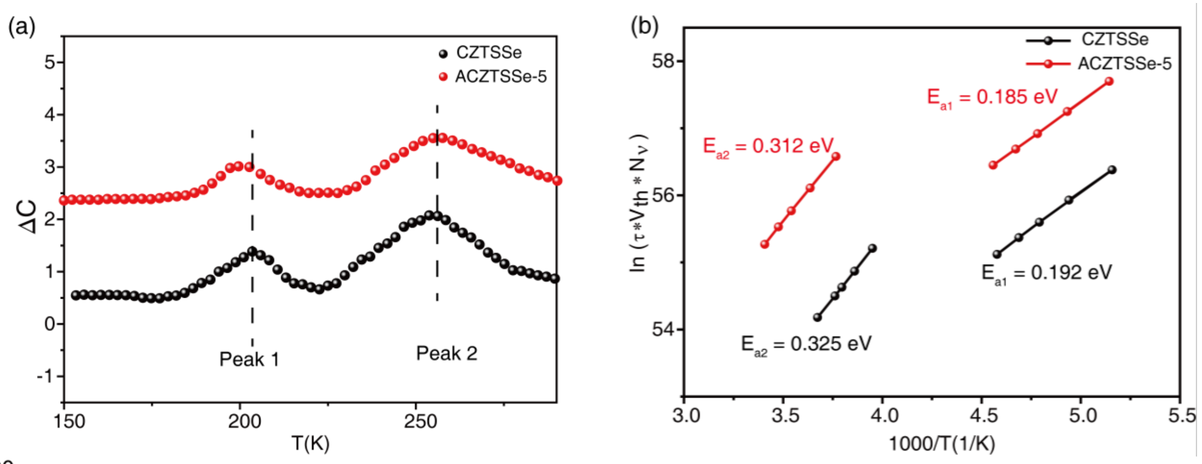

Device	Defect	N_T (cm^{-3})	Lowest reported
No Ag	Cu_{Zn}	2.84×10^{13}	5.79×10^{13}
	Cu_{Sn}	2.22×10^{13}	8.32×10^{13}
Ag (5%)	Cu_{Zn}	5.12×10^{12}	1.50×10^{13}
	Cu_{Sn}	1.48×10^{13}	3.25×10^{13}

Total area: 12.5%

Active area: 13.5%

V_{oc}/V_{oc}^{SQ} = 64.2%

- **Suppresses Cu_{Zn} and Cu_{Sn}**
- **E_U decreased 2.1 meV, V_{oc} increased 23 mV**

3. 异质结界面缺陷与调控

Optimization of JHT Temperature

JHT (12h, in N_2 filled glovebox)

ACZTSSe-10

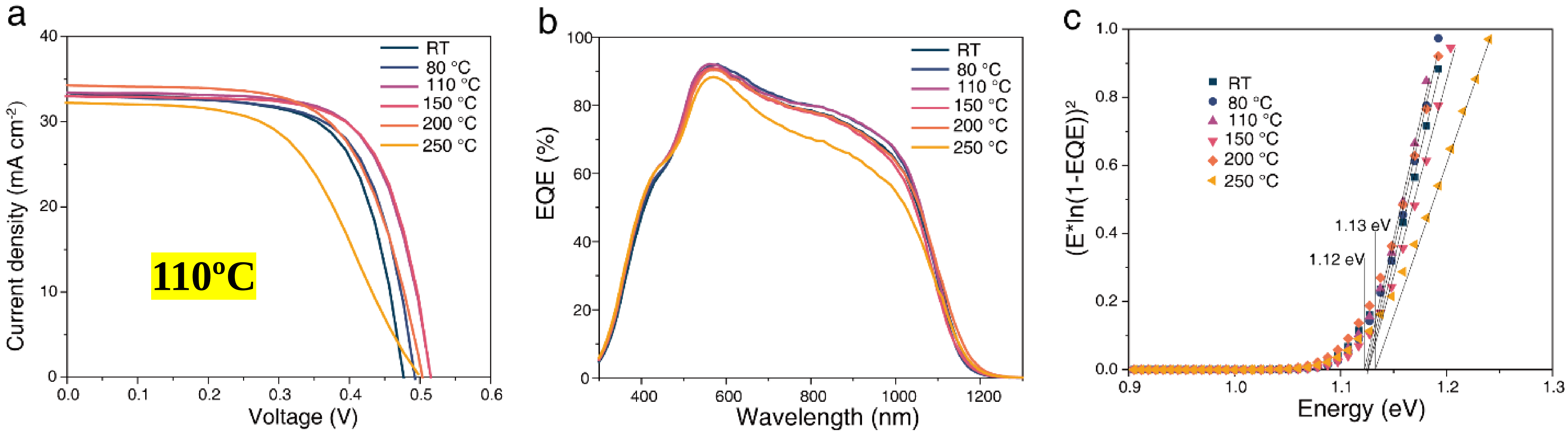

- V_{OC} increase observed at temperature as low as 80ºCwith 110ºC/150ºC the best
- No band gap increase at the optimized temperature
- No obvious improvement on Cu-Zn order level

Nature Energy, 2022.

Low-Temp Junction Heat Treatment (LT-JHT)

110ºC

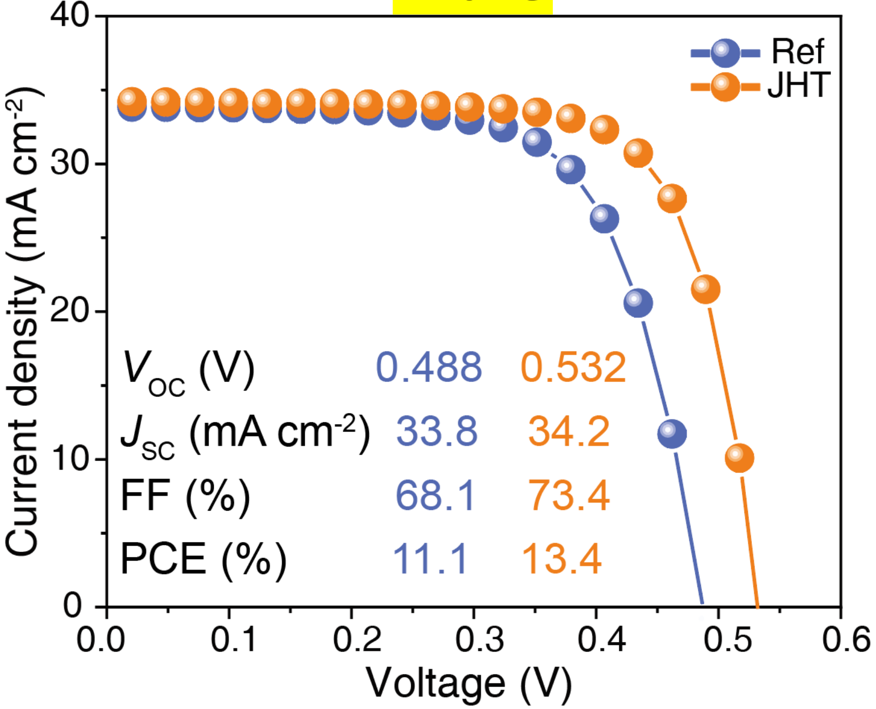

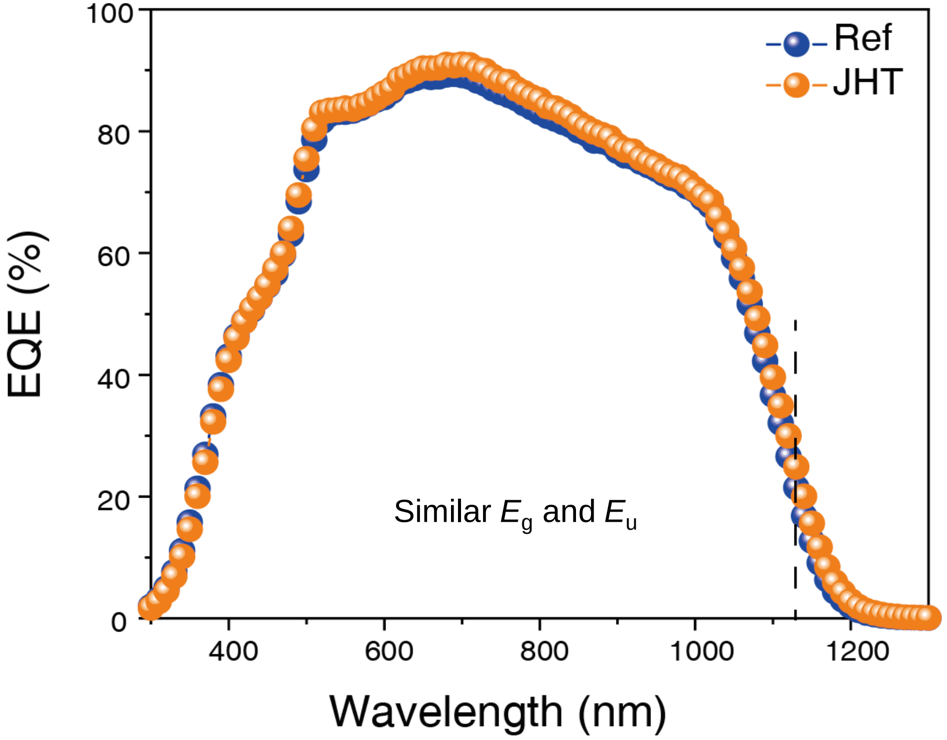

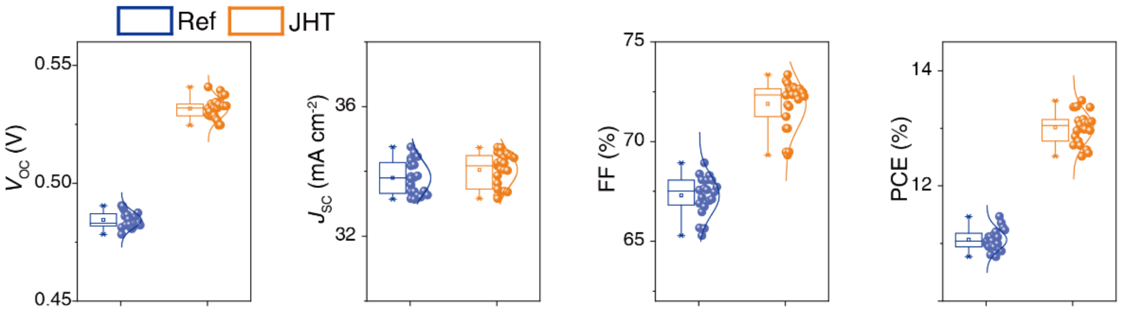

- **No change on band gap, same E_U**
- **No obvious improvement on absorber bulk**
- **Improvement comes from heterojunction**

JHT of CZTS/CdS and CZTSe/CdS

CZTS/CdS

270 °C/10 min

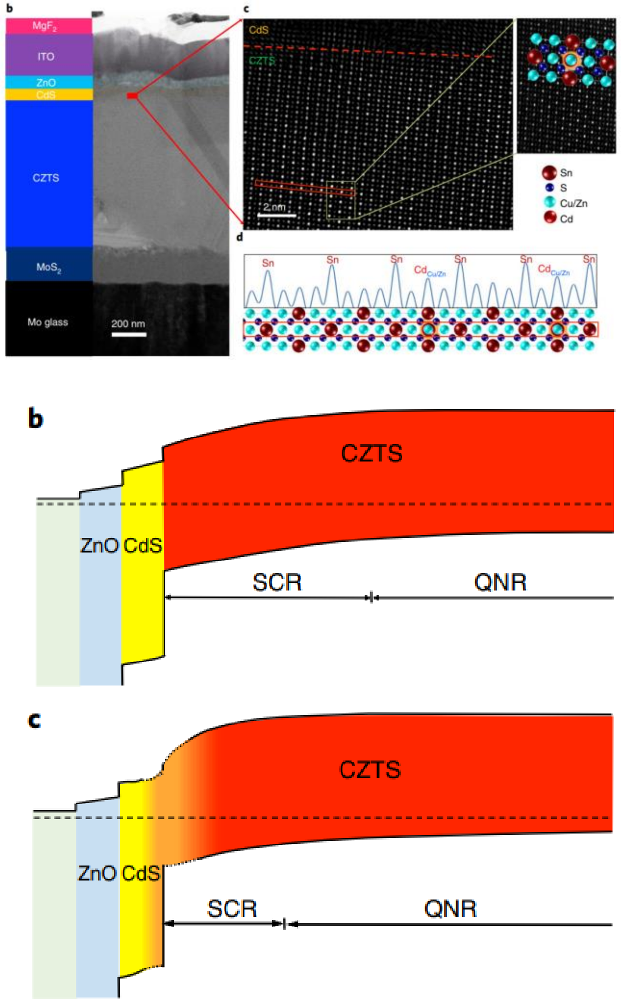

Yan C et al. Nat. Energy, 2018, 3(9): 764-772.

300 °C/8 min

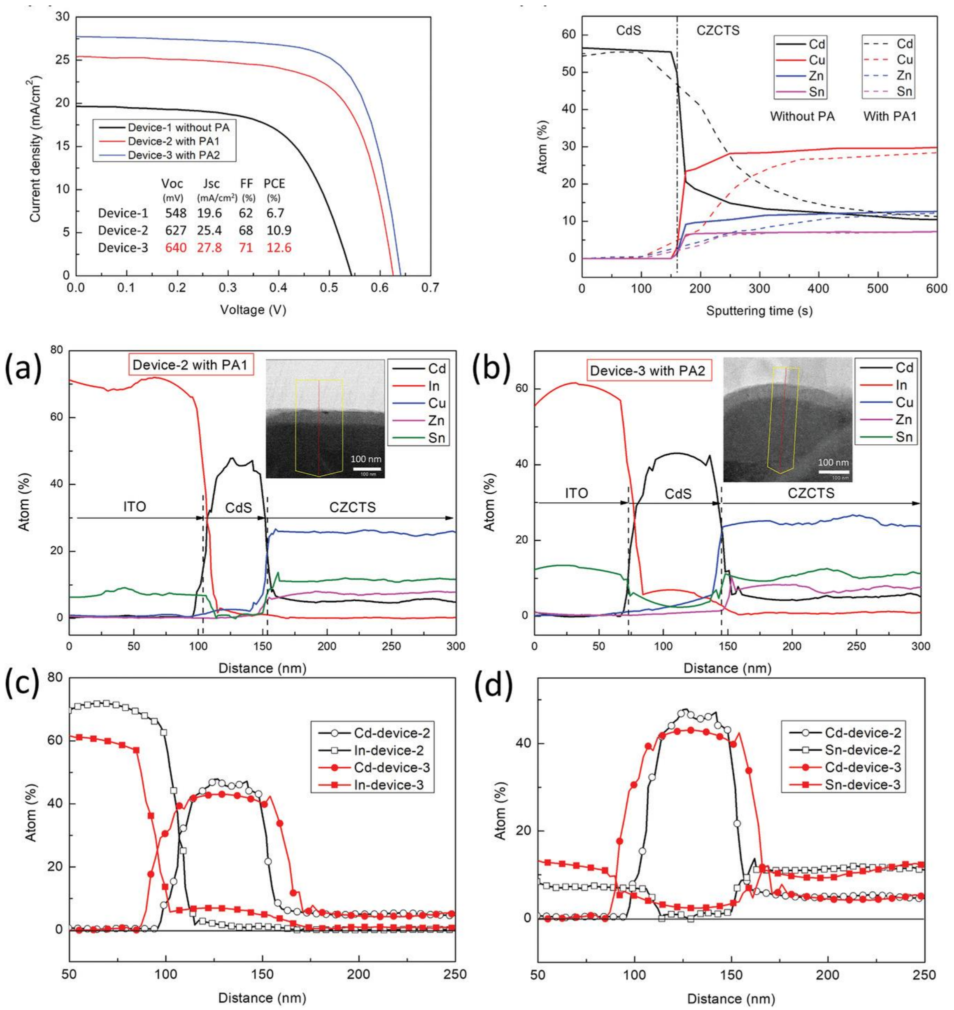

Su Z et al, Adv. Mater. 2020, 32, 2000121

CZTSe/CdS

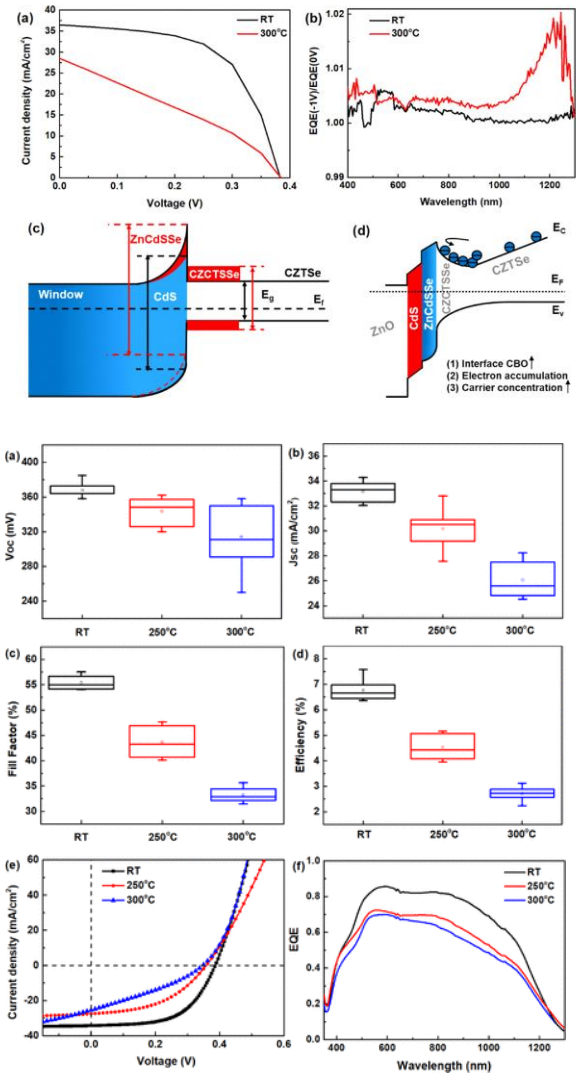

Wang S et al. ACS AMI 2021, 13, 12211.

Interface Recombination Dynamics and Defect Property

M-TPV/M-TPC

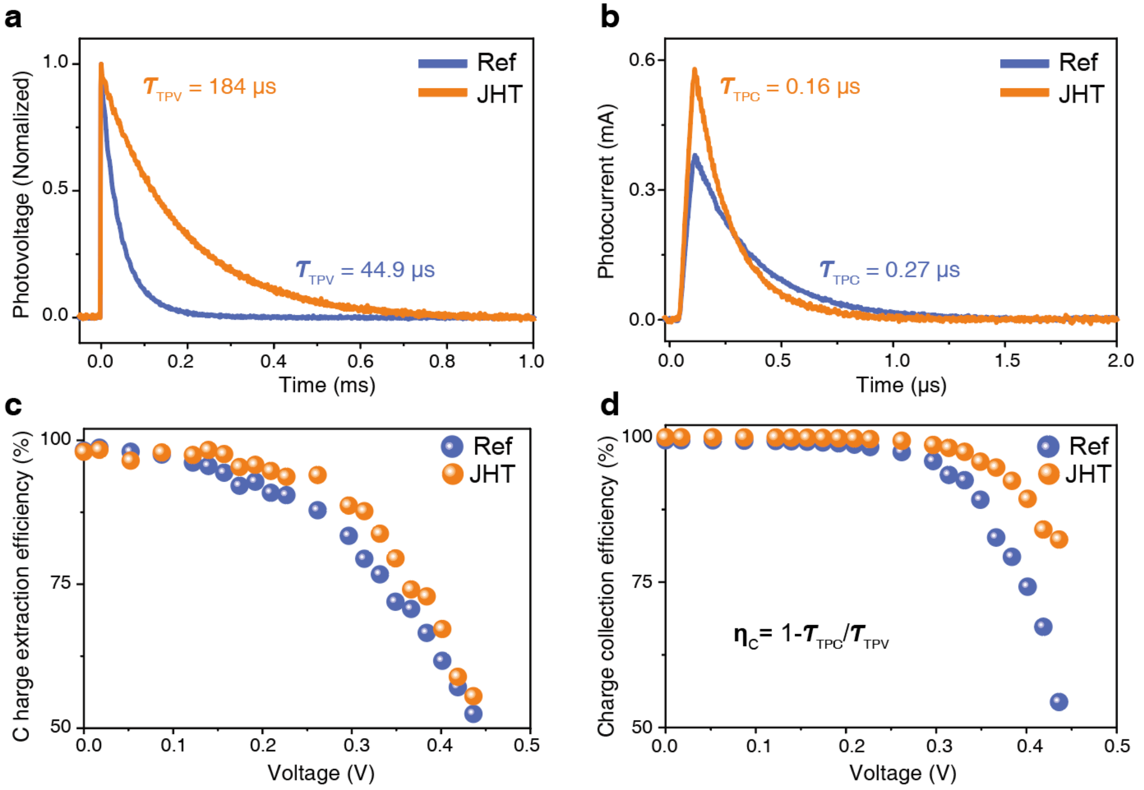

charge extraction efficiency — charge collection efficiency

recombination within the absorber — recombination at the heterojunction

CV/DLCP

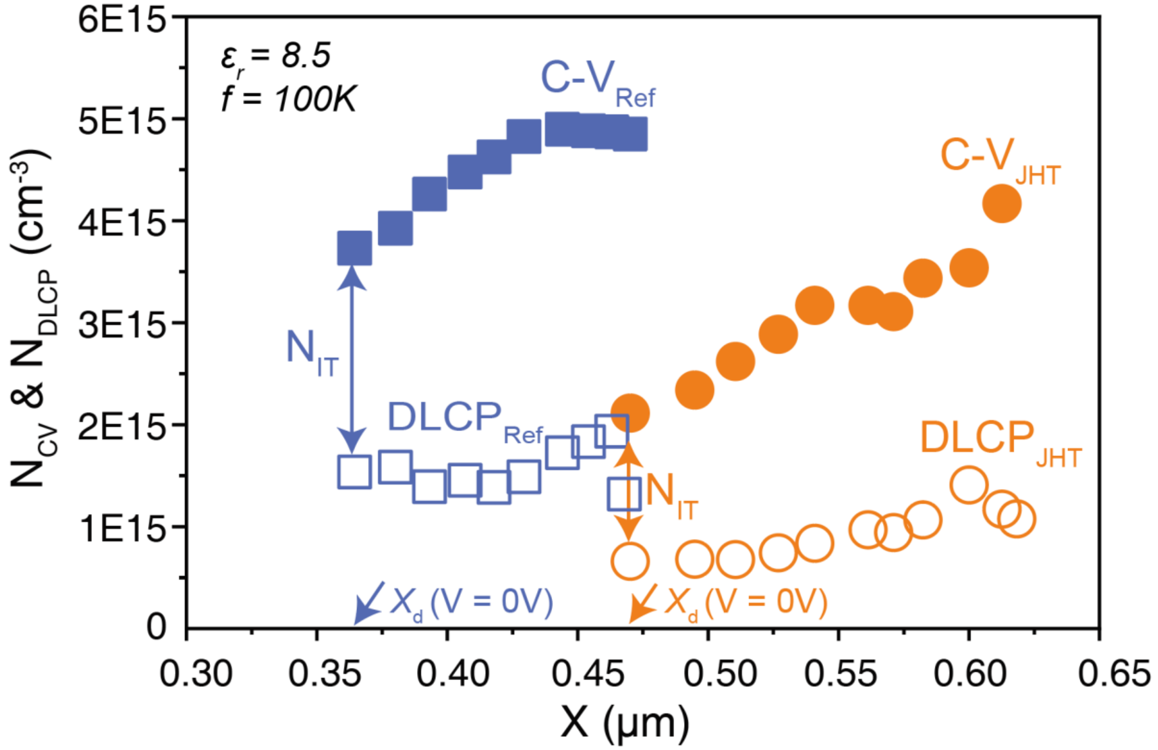

- **LT-JHT significantly reduces interface recombination**
- **LT-JHT greatly reduces interface charge density**

Interface Recombination: CZTSSe vs CISSe

V_{OC}-T

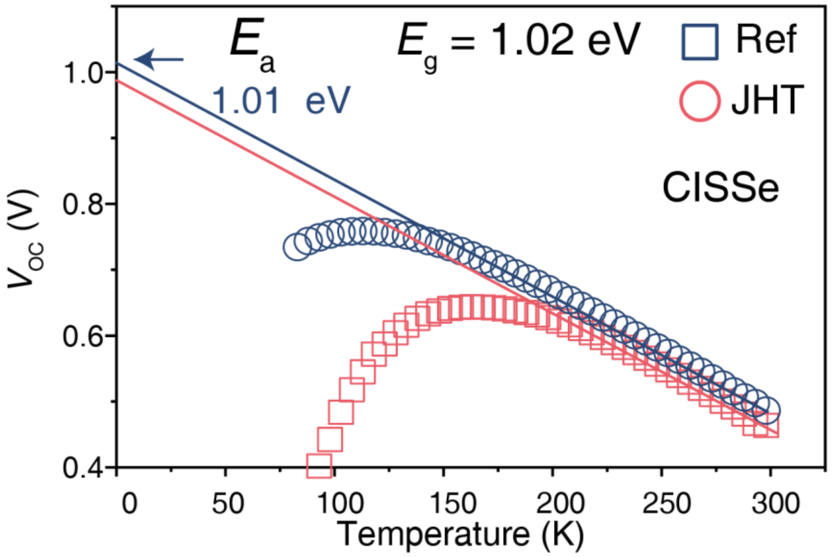

V_{OC}-T

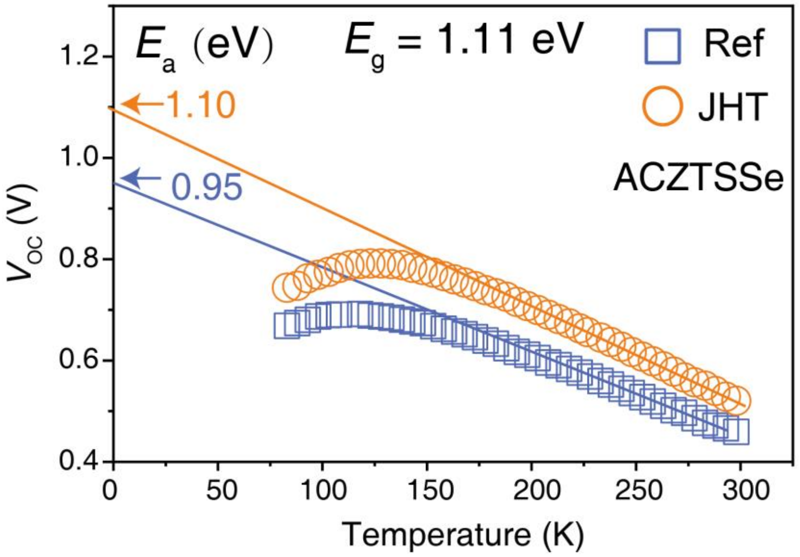

Raman

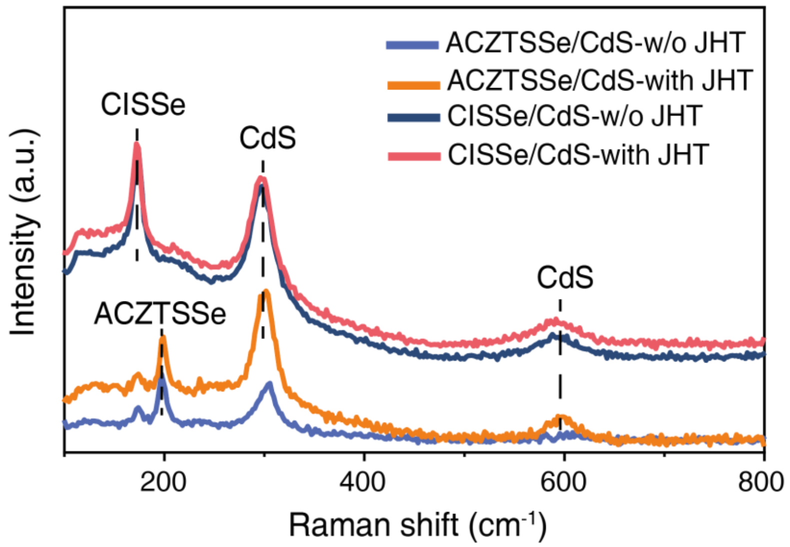

CISSe

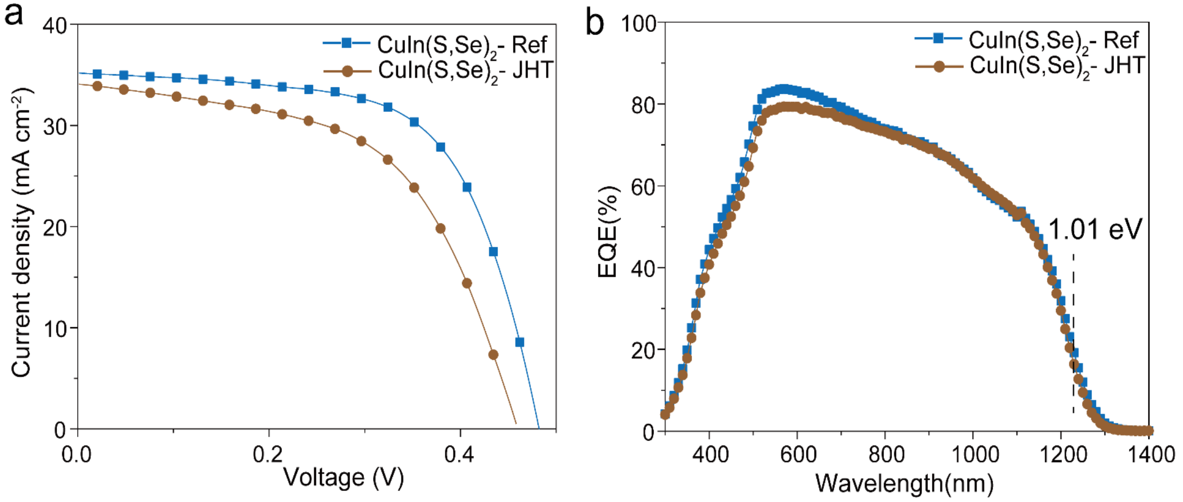

CZTSSe

- **JHT almost eliminates interface recombination**
- **Low CdS crystallinity**
- **JHT significant improves crystallinity of CdS**

CISSe

- **Perfect heterojunction interface**
- **JHT deteriorates interface**
- **High CdS crystallinity**
- **JHT has little effect on CdS**

LT-JHT Induces Interface Elemental Di-Mixing

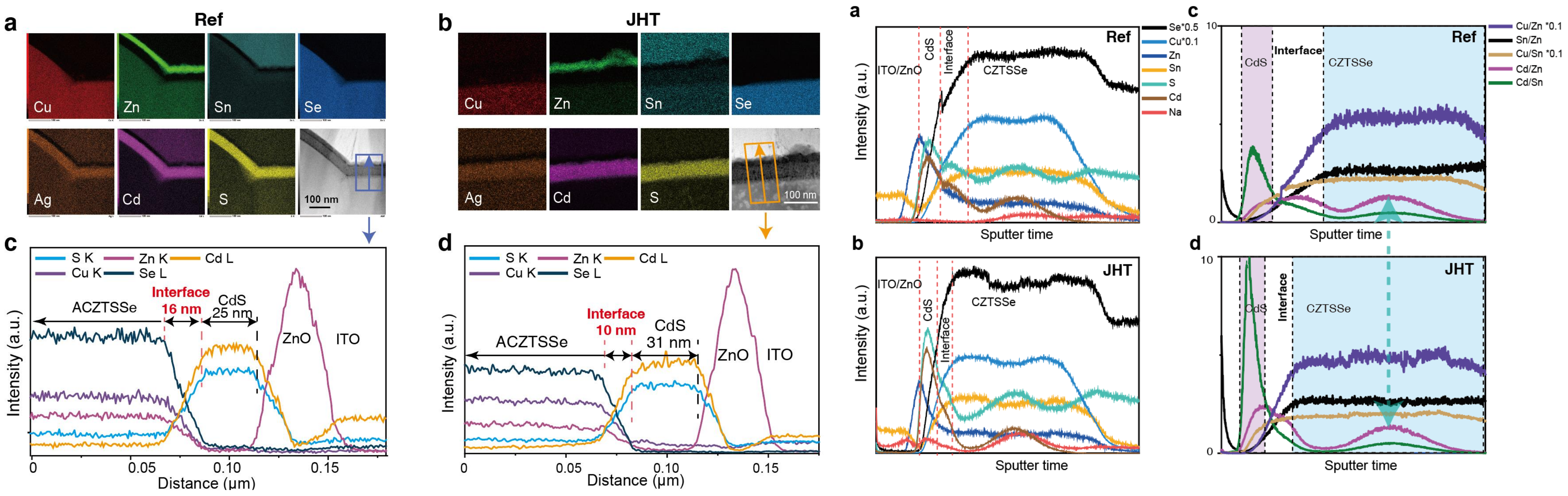

- Cd in CZTSSe and Zn in CdS are observed in Ref sample
- Interface narrows and sharps upon low-temperature JHT
- Elemental di-mixing: Cd and Zn back to original position
- Interface moves toward CdS layer

Elemental Di-mixing Enables Epitaxial Interface

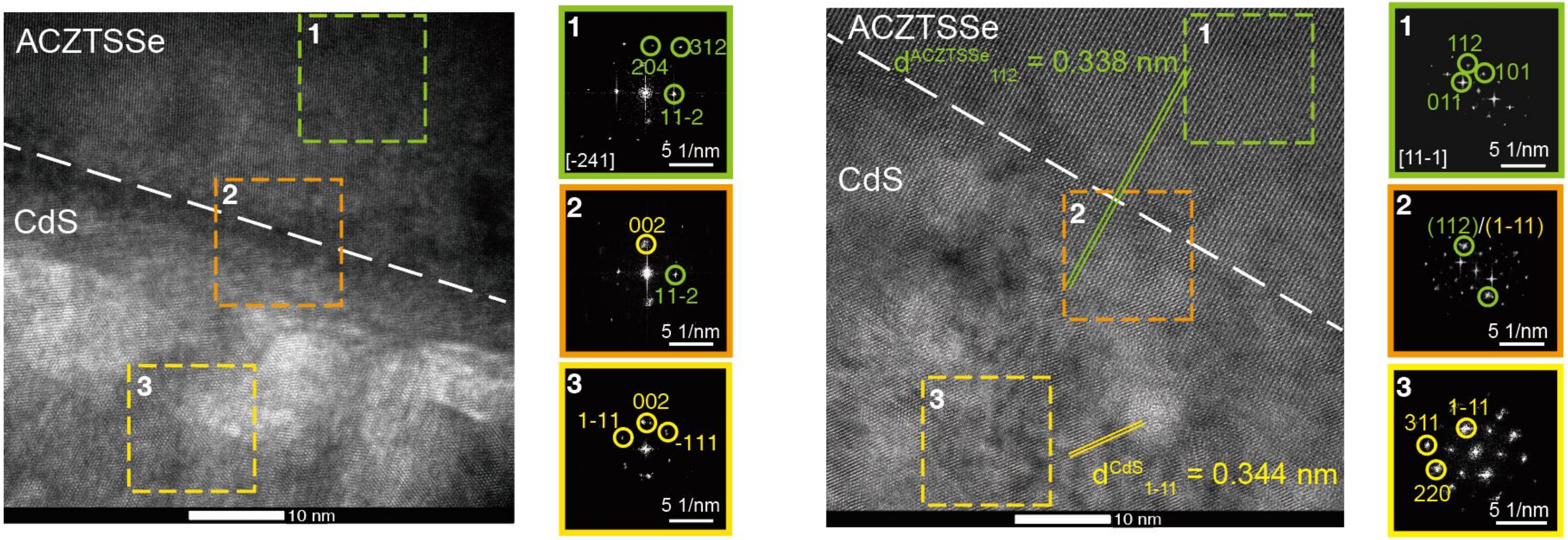

- Low crystallinity of CZTSSe and CdS
- Defective and non-coherent interface

- Improved crystallinity for CZTSSe and CdS
- Coherent interface: CZTSSe(112)ǁCdS(111)

Nature Energy, 2022.

Heterojunction Interface: CZTSSe vs CISSe

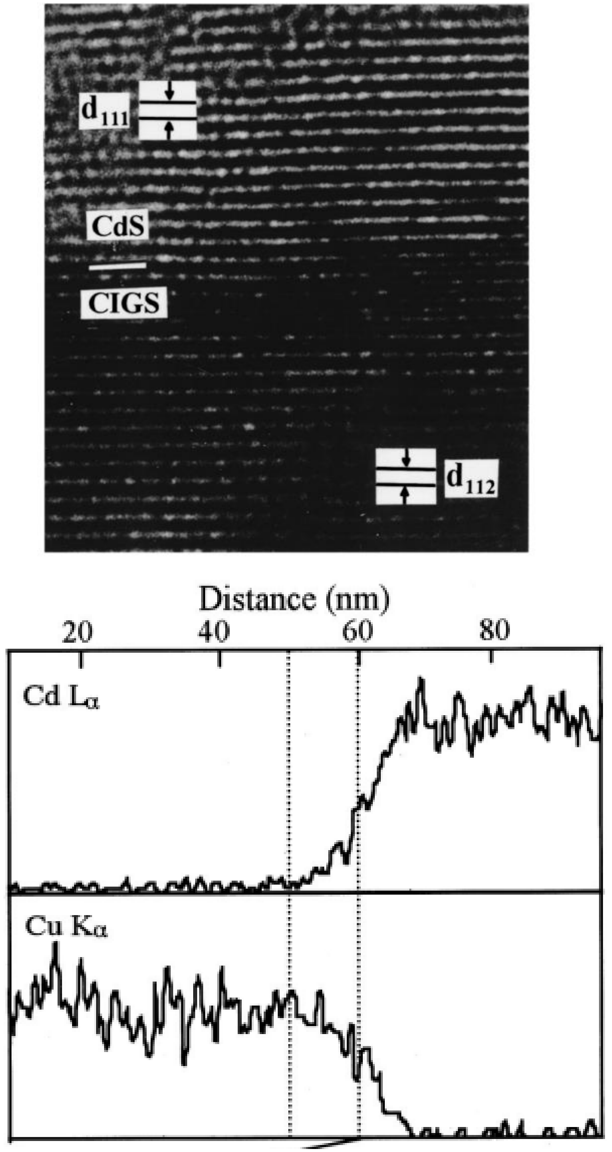

Nakada T et al. . Appl. Phys. Lett., 1999.

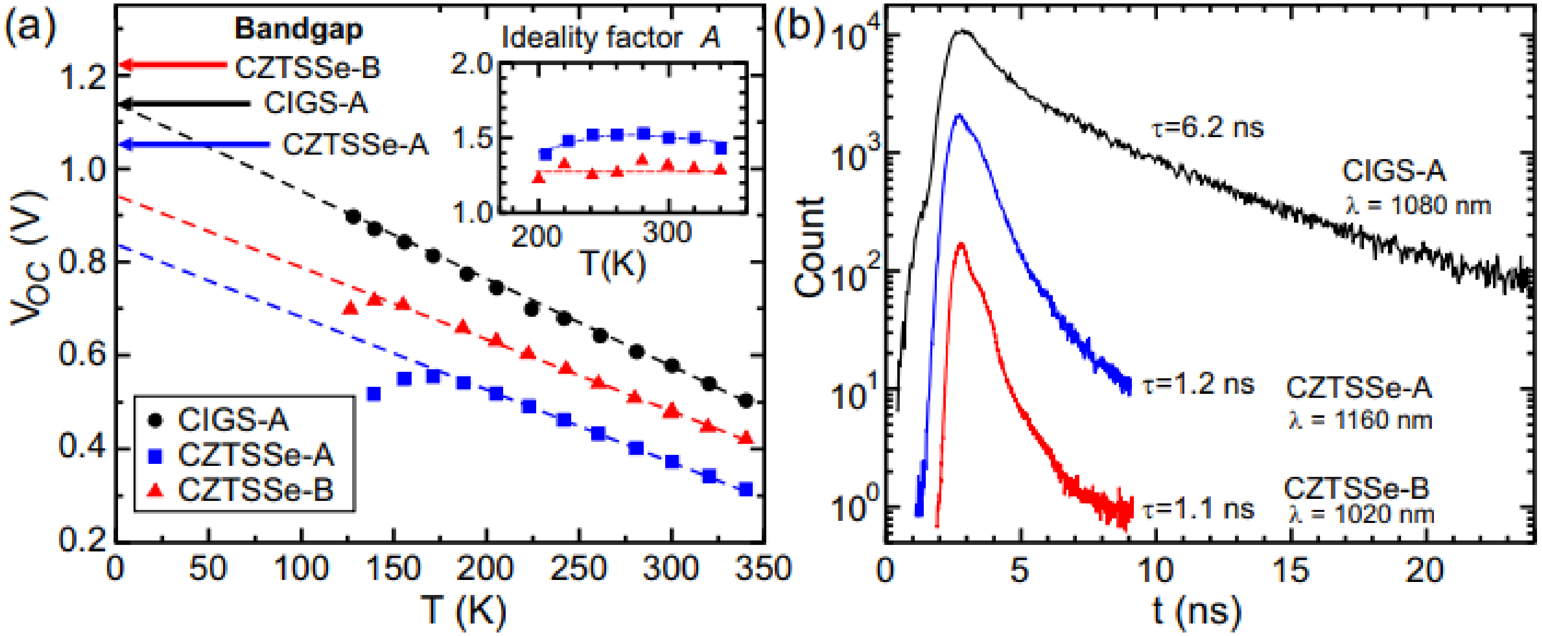

Gunawan O et al. Appl. Phys. Lett., 2010.

CIGS/CdS:

- $E_a \approx E_g$
- less interface recombination
- epitaxial heterointerface
- Cu-poor surface
- Cd^{2+} occupies V_{Cu}
- buried pn junction

CZTSSe/CdS:

- $E_a < E_g$
- serious interface recombination
- Defective heterointerface
- Cu-poor surface ??
- Cd^{2+} occupies V_{Cu}??
- buried pn junction??

Construction of CZTSSe/CdS Interface

NH$_4$OH etching

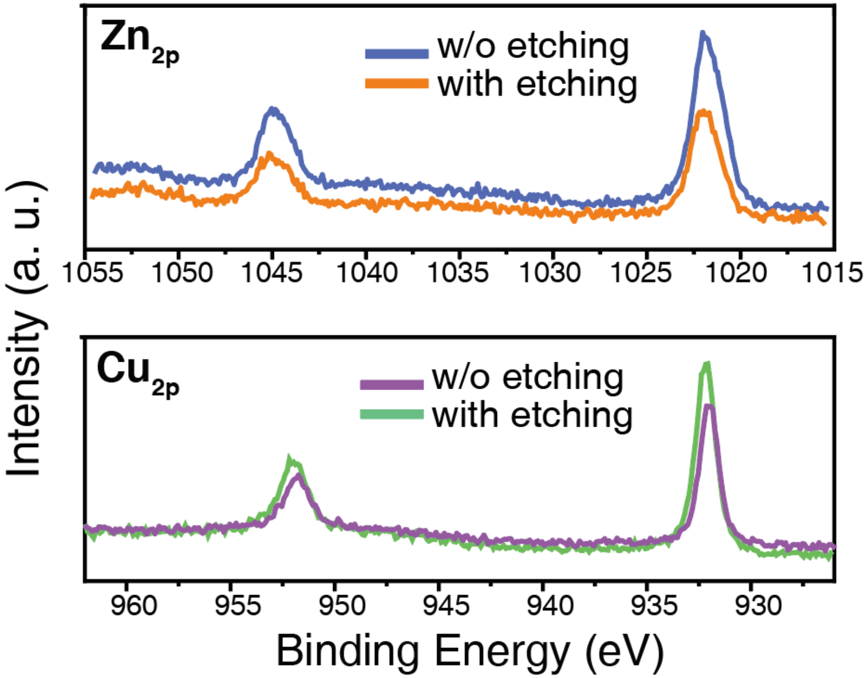

Zn Cu intensity change

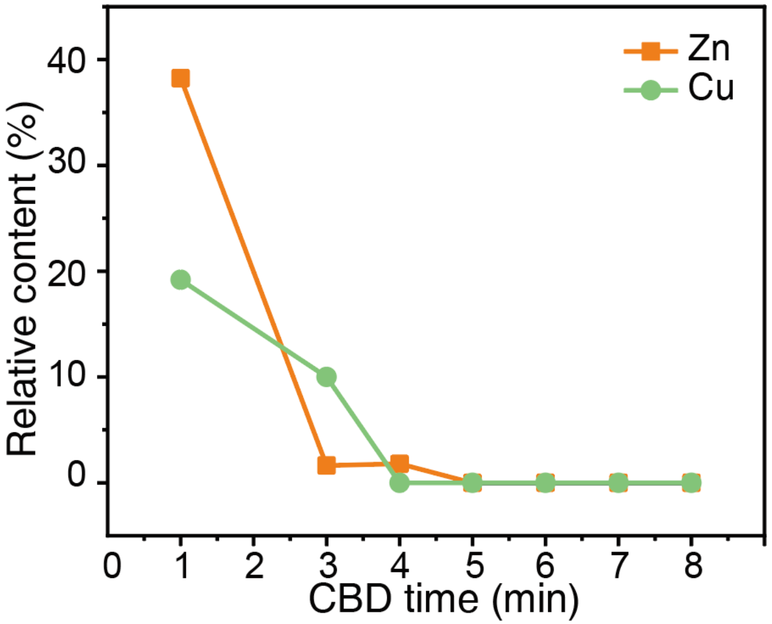

Device with etching and JHT

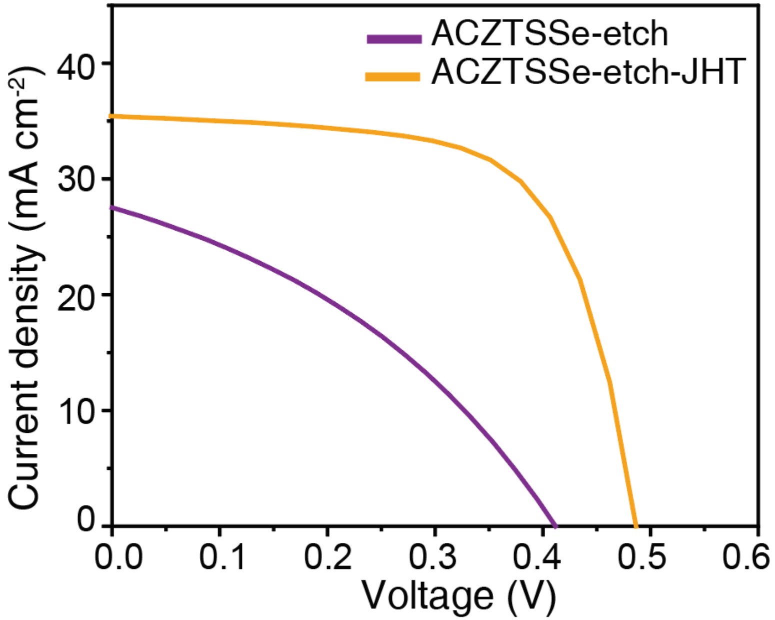

$Cu_2Se + 4NH_3 = 2[Cu(NH_3)_2]^+ + Se^{2-}$

$K = 8.2 \times 10^{-40}$

$ZnSe + 4NH_3 = [Zn(NH_3)_4]^{2+} + Se^{2-}$

$K = 1.48 \times 10^{-17}$

- Zn dissolves with etching (during CBD)
- Cu poor/Zn-rich surface
- CdS constructed on Zn-poor surface (not Cu-poor as in CIGS)
- Zn re-deposition into CdS
- JHT recovers interface: Zn moves towards surface

Lattice Constrain and Band Alignment

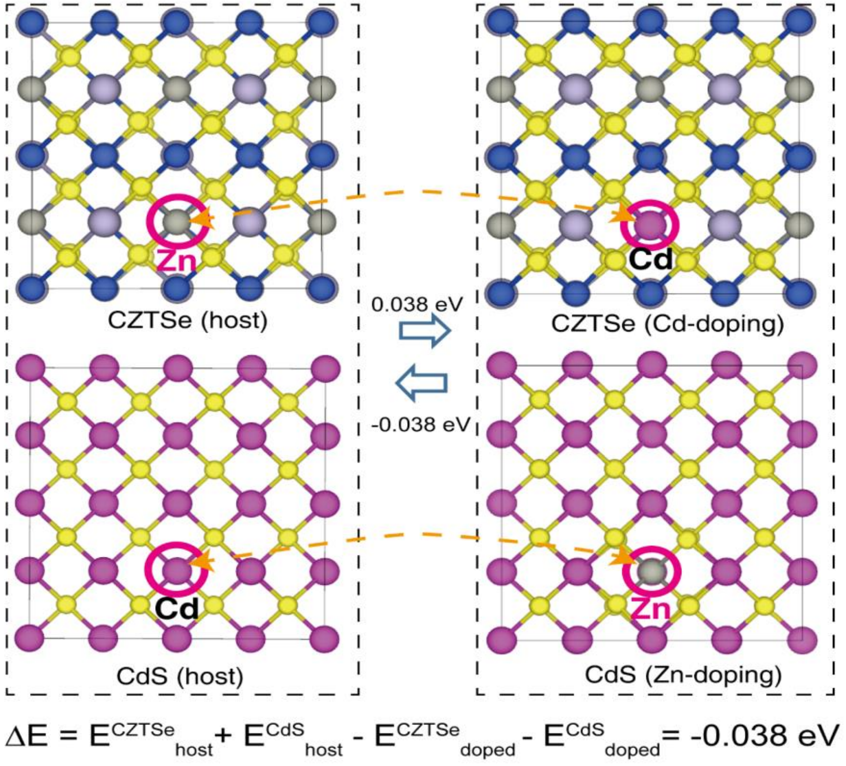

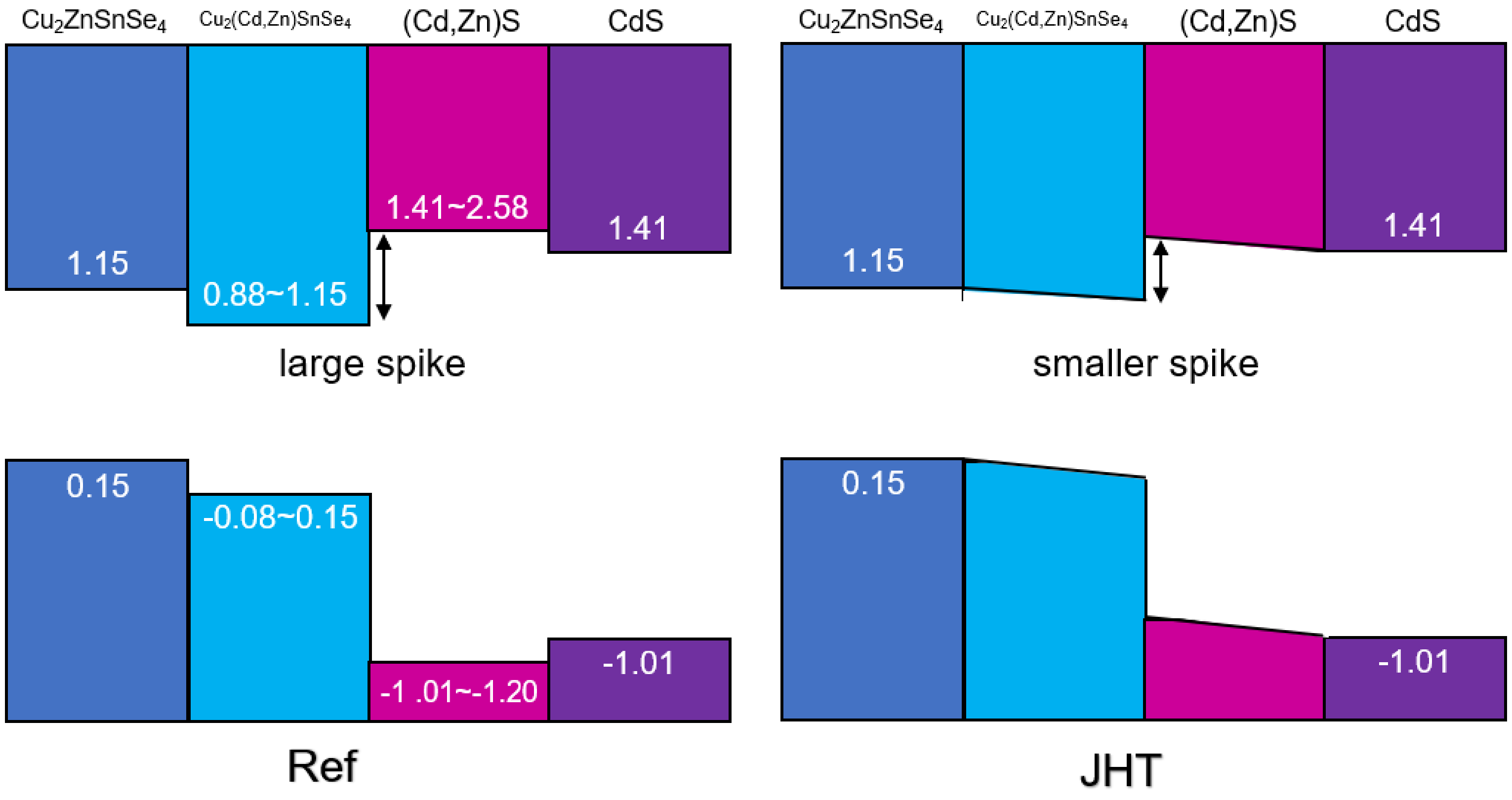

CZTSSe/CdS Interface: Defective to Epitaxial

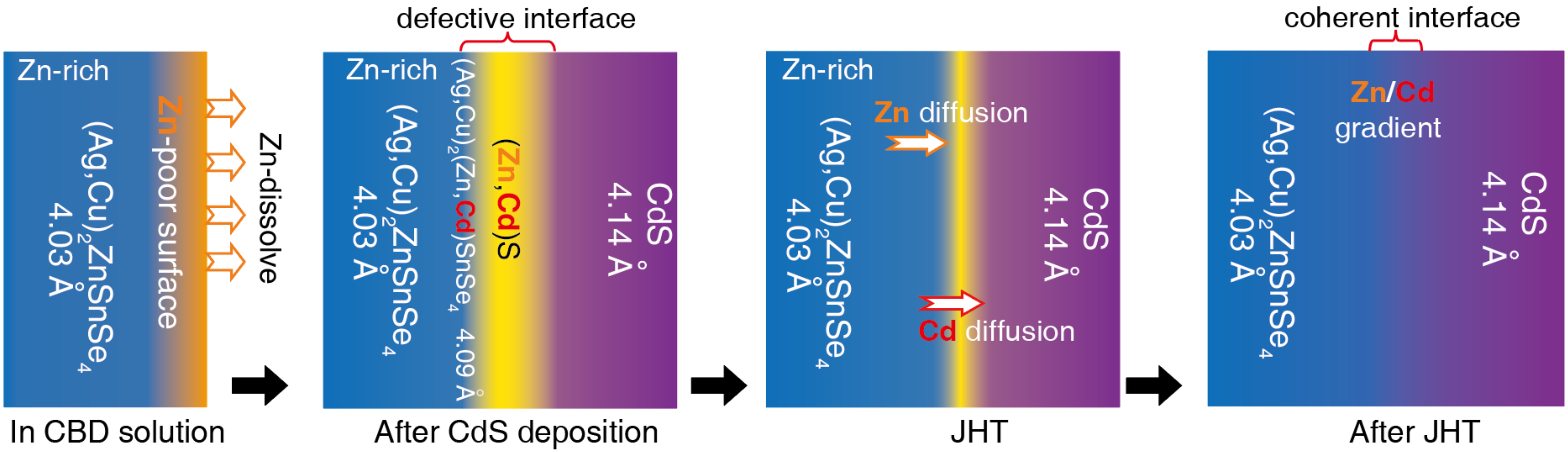

- Cd in CZTSSe and Zn in CdS are observed in Ref sample
- Interface narrows and sharps upon low-temperature JHT
- Elemental di-mixing: Cd and Zn back to original position
- Interface moves toward CdS layer

Nature Energy, 2022.

Record Efficiency Device via Low-Temp JHT

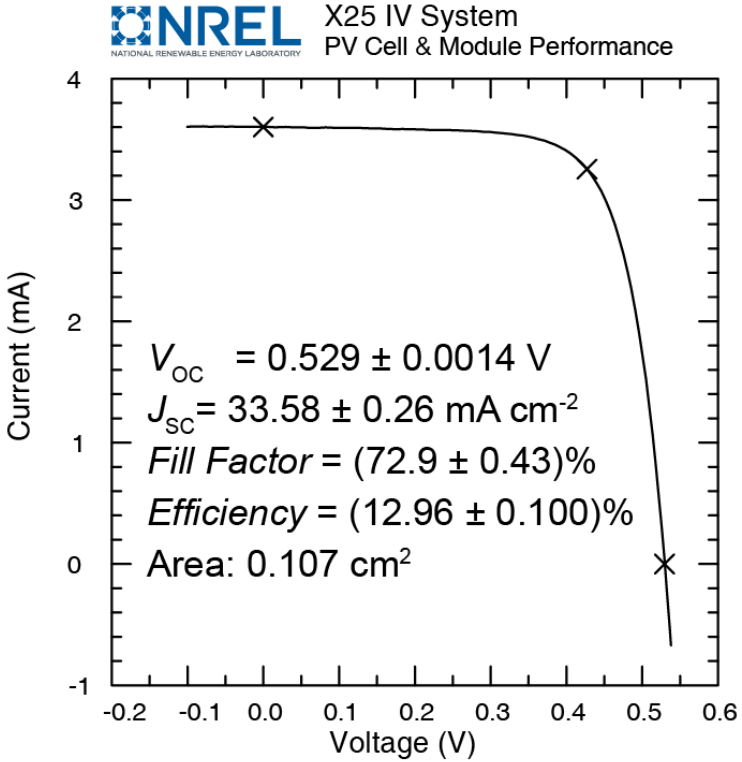

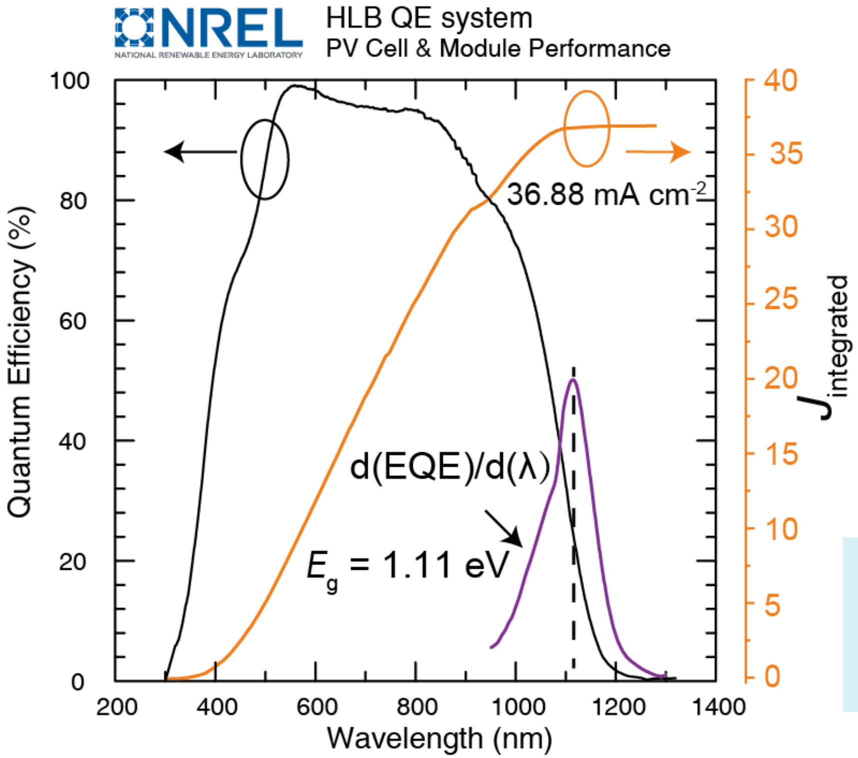

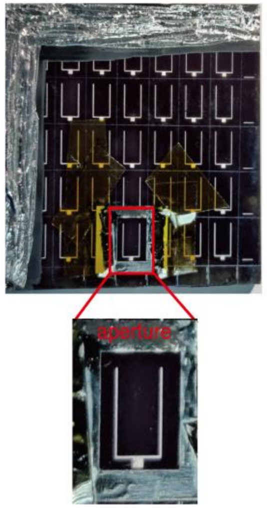

0.107 cm² Cell

Aperture area: 12.96%
Active area: 14.22%

Device	Absorber	Area (cm²)	V_{OC} (V)	J_{SC} (mA/cm²)	FF (%)	Eff. (%)	n	J_0 (A/cm²)	R_s	E_g (eV)	$V_{OC\text{-}def}$ (V)	Certifying Center
This work	ACZTSSe*	0.107	0.529	33.7	72.9	13.0	1.35	8.2×10^{-9}	0.35	1.11	0.337	NREL
IBM cell[6]	CZTSSe	0.420	0.513	35.2	69.8	12.6	1.45	7.0×10^{-8}	0.72	1.13	0.373	Newport
DGIST cell[7]	CZTSSe	0.480	0.541	35.4	65.9	12.6	1.88	9.6×10^{-7}	0.87	1.13	0.345	Newport
UNSW cell[2]	CZTS	0.233	0.730	21.7	69.3	11.0	1.44	6.8×10^{-8}	2.58	1.50	0.500	NREL
IBM cell[27]	CZTSe	0.43	0.423	40.6	67.3	11.6	1.57	1.3×10^{-6}	0.32	1.00	0.342	Newport

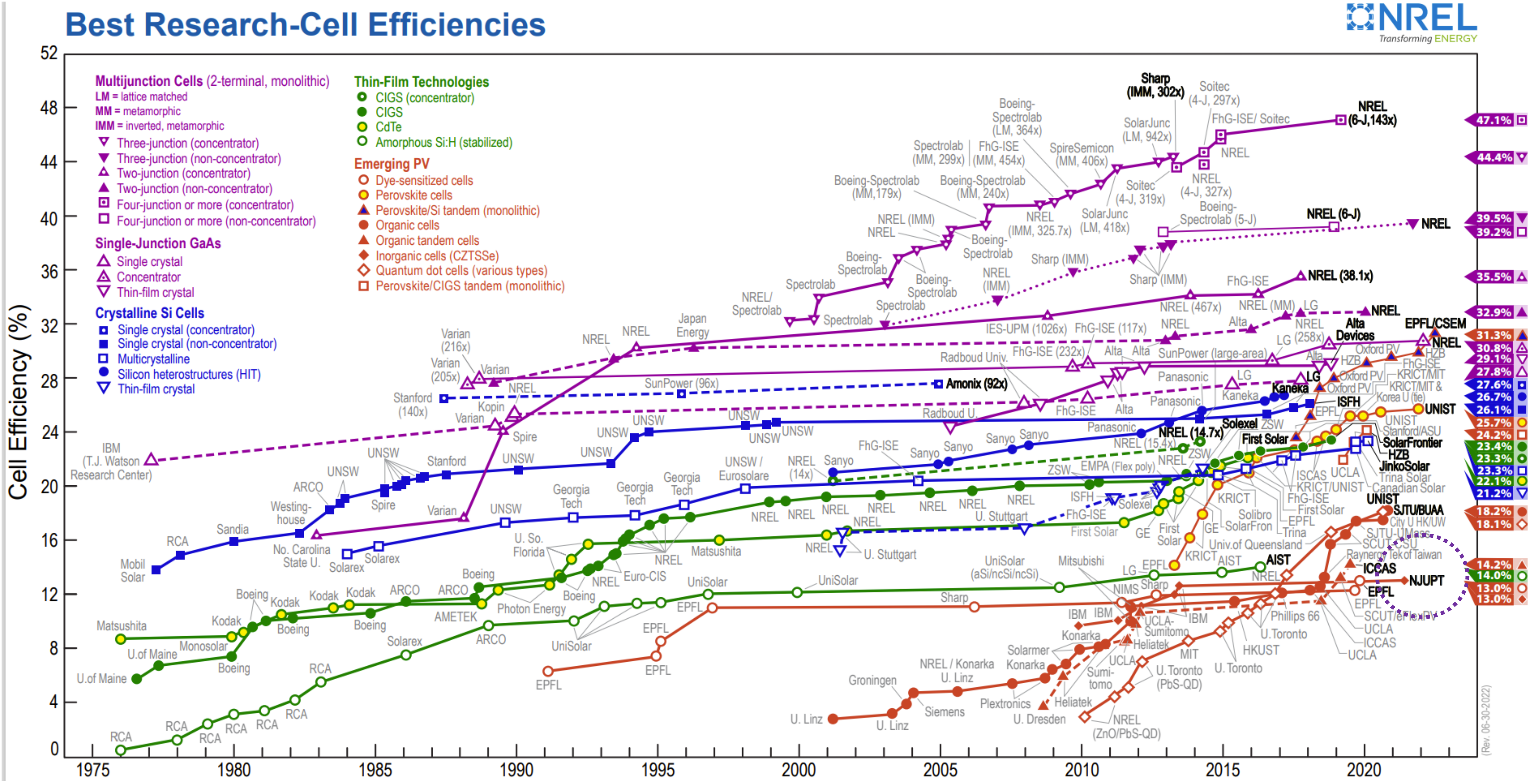

[Best Research-Cell Efficiency Chart | Photovoltaic Research | NREL]

Solar Cells on 1-cm² Area and Device Stability

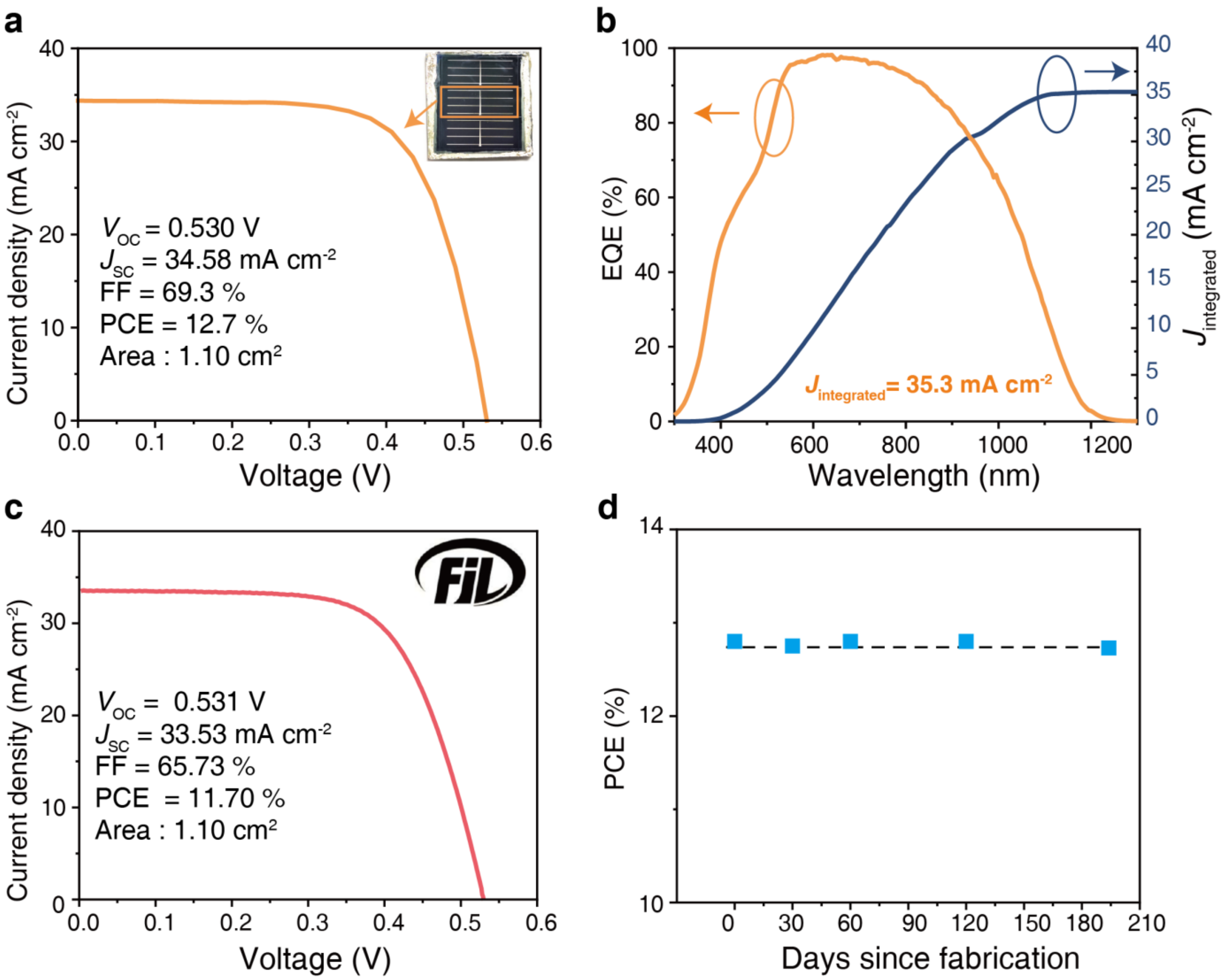

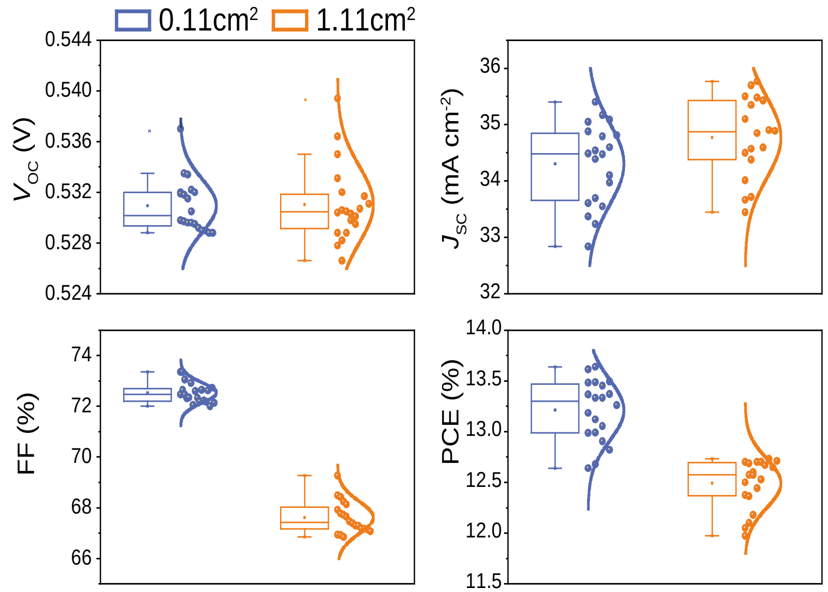

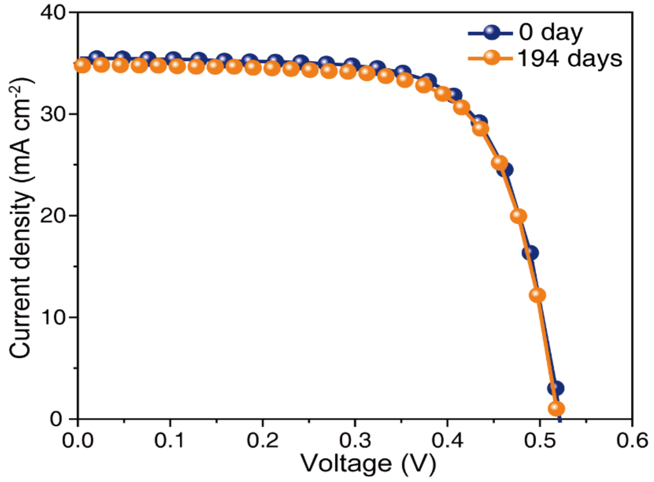

Certification of 11.7% 1-cm^2 Size Device

福建省计量科学研究院
FUJIAN METROLOGY INSTITUTE
（国家光伏产业计量测试中心）
National PV Industry Measurement and Testing Center

ilac-MRA CNAS 中国认可 国际互认 检测 TESTING CNAS L0131

检 测 报 告
Test Report

报告编号：21Q3-00174
Report No.

客户名称 Name of Customer	Nanjing University of Posts and Telecommunications
联络信息 Contact Information	No. 9, Wenyuan Road, Qixia District, Nanjing city, Jiangsu Province, China
物品名称 Name of items	NJUPT-CZTSSe-1
型号/规格 Type /Specification	Area：1.11cm^2
物品编号 Items No	1
制造厂商 Manufacturer	Nanjing University of Posts and Telecommunications
物品接收日期 Items Receipt Date	2021-06-09
检测日期 Test Date	2021-06-09

1.11 cm^2

（盖章处）
Stamp

批准人 Approved by 黎健生
核验员 Checked by 何翔
检测员 Test by 游宏亮

发布日期 Date of Report 2021 年 Year 06 月 month 21 日 Day

扫一扫 查真伪

本院/本中心地址：福州市屏东路 9-3 号 Address：9-3 Pingdong Road,Fuzhou,China
电话：0591-87845050 Telephone
传真：0591-87808417 Fax
邮编：350003 Post Code
网址：www.fjjl.net Web Site
咨询电话：0591-87845050 Inquire line
投诉电话：0591-87823025 Fax for complaint

福建省计量科学研究院
FUJIAN METROLOGY INSTITUTE
（国家光伏产业计量测试中心）
National PV Industry Measurement and Testing Center

报告编号：21Q3-00174
Report No.

检测结果/说明：
Results of Test and additional explanation.

1 Standard Test Condition (STC)：Total Irradiance：1000 W/m^2
Temperature：25.0 °C
Spectral Distribution：AM1.5G

2 Measurement Data under STC

Test Times	I_{sc} (mA)	V_{oc} (V)	I_{MPP} (mA)	V_{MPP} (V)	P_{MPP} (mW)	*FF* (%)	*η* (%) total area	*η* (%) effective area (with subtracted busbars area)
1	36.89	0.5305	32.81	0.3929	12.89	65.87	11.70	12.38
2	36.92	0.5315	32.77	0.3935	12.89	65.69	11.70	12.38
3	36.92	0.5319	32.79	0.3931	12.89	65.64	11.70	12.38
Average Value	36.91	0.5313	32.79	0.3932	12.89	65.73	11.70	12.38

Mismatch factor: 1.019

3 I-V & P-V Characteristic Curves under STC

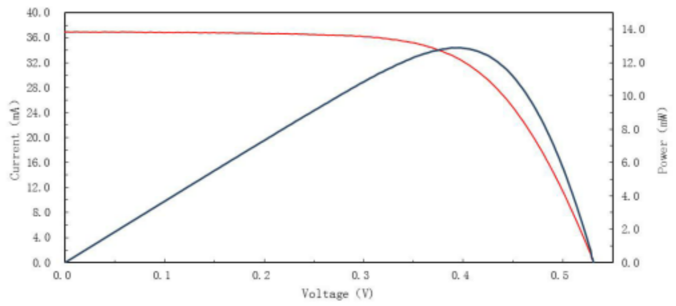

Figure 1. I-V and P-V characteristic curves of the measured sample under STC

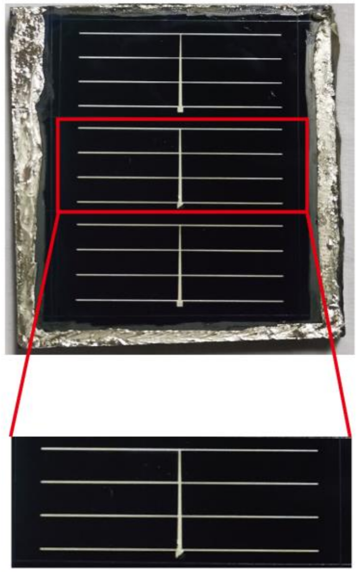

Total area: 11.70%
Active area: 12.38%

V_{oc} = 0.5313 mV

FF = 65.73%

Recombination-free Heterojunction Interface

epitaxial interface (matched lattice constants)

	Zinc-blende	(112)/(111) in-plane cons.	layer distance
CdS	5.848	4.136	3.376
$CuInSe_2$	a=5.781, c=11.642	4.103	3.349
$Cu_2ZnSnSe_4$	a=5.680, c=11.360	4.016	3.278
$Cu_2CdSnSe_4$	a=5.826, c=11.394	4.074	3.326
$Ag_2ZnSnSe_4$	a=6.036, c=11.301	4.134	3.375
Cu_2ZnSnS_4	a=5.429, c=10.847	3.837	3.132
Cu_2CdSnS_4	a=5.590, c=10.840	3.893	3.178
Ag_2ZnSnS_4	a=5.776, c=10.869	3.965	3.237

reasonable CBO (small spike)

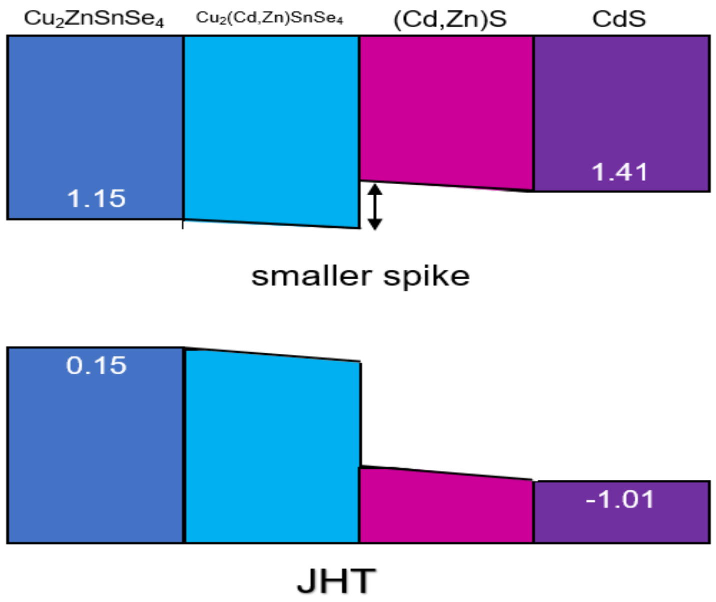

uniform surface (less defective)

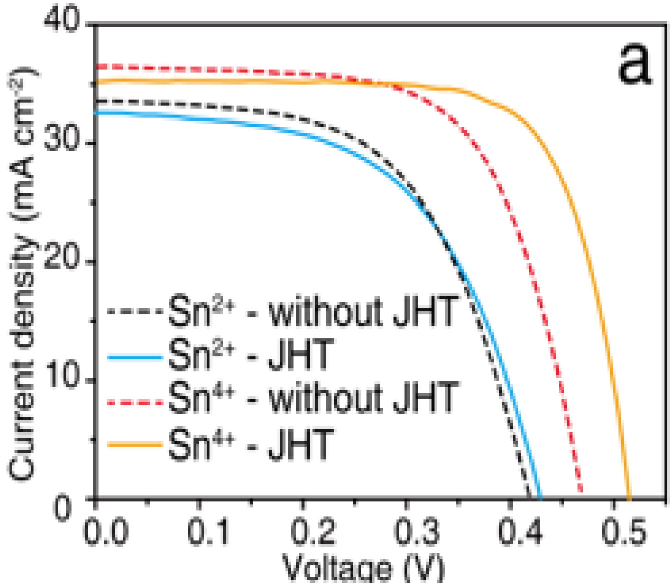

Wang, et al. *J. Alloy. Compd.* **509**, 9959-9963 (2011).
Knight, et al. *Mater. Res. Bull.* **27**, 161-167 (1992).
Das, S. et al. *J. Cryst. Growth* **381**, 148-152 (2013).
Babu, et al. *Semicond. Sci. Technol.* **23**, 085023 (2008).
Shi, et al. *J. Alloy. Compd.* **683**, 46-50 (2016).
Chetty, et al. *Intermetallics* **72**, 17-24 (2016).
Nagaoka, et al. *J. Cryst. Growth* **555**, 125967 (2021).
Gurieva, et al. *Phys. Status Solidi (C)* **12**, 588-591 (2015).

- ➢ CdS is a good buffer layer for CZTSe but not for CZTS
- ➢ Uniform surface (grain growth) is crucial for kesterite

4. 总结与展望

- Controlled solution chemistry enables fabrication of CZTSSe through direct phase transformation grain growth, which sufficiently suppresses defects and band tailing.
- For the first time unveils that the kesterite/CdS heterojunction is constructed on a Zn-poor surface (not Cu-poor surface as CIGS), accounting for the defective heterojunction interface.
- Low temperature JHT induces elemental di-mixing, which reconstructs epitaxial interface.
- We have achieved 13% new record efficiency and 11.7% certified efficiency on 1 cm^2 size.
- The findings are expected to advance the development of kesterite solar cells.
- The strategies developed here can be applied to other solution based multi-element semiconductors.

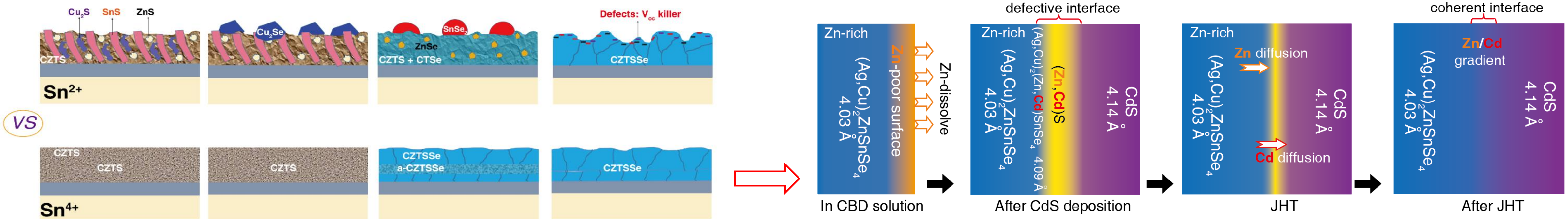

Acknowledgements

Prof. David S. Ginger
Prof. Hugh W. Hillhouse
Dr. Rajiv Giridharagopal
Prof. Sixin Wu
Prof. Xiaojing Hao
Dr. Zhenghua Su
Dr. Junjie Fu

Dr. Weibo Yan
Dr. Jingjing Jiang
Shaotang Yu
Yuancai Gong
Sanping Wu
Yifan Zhang
Ruichan Qiu
Chuanyou Niu
Qiang Zhu
Yage Zhou

中华人民共和国科学技术部
Ministry of Science and Technology of the People's Republic of China

NSFC

南京邮电大学
Nanjing University of Posts and Telecommunications

(2019YFE0118100) (21571106, U1902218, 22075150)